CONFIGURAL AND PERCEPTUAL FACTORS INFLUENCING THE PERCEPTION OF COLOR TRANSPARENCY

THÈSE N^{O} 3181 (2005)

PRÉSENTÉE À LA FACULTÉ INFORMATIQUE ET COMMUNICATIONS

Institut de systèmes de communication

SECTION DES SYSTÈMES DE COMMUNICATION

ÉCOLE POLYTECHNIQUE FÉDÉRALE DE LAUSANNE

POUR L'OBTENTION DU GRADE DE DOCTEUR ÈS SCIENCES

PAR

Peggy GERARDIN

licence de sciences cognitives, Université Lumière, Lyon 2, France
et de nationalité française

acceptée sur proposition du jury:

Prof. S. Süsstrunk, directrice de thèse
Prof. M. D'Zmura, rapporteur
Prof. M. Herzog, rapporteur
Dr K. Knoblauch, rapporteur

Lausanne, EPFL
2005

Acknowledgments

Many people supported me during the completion of this thesis with criticism, helpful assistance and references. This work would have never been possible without them.

First of all, I would like to express my gratitude to my supervisor Prof. Sabine Süsstrunk who gave me the opportunity to join her group, the best research environment I ever had. I would like to thank her for her guidance, encouragement and excellent advice throughout this study.

I owe a special thank to Dr. Kenneth Knoblauch (INSERM U371, Lyon, France), whose patience, assistance and motivation were greatly appreciated. I stopped counting the numerous emails we sent to each other, the abundant lunches we shared and the million discussions we had on color vision.

I would like to give a special thank to Prof. Michael D'Zmura, who welcomed me in his laboratory at the University of California, Irvine (USA). He proposed me a very interesting subject and helped me during all my stay. I thank him for the nice barbecues we had together and private concerts at home. I also thank Prof. Don Hoffman (UCI, USA) for the nice classes I attended to, and for the interesting discussions we had facing some good sushi.

I thank all members of my thesis committee, including Prof. Michael Herzog, for accepting to read the thesis and to comment my defense.

In particular, I would like to thank my colleague Roberto for being a very quiet officemate, not disturbing me with phone calls and not singing all day long, especially when I had to concentrate at work. I also thank Philippe for continuing working with me, even after his diploma. Many thanks to Vladan for the numerous coffee breaks, and to Jocelyne, Laurence, Patrick, Luciano, Andrea, Williams, Martin and all LCAV members, and for their interesting questions after each of my talks, such as 'Do Inuits see colors like Europeans'? I really enjoyed working in this group.

All my gratitude to my friends who shared these four years in Lausanne with me, in particular to David, Véronique, Elena, Gianluca, Gloria, Daniela and Stefan. I enjoyed travelling and partying with them, especially when I was discouraged and wanted to give up and become a florist. Also many thanks to Erin, for her gentleness and for the numerous rides we had in California. I also thank all my friends in France for their precious support.

Last but certainly not least, I would like to thank my parents and my brother for their support and their numerous encouragements for each step that a thesis involves. I really enjoyed our relaxing and refreshing barbecues in our country house. Their visit in California was also one of my best memories.

Finally, my warmest thanks go to Nicolas, for his understanding and his fantastic support. We endured numerous geographical distances during all my studies. During my thesis, a total of 72,240 km has been done to see each other. This does not include the time when I was in California. I dedicate this thesis to him, with love.

Abstract

The mechanisms by which the brain represents colors are largely unknown. In addition, the large number of color phenomena in the natural world has made understanding color rather difficult. Color transparency perception, which is studied in this thesis, is precisely one of these interesting phenomena: when a surface is seen both in plain view and through a transparent overlay, the visual system still identifies it as a single surface. Processes of the visual system have widely inspired researchers in many domains such as neurosciences, psychology, as well as computer vision. The progress of digital imaging technologies requires research engineers to deal with issues that demand knowledge of human visual processing. To humans, an image is not a random collection of pixels, but a meaningful arrangement of regions and objects. One thus can be inspired by the human visual system to investigate color representation and its applicability to digital image processing. Finding a model of perception is still a challenging matter for researchers among multidisciplinary fields.

This thesis discusses the problem of defining an accurate model of transparency perception. Despite the large number of studies on this topic, the underlying mechanisms are still not well understood. Investigating perceptual transparency is challenging due to its interactions with different visual phenomena, but the most intensively studied conditions for perceptual transparency are those involving achromatic luminance and chromatic constraints. Although these models differ in many aspects, a broad distinction can be drawn between models of *additive* and *subtractive* transparency. The General Convergence Model (GCM) combines both additive and subtractive color mixtures in showing that systematic chromatic changes in a linear color space, such as translation and convergence (or a combination of both), lead to perceptual transparency. However, while this model seems to be a necessary condition, it is not a sufficient one for transparency perception.

A first motivation of this thesis was to evaluate and define situations more general than the GCM. Several chromatic changes consistent or not with the GCM were generated. Additional parameters, such as configural complexity, luminance level, magnitude of the chromatic change and shift direction were tested. The main results showed that observers' responses are influenced by each of the above cited parameters. Convergences appear significantly more transparent when motion is added for bipartite configurations, or when they are generated in a checkerboard configuration. Translations are influenced by both configuration and motion. Shears are described as opaque, except when short vector lengths are combined with motion: the overlay tends to be transparent. Divergences are strongly affected by motion and vector lengths, and rotations by a combination of checkerboard configuration with luminance level and vector length. These results question the generality of the GCM.

We also investigated the effects of shadows on the perception of a transparent filter. An attempt to extend these models to handle transparency perception in complex scenes involving surfaces varying in shape and depth, change in conditions of illumination and shadow, is described. A lightness-matching task was performed to evaluate how much constancy is shown by the subject among six experimental conditions, in which shadow position, shadow blur, shadow and filter blending values were varied. The results showed that lightness constancy is very high even if surfaces were seen under both filter and shadow. A systematic deviation from perfect constancy in a manner consistent with a perceived additive shift was also observed. Because the GCM includes additive mixture and is related to color and lightness constancy, these results are promising and may be explained ultimately by this model.

Version Abrégée

Les mécanismes par lesquels le cerveau se représente la couleur sont encore méconnus. De plus, le grand nombre de phénomènes colorés traités rend la tâche encore plus difficile. La perception de la transparence colorée, qui est étudiée dans cette thèse, est justement l'un de ces phénomènes : lorsqu'une surface est vue à la fois sous un filtre et en dehors, le système visuel l'identifie comme une seule et même surface. Les processus de traitement du système visuel ont largement inspiré les chercheurs dans des domaines aussi variés que les neurosciences, la psychologie et les sciences de l'informatique. Les progrès grandissants des technologies de l'imagerie numérique incitent les chercheurs à acquérir des connaissances sur le traitement visuel humain. Pour lui, une image n'est pas une collection de pixels, mais un arrangement de régions et d'objets qui a un sens. Il serait donc utile d'en être inspiré pour explorer la représentation de la couleur et ses applications dans le traitement de l'image numérique.

Cette thèse traite du problème de définition d'un modèle précis de la perception de la transparence. Malgré le grand nombre d'études sur ce sujet, les mécanismes sous-jacents à ce phénomène sont encore peu compris. Explorer la perception de la transparence est un défi , dû à ses interactions avec de nombreux phénomènes visuels. Cependant, les modèles les plus étudiés sont ceux relatifs à la luminance achromatique et aux contraintes chromatiques. Même si ces modèles diffèrent par de nombreux aspects, ils peuvent être divisés en deux: les modèles de transparence *additifs* et *soustractifs*. Le Modèle Général de Convergence (GCM) combine ces deux mixtures de couleurs et montrent que des changements chromatiques systématiques dans un espace de couleurs linéaire, tels qu'une tranlation ou une convergence (ou bien la combinaison des deux), permettent la perception de la transparence colorée. Seulement, ce modèle est une condition nécessaire mais non suffisante à cet effet.

Nous avons évalué et défini dans cette thèse des situations plus générales que celles qu'englobe le GCM. Plusieurs changements chromatiques cohérents et non cohérents avec ce modèle ont été générés. Des paramètres supplémentaires, tels que la complexité de la configuration, le niveau de luminance, la magnitude des changements et leurs directions ont été testés. Nos résultats montrent que les réponses des sujets sont influencées par chacun de ces paramètres. Les convergences apparaissent plus transparentes lorsque le mouvement du filtre est ajouté pour les configurations de type *bipartite*, ou bien lorsqu'elles sont générées pour des configurations de type *damier*. Les translations sont influencées par tous les paramètres. Les cisaillements sont décrits comme opaques, excepté pour les petites longueurs de vecteur. Les divergences sont fortement affectées par le mouvement, et les rotations par une combinaison entre la configuration de type damier, la luminance et les longueurs de vecteur. Ces résultats mettent en péril la généralité du GCM.

Nous avons aussi exploré les effets des ombres sur la perception de la transparence. Une tentative d'étendre ces modèles perceptifs à des scènes plus complexes, incluant des surfaces dont varient la forme, la profondeur, les conditions d'éclairage et les ombres a été entreprise. Une tâche d'appariement a été adoptée à travers six expériences testant la constance à la luminosité d'un sujet, dans lesquelles la position de l'ombre, sa netteté et son intensité variaient. Nos résultats montrent une déviation systématique de la constance parfaite, de manière cohérente avec la perception d'un changement additif, et pourront ainsi être expliqués plus tard par le GCM.

Contents

Chapter 1

Introduction

1.1 Motivations

Color representation mechanisms are still unknown. Theories try to link color appearance to physiological and physical mechanisms, and the large number of color phenomena in the natural world has made understanding color rather difficult. *Color transparency* is precisely one of these interesting phenomena: when a surface is seen both in plain view and through a transparent overlay, the visual system still identifies it as a single surface. Many studies have stressed its relation to color constancy, and despite the growing number of studies on this topic over the last century, the underlying mechanisms are still not well understood.

The light reflected from an object changes considerably under different conditions of illumination. Nevertheless, the color of the object remains approximately the same. This property, so-called color constancy, is one of the most important properties of the visual system. For example, an apple looks green in the early morning daylight, whose main component appears bluish, and also in the late afternoon, when light appears reddish. This allows to easily identify objects in a world where attributes are continuously in motion and vary considerably. The visual system has to detect rapid changes that occur (an object in motion), but has to hold constant certain properties of this object (color, form). This ability has widely inspired researchers in many domains such as neurosciences, psychology, as well as computer vision.

The progress of digital technologies (digital image analysis, for example) requires research engineers to deal more and more with problems that demand knowledge of human visual processing. For example, more and more images are used in HTML documents on the World Wide Web. Ideally, a tool should be available, i. e. an image search engine, that can retrieve relevant images quickly on demand. Effectively, digital image databases have seen an enormous growth over the last years. Since many image collections are indexed or annotated, there is a great need for automated, content-based methods that could help users retrieve or structure image databases. Given the current state of the art in computer vision, no robust general purpose methods exist that could perform, for example, object recognition in a broad domain. This performance requires information about how the visual system performs recognition. One needs an image analysis system where the image color representation would not be based on a pixel-by-pixel encoding, but would take into account its contextual factors. However, solving this problem requires elucidating how the human visual system extracts an object from its context.

To humans, an image is not a random collection of pixels, but a meaningful arrangement of regions and objects. To this effect, one can be inspired by the human visual system to investigate color representation and its applicability to digital image processing. Finding an accurate model of perception is still a challenging matter for researchers among multidisciplinary fields. Establishing an accurate model of transparency perception greatly contributes to such challenges.

1.2 Investigated Approach

The objective of this thesis is to analyze, test and extend a model of color transparency perception: the *General Model of Convergence* (GCM) [D'Zmura et al., 1997]. This model predicts that certain systematic chromatic changes in a linear chromatic space across a region in the image lead to the perception of color transparency. For example, convergences or translations result in a transparent overlay as seen in Figure 1.1. The base of each vector represents chromatic properties of surfaces seen in plain view, while the arrowhead represents chromatic properties of the same surfaces but appearing under a filter. An interesting aspect of this model is that it incorporates several aspects of color transparency perception such as light absorption or light addition. Both can be found in the real world (like an absorption filter or a spotlight, respectively). Moreover, this model covers equiluminant chromatic changes for which a resulting filter cannot be realized in the physical world. Defining optimal conditions for perceiving transparency will permit in the future

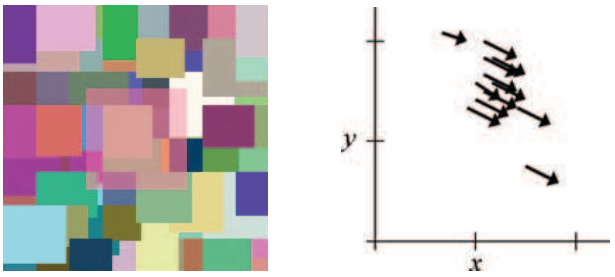

(*a*) (*b*)

Figure 1.1: (*a*) Pink filter obtained by a translation towards the L cardinal point of the L-M-cone axes [D'Zmura et al., 1997]. (*b*) Illustration of plots in the *CIE* 1931 Yxy color space of the equiluminant translations.

an extension to color imaging applications, such as color image rendering algorithms, gamut mapping algorithms, etc.

In this thesis, several conditions were investigated to test the specificity of the GCM. First, a psychophysical experiment was designed to analyze statistically the effects of vector length for several types of systematic chromatic changes. A second psychophysical experiment investigated such effects in a more uniform color space. Additional factors such as configural complexity and motion were also included in the experiment. These factors were added to test the robustness of the model and to examine their possible interactions with the systematic chromatic changes on the appearance of transparency. Finally, a third psychophysical experiment considered the effect of the position of a filter and its related shadow in a given three-dimensional scene. This last part of the thesis did not test the GCM, but was an investigation on the effects of shadows on transparency in simulated displays with both filters and shadows lying in front of surfaces.

1.3 Main contributions

The main contributions of this work can be summarized as follows:

- An extensive analysis of the GCM with different vector lengths in a simple configuration. In a first psychophysical experiment, filters resulting from different systematic chromatic shifts were presented to subjects, including convergences, translations, shears (described as opaque) and divergences. This study was designed to analyze statistically the effect of these different color shifts.

- Extension of the GCM to moving color transparency and its consequences/implications for the appearance of chromatic changes. The main goal of this experiment was to examine whether motion is neutral with respect to the effects of systematic color changes. This experiment also explores the effect of the stimulus configuration, from simple to more complex figural constraints.
- A study of the effects of shadows on transparency perception. This experiment includes filters and their shadows, used as a cue for a three-dimensional scene. The interest is in studying transparency in an environment closer to real scenes, and to investigate the effect of shadows on the perception of a transparent filter and the surfaces behind it.

1.4 Organization of the thesis

This thesis is organized as follows: **Chapter 2** presents an overview of color vision, from physical data to neural structures. It also introduces the notion of color appearance and related phenomena such as color constancy. **Chapter 3** outlines the main aspects of transparency perception. It reviews recent models and the state of the art on this topic. **Chapter 4** develops experiments on color transparency according to systematic color changes with several vector lengths and spatial configurations. The contribution of motion on systematic color changes is described in **Chapter 5**. Seeing transparency with shadows is investigated in **Chapter 6**. **Chapter 7** concludes the thesis and explores directions for future work. **Appendix A** presents a short introduction to colorimetry, **Appendix B** provides an explanation of statistics used in two of the three experiments, **Appendix C** shows complementary results for **Chapter 5**.

Chapter 2

Color Vision

2.1 Introduction

The perception of color is a central component in primate vision. Color facilitates object perception and recognition, and has an important role in scene segmentation [Gegenfurtner, 1999]. Color vision has a long history, but one has still to know about physics, physiology and psychology to understand its bases. Entire books are devoted to this challenging topic. In this chapter, color vision is first presented through a review of physical and physiological studies. Light is captured by the eye and then transmitted to the brain through different pathways. However, despite numerous studies dedicated to such physiological processes, color perception is still not well understood. Among the variety of color phenomena (such as color constancy and color transparency), psychological (and mainly psychophysical) studies color perception with an implicit reference to the underlying neurological processes. A second part of this chapter enumerates some of these color phenomena. The purpose of this review is to introduce the fundamental notions that will be of use for the understanding of the color transparency phenomenon.

Early investigations on color vision were focused on the coding of spectral characteristics of light [Knoblauch, 2002]. In the three last decades, studies have shown that color perception depends on the context as well. As a matter of fact, the color we see at a point does not, in general, depend only on its spectral characteristics at that point (For example, see Figure 2.1). Moreover, the characteristics of light

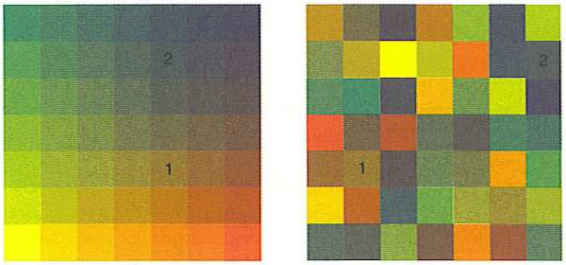

Figure 2.1: Color shuffle, devised by J. Koenderink [Hoffman, 1998]. On the left an array of color squares arranged so as to create a smooth transition of colors. On the right the same squares but randomly shuffled. One can notice how different corresponding squares (1 and 2 in the figure) appear, even though their spectra are identical.

vary during the day, and these changes can have a considerable impact on the object reflected by light. Our visual system compensates for these light variations by assigning constant colors to the objects. This

phenomenon is well known as *color constancy*.

This chapter discusses the physics of light and surface reflectances, as well as physiology and psychology approaches (including color appearance and color constancy) of color perception. Section 2.2 gives an overview of physical sources involved in color vision, such as light and surface reflectances. Structures and pathways involved in light coding are shown in Sections 2.3 and 2.4, as well as cortical mechanisms in Section 2.5. Context is also important when trying to understand color perception. Section 2.6 introduces first theories on color appearance, different color phenomena such as simultaneous color contrast and color constancy. This review is helpful to understand **Chapter 3** and focuses on some aspects relevant to color transparency phenomenon.

2.2 Physical data

The light reaching the retina comes from two types of emitters: *sources* as the sun, lamps, etc., and *surface reflectances* that are illuminated by sources.

2.2.1 Sources

Light is electromagnetic waves that propagate in space and time. They are characterized by their *wavelength* λ and their frequency v. Both are related by

$$\lambda = cv^{-1} \tag{2.1}$$

where $c = 2.9979$ x 10^8 m$\cdot$ s^{-1} is the velocity of light *in vacuo* [Wyszecki and Stiles, 1982]. The visible light is a narrow window in the entire ensemble of electromagnetic waves which comprise gamma rays, X-rays, ultra-violet, infrared, radio waves, etc. The visible spectrum ranges from 380nm to 780nm (Figure 2.2). The energy E of a single photon is proportional to its radiation frequency v with

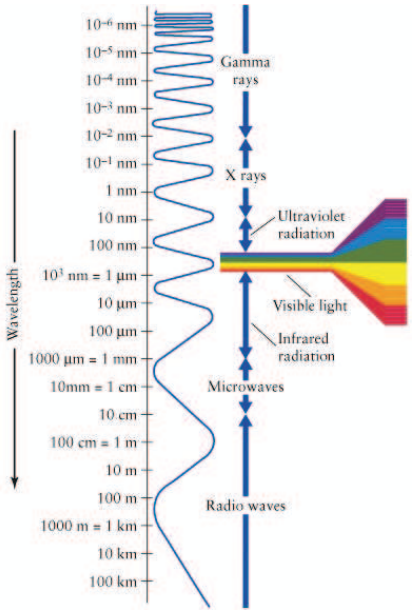

Figure 2.2: Visible light spectrum in a range of [380nm, 780nm].

$$E = hv \tag{2.2}$$

where h = 6.6262 x 10^{-34}J· s is Planck's constant. Every light is characterized by its energy as a function of frequency, and by extension of wavelength. Light is generally composed of a mixture of energy at different wavelengths. The power emitted at each wavelength gives an indication of the spectral power distribution of the light source. Some of them have been standardized by the Commission Internationale de l'Eclairage (CIE) and thus were classified as standard illuminants, such as illuminant CIE D65, for example, representing daylight (See Figure 2.3). The most important natural light source is the sun. Direct

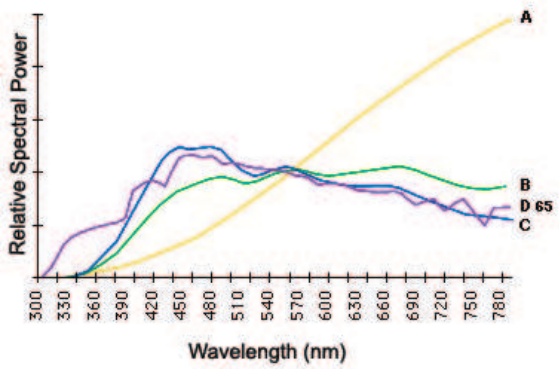

Figure 2.3: Relative spectral distribution of different standard illuminants, such as CIE D65 (daylight), CIE A (tungsten lamp), CIE B (direct sunlight) and CIE C (average daylight with sun).

sunlight and sunlight scattered by the atmosphere are the components of daylight that play a key role in color science. Many spectroradiometric measurements[1] of daylight have been made and reported in the literature. An approximate characterization of the sun light is to consider it as a *point light source at infinity*, when it can be assumed that the power at a surface due to the point source does not decrease with the distance to the source.

Additive and subtractive mixtures

Light sources have different rules when they are interacting with only themselves or with surfaces. When two light sources are combined, the resulting spectrum is the sum of the two. This rule is named *additive* mixture. However, when two reflectances are combined, some light is lost: this is called the *subtractive* color mixture. One can find a similar relationship with subtractive color mixture and filters applied on surfaces. As a matter of fact, many models of transparency perception are inspired from the color mixture properties (See Section 3.3).

2.2.2 Surfaces

Light interacts with surfaces. Some of them can absorb, reflect or transmit it. Most surfaces absorb and reflect wavelengths differently. These different surface properties will be considered in this thesis, since a given filter can partly absorb and transmit the light (See Section 3.2 for a definition of physical transparency). Finally, the light can be reflected by surfaces under the filter. The basic quantity that characterizes the process of reflection is called *reflectance* $R(\lambda)$. The reflectance can be defined as a ratio of the reflected

[1] Spectroradiometry is the measurement of radiometric quantities as a function of wavelength.

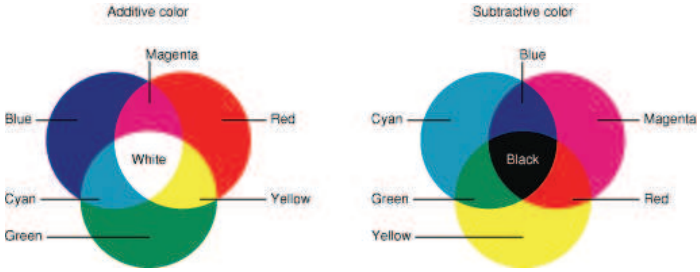

Figure 2.4: Additive and subtractive color mixtures.

radiant flux (or energy E_r) to incident radiant flux (or energy E_i), that is

$$R(\lambda) = \frac{E_r(\lambda)}{E_i(\lambda)} \tag{2.3}$$

If a surface is perfectly matte (i.e., Lambertian, when the surface reflects equally in any direction), the spectrum reaching the eye is $E_i(\lambda)R(\lambda)$. Most surfaces have both *specular* (when light is reflected back at the angle of incidence) and *matte* (when light is reflected uniformly in all directions) components.

2.3 Spectra coding

The information encoded from the visible radiant flux incident on the eye follows a complex pathway to get the cortex. This section summarizes the main cerebral components involved in spectra coding.

2.3.1 Eye

Structure

The human eye is an egg-like structure under the mechanical control of six muscles (Figure 2.5). Its envelope is called the *sclera*, made of dense white fibers, except where the *cornea* is exposed. Inside, the eye is filled with a transparent fluid named the *vitreous humor*, in which the *lens* is suspended by a system of muscle tissue. The visible radiant flux passes through the cornea, the lens, and the vitreous humor, where light is focused on the *fovea*. The inside back wall is covered with a layer of light sensing cells and a neural network, the *retina*.

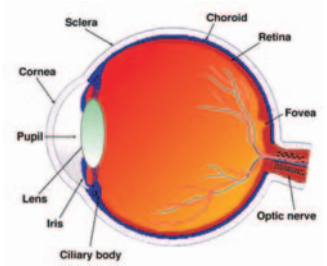

Figure 2.5: Schematic vertical section of an adult human eye.

2.3.2 Retina

Structure

The retina contains about one hundred twenty million photosensitive receptors: *rods* and *cones*. They project to several neuron layers (Figure 2.6). This figure shows rods and cones connected to several cells,

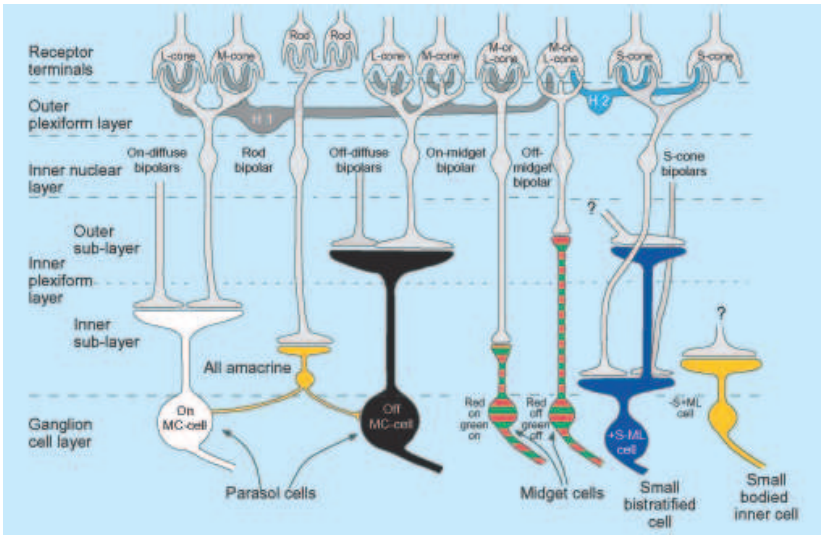

Figure 2.6: Schematic diagram of connectivity of primate retina [Lee, 2004]. Photoreceptors (cones and rods) make specific contact with various bipolar cell types. Horizontal cells also make specific cone contacts. In inner retina, the bipolar cells transmit signals to the main ganglion cell types. The only amacrine cell shown is the AII (there are about twenty different kind of amacrine cells), which receives excitatory input from rod bipolars and makes gap junction contacts with ON parasol cells and inhibitory synapses with OFF parasol cells. It is supposed that only two types of horizontal cells in primates, one (H1) making contacts with L and M cones and avoiding S cones and another (H2) making substantial contacts with S cones but also making some contacts with the L and M cones.

as *horizontal cells*, *bipolar cells*, themselves connected to *amacrine* and *ganglion cells*. Descriptions of these retinal neurons are stated in following subsections. The ensemble of axons of ganglion cells forms the optic nerve.

Photoreceptors

The distribution and relative number of rods and cones vary across the retina. The cones are about seven million in number and are of highest density in the fovea. When moving away from the fovea, the number of rods increases. Thus, the ratio of rods and cones varies from all cones and no rods in the fovea to nearly all rods and very few cones beyond about $40°$ from the visual axis. Rods are functionally and photochemically different from cones. Their photosensitive pigment (called *rhodopsin*) absorbs light at low level (below $0.001\ cd/m^2$). This is *scotopic* vision. There is a gradual change when rods and cones make both significant contribution to light response, called *mesopic* vision. At about $3\ cd/m^2$, rod receptors saturate, and *photopic* vision occurs solely: cones are functional.

Spectral coding by the cones Cones are involved in spectral coding and have varied spectral sensitivities. In humans, three classes of cones are sensitive to short-, medium and long-wavelengths: S-cones, M-cones and L-cones, respectively. Their distributions are not equal. Whereas S-cones are less than 10%, M- and L-cones distribution varies from $1:1$ to $4:1$ according to individuals [Roorda and Williams, 1999]. As a matter of fact, S-cones have a very different relative spectral sensitivity compared to M- and L-cones. Figure 2.7 shows the most recent and precise cone fundamentals [Stockman and Sharpe, 2000]. Each curve was normalized to its maximum. The curves show the cone sensitivity profiles. The M- and L-cones sensitivities overlap to a large extent and cover almost the entire visible spectrum. M- and L-cone

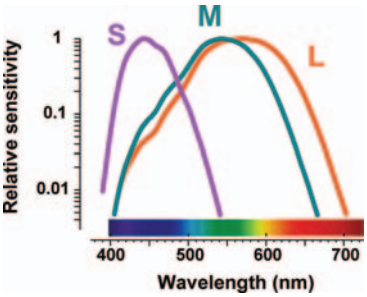

Figure 2.7: The relative sensitivities of the Short- (S), Middle- (M) and Long- (L) wavelength sensitive cones as a function of wavelength, after [Stockman and Sharpe, 2000].

absorption peaks in humans are at about 535nm and 565nm, respectively, whereas the S-cone absorption is clearly separated from them with a peak at 440nm. The visual system seems to treat M- and L-cones equally, trading chromatic comparison, in achieving the highest possible acuity at the fovea center. Thus, the small separation between M- and L-cones might be the compromise between the needs for high-contrast chromatic vision and high luminance acuity [Gegenfurtner and Kiper, 2003; Osorio et al., 1998]. This would be consistent with the fact that there are no S-cones in the foveola.

Trichromacy Whereas the light stimulus is determined by its intensity of wavelengths continuously distributed between 380 and 780nm (See Section 2.2.1), the output of the cones can be characterized by only three numbers. This is the principle of *trichromacy*. Thus, different light sources can produce equal distribution of quantum absorption across the three photoreceptors and match: this phenomenon is called *metamerism*. The number of photons absorbed by each cone will generate an electrochemical signal through a complex photochemical reaction: the *phototransduction*.

Univariance Once absorbed, the only remaining information is the photon count in each cone, not the wavelength of absorbed photons: a principle named *univariance*. An increase in photons can be due to an increase in light intensity, a change to a more favorable wavelength, or both (for example, an increase in one of the S-, M- or L-cone could be an increase of light intensity or that light comes closer to the peak of one of these cones). The reduction to the three dimensions results in a loss of wavelength information. Photons of different wavelength will be absorbed by corresponding cones. The cone signal is a function of the spectral sensitivity combined with the spectral energy distribution of the incident light [Knoblauch, 2002]. A dot product may be a discrete representation of this integration,

$$\rho = f(S_\lambda \cdot E_\lambda) \tag{2.4}$$

with S_λ the spectral sensitivity of a cone class as a function of wavelength, E_λ the spectral distribution, ρ the cone signal and f a function that represents the transmitted signal cone to the next retina cells. Therefore, the magnitudes of the output signals of the three cones must be compared. This is performed at the next level by horizontal cells and ganglion cells in the retina.

Retinal neurons

Photoreceptors project to two major neurons layers: horizontal cells and bipolar cells [Kaiser and Boynton, 1996] (see Figure 2.6). Several groups of dendrites belong to horizontal cells, connected to different cones, while contacts with rods are distant and have long axons. Five classes of bipolar cells are cone-specific, only one is connected to rods. Thus, this cone specificity leads to a very high visual acuity, on the contrary for rods, when sensitivity is primordial. Amacrine cells make connections with bipolar cells and a third nuclear layer formed with ganglion cells.

Ganglion cells Information from the cones is sent to the lateral geniculate nucleus (LGN) in the thalamus and the superior colliculus via axons of the ganglion cells in the optic nerve. Many converging signals through different retinal cells must be differentiated. Ganglion cells have a *center-surround receptive field*, which is spatially antagonistic (Figure 2.8). Light reaching the center of this field may either inhibit or excite the ganglion cell while its surrounding region behaves in the opposite way. Many ganglion cells with small receptive fields (*P-cells*) are usually chromatic sensitive and respond well to detailed contrasts on the retina, contributing to form vision. Others have larger receptive fields (*M-cells*) and highly respond to contrasts, serving to detect directional movement of objects across the retina. There are also small *bistratified cells* whose signal is entirely chromatic. Ganglion cells responses are then grouped in three classes, called *opponent-channels*, each represented by different combinations of cone signals.

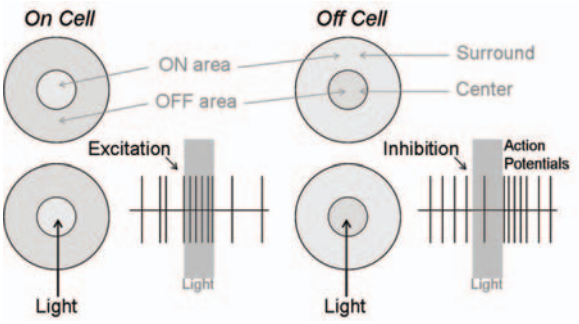

Figure 2.8: Schematic center-surround receptive fields of retinal ganglion cells.

Opponent channels In the retinal ganglion cells, three channels convey information from cones to the brain: a luminance channel, combining signals from L- and -cones (L + M); a channel subtracting L-cones to M-cones signals (L - M); a channel subtracting S-cones signals to the sum of L- and M-cones signals (S - (L + M)). Figures 2.9 and 2.10 illustrate the transformation from the cone signals into chromatic-opponent signals. These three channels are functionally independent and transmitted in anatomically distinct retino-geniculo-cortical pathways.

2.4 Chromatic and luminance pathways

2.4.1 Optic pathways

The optic pathways are composed into three steps: the first one origins at bipolar cells in the retina that transmit signals from cones and rods to ganglion cells. The second step represents ganglion cells whose axons form the *optic nerve* and project to the *lateral geniculate nucleus* (LGN) (See Section 2.4.2). Finally, a third step is constituted with LGN cells forming the *optic radiation* that project to the *striate area* of the visual cortex (See Section 2.5.4). Figure 2.11 illustrates in more details these optic pathways.

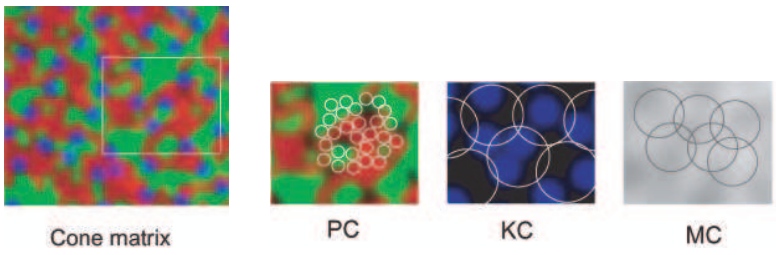

(*a*) (*b*)

Figure 2.9: Chromatic and spatial organization of subcortical pathways (from [Martin, 2004]). A patch of perifoveal cone mosaic based on data from [Roorda et al., 2001] is shown in (*a*). The sampling density of *ON-center* projecting cells (Parvocellular pathway (**PC**)) is shown in (*b*). Each white circle shows anatomical sampling aperture of one midget cell. Sampling density of *ON-center* cells relative to the Koniocellular pathway (**KC**) is shown by white circles and sampling density of *ON-center* cells from Magnocellular pathway (**MC**) is shown by grey circles.

2.4.2 The lateral geniculate nucleus (LGN)

The total number of cells in the LGN is about one million and corresponds to the number of optic nerve fibers. These optic nerve fibers usually terminate on 5 or 6 cells in diverse cellular layers. The LGN also receives fibers from the occipital cortex to assure the regulation of the afferences. The LGN is *topologically organized*, e.g. it is possible to predict where signals from the retina will be received in the LGN. Direct and crossed fibers of the optic tract join different layers of the thalamic LGN: four *parvocellular* layers, two *magnocellular* layers and thin intercalated layers named *koniocellular*, adjacent to the parvocellular layers. Functional properties of these different layers are described in the following Section.

Magno-, Parvo- and Koniocellular pathways

Figure 2.12 illustrates projections of these different pathways, from the retina to the LGN, and then projections to the different layers of primary cortex (or *striate area*).

Magnocellular layers First, cells in the magnocellular (M-) layers of the LGN receive input from retinal *M-cells* which in turn receive their signals from L- and M-cones, via diffuse bipolar cells [Derrington et al., 1984]. An ON-center receptive field of a ganglion cell will show +L+M in its center and -L-M in its surround. An OFF-center receptive field will receive inhibition in its center (-L-M) and excitation in its surround (+L+M). Geniculate M-cells have high contrast sensitivity for *luminance* stimuli [Shapley and Hawken, 1999]. The (M-)pathway seems to be the precursor of a system that establishes movement and depth as well.

Parvocellular layers The parvocellular (P-) pathway originates with L- and M-cones via midget bipolar cells providing input to retinal *P-cells* [Rodieck et al., 1993]. P-cells receive inhibitory inputs from M-cones in the whole receptive field and excitory inputs from L-cones in the center. The sign difference between these cones gives this neuron its chromatic-opponency. The parvocellular layers contribute about 80% of the total retinogeniculate projections. The (P-)pathway is thought to be the precursor of a system that establishes the surface properties and shapes of objects.

Koniocellular layers The Koniocellular (K-) pathway is the most recently discovered [Casagrande, 1994], and mainly carries signals from S-cones, via small retinal *bistratified cells*. These also receive input from diffuse bipolar cells forming S-(L+M) cells.

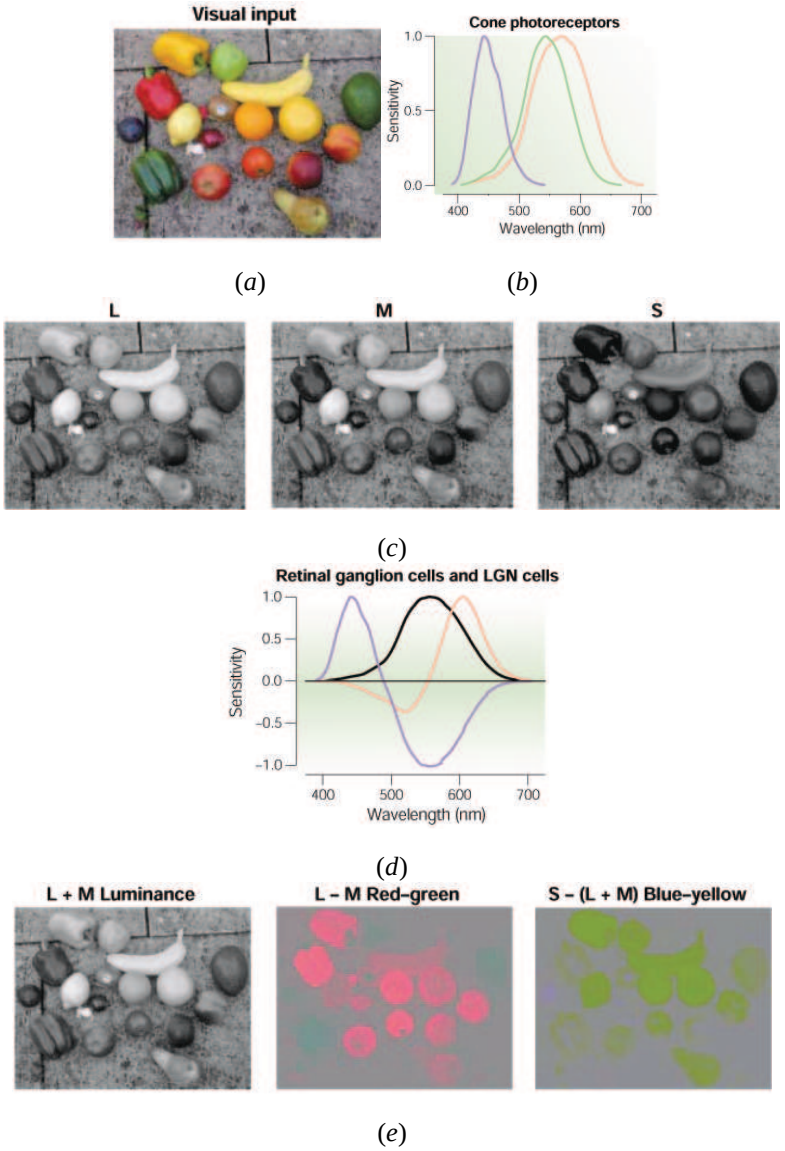

Figure 2.10: Early stages of color processing after [Gegenfurtner, 2003]. Color vision, for example, of the picture shown in (*a*), starts with the absorption of light by three types of cone photoreceptors (L, M, and S) in the eye (*b*). The three black and white pictures (*c*) show how the three cones are excited by the image (*a*). The L- and M-cone images are similar. The electrical signals generated by these photoreceptors go through complicated circuitry (*d*) that transforms the signals into three channels - one carrying luminance and the other two being chromatic-opponent (*e*). These chromatic-opponent signals are sent to the visual cortex by the way of the thalamic lateral geniculate nucleus (LGN).

To the cortex

Projections from the magno-, parvo- and koniocellular pathways terminate in different layers in the primary visual cortex (*striate area*) (See Section 2.5.4 and Figure 2.12). The magnocellular pathway mainly projects

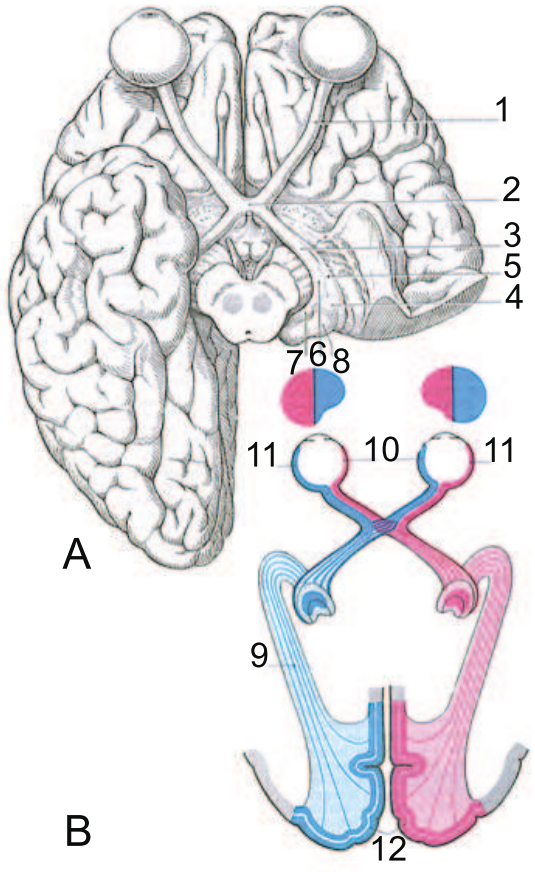

Figure 2.11: Optic pathways in the human brain (transverse section). Both optic nerves (**A1**) form the *optic chiasm* (**A2**). Optic nerves from nasal halves (**B10**) of the retina cross to the opposite side into the optic chiasm. Fibers from temporal halves of the retina (**B11**) stay at the same side. From there, fibers are named *optic tract* (**A3**) and split into two roots: the *lateral* (**A5**) and *median* (**A6**) roots. This is the lateral roots that reach the two *lateral geniculate nuclei (LGN)* (**A4**). *Optic radiation* (**B9**) originate from the LGN and finish to the *striate area* (**B12**). Thus, right hemisphere receives information from both left halves of the visual field and left hemisphere receives information from both right halves of the visual field.

to layer $4C_\alpha$ and layer 6. Parvocellular neurons project principally to $4C_\beta$ and layers $4A$ and 6. Koniocellular neurons terminate in blobs in layers 2 and 3, and in layer 1. The next Section 2.5 reviews principal chromatic properties of striate and extrastriate cortex, and investigates a possible independent color system throughout the visual cortex.

2.5 Cortical mechanisms of color vision

The visual cortex is situated in the *occipital lobe* (Figure 2.13). Signals from the LGN reach the *striate area*, or *primate visual area*. Then the signals carried by these pathways give rise to the *dorsal* and *ventral* functional streams described in extrastriate cortex.

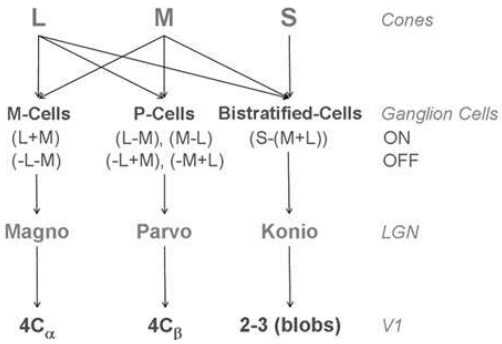

Figure 2.12: Principal retino-geniculo-cortical pathways involved in human color vision after [Knoblauch, 1999].

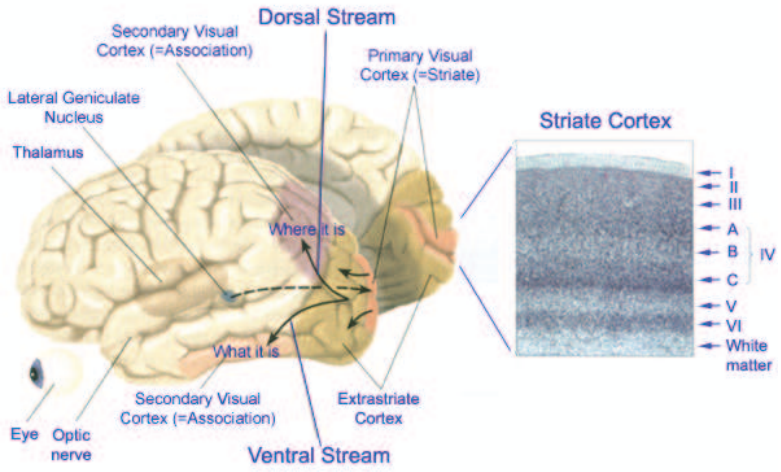

Figure 2.13: Schematic *dorsal* and *ventral* streams. Signals from the retina arrive to the LGN via the optic nerve. Fibers from the LGN reach the striate cortex (divided in different layers (right)) and then the extrastriate cortex. The (P-) pathway through the parvocellular division of the LGN drives the *ventral stream* in cortex (located in the temporal lobes and mainly involved in the 'what it is'), while the (M-) pathway through magnocellular LGN provides the major input to the *dorsal stream* in cortex (located in the parietal lobes and mainly involved in the 'where it is').

2.5.1 Connections in visual cortex

The visual information is immediately divided in the striate area (V1) into parallel streams[2]. Chromatic cells in blobs of V1 preferentially project to a particular area of V2 named the *thin stripe* area (See Section 2.5.4). These thin stripes contain cells that are involved in color processing and project to an area called V4, that

[2]There are many connections between the different visual areas in the brain. This section only focuses on few of them (mainly V1 to V4) and does not represent the high complexity of the visual system.

is also color specific. For example, if a damage occurs in this area, a patient will have difficulty to perceive color in the opposite visual field. Another pathway (motion specific) also projects from V1 to the *thick stripes* of V2, and then to areas named V3 and MT. An injury to this pathway will produce a specific motion deficit. For example, a patient would recognize cars in traffic but would be unable to see them moving.

Weights of projections

The extrastriate visual cortex is cytoarchitectonically quite homogeneous, thus the density of afferent axons entering any area is fairly uniform. Given this assumption and the sizes of the areas (receptive field size increases from V1 to V4), a fraction of V1 output can be estimated [Lennie, 1998]. By this criterion, V2 receives at most 89%, V3 receives at most 8%, and MT receives at most 1% of V1 output. The same analysis to the main outputs from V2 can be applied (V4, V3, V3A, MT) in proportion to their sizes. Then, V4 receives at most 53% of V2 output, V3 receives 32%, V3A receives 11%, and MT receives 4%. Finally, if the output from V3 is assigned to V4 and MT in proportion to their areas, V3A receives 22%, V4 receives 72%, and MT receives 6%. The underlying assumption is that visual information is more relevant to object analysis then to motion detection.

2.5.2 Visual responses of neurons

Neurons in V2, V3 and V4 (MT excepted) behave similarly as those of cells in V1. Figure 2.14 illustrates this problematic: either techniques used to characterize individual cells are not efficient enough, or they differ in a way that is not captured yet. However, in contrast to the single cell recordings, most of the

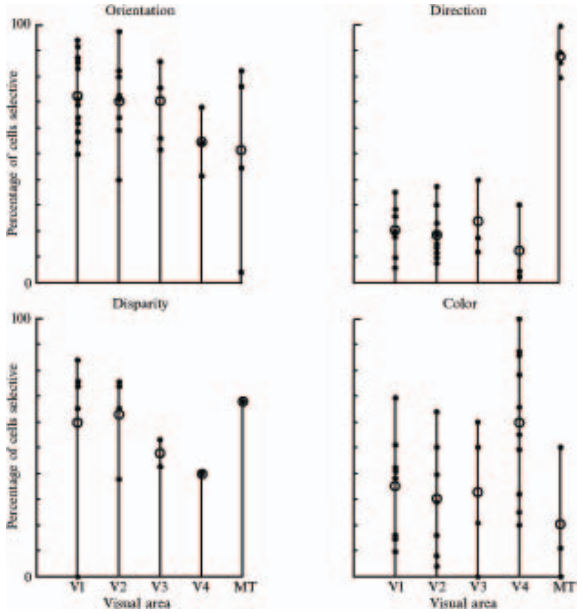

Figure 2.14: Proportions of neurons in visual areas V1, V2, V3, V4 and MT that respond selectively to orientation, direction of movement, binocular disparity, and color. Filled points represent a single study. Open circles show the unweighed averages. These values are taken from [Lennie, 1998] and are a mix of different studies (See references of these studies in [Lennie, 1998], p.899).

activity that is detected by functional Magnetic Resonance Imaging (fMRI)[3] of visual cortical areas V1 and V2 in humans is due to the activity of chromatic-opponent cells. Neurons responses to chromaticity are greater with fMRI than those based on single-cell recording in monkeys (however similar to those in humans), and the fMRI measurements are about 100 times less sensitive than the psychophysical measurements. Thus, the implication would be that there is a temporal filtering of the chromatic signal after the V1 region (Figure 2.15 illustrates spatial and temporal resolutions of these methods). This leads to the question whether a fMRI signal simply reflects the average activity of all neurons, and how specific is the response of an individual neuron to a particular stimulus. To reconcile the results from different techniques more formally, [Schluppeck and Engel, 2002] used electrophysiological data to predict the outcomes of neuroimaging experiments and found a convergence of fMRI and single-unit data to show that large numbers of chromatic-opponent neurons exist in V1 (See Section 2.5.4). An interesting hypothesis [Gegenfurtner, 1997] may be that the visual system wants to attach a chromaticity to each stimulus, independently of its other characteristics. So it would make sense for chromatic cells to respond in a less specific manner to these other features.

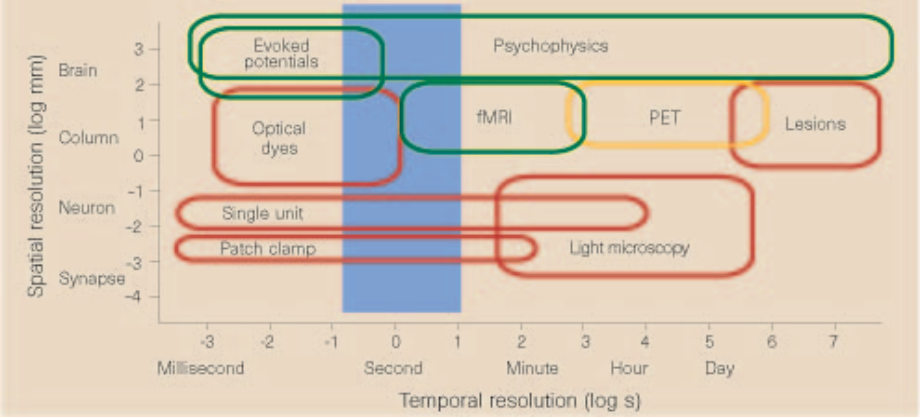

Figure 2.15: Spatial and temporal resolution of some techniques and experimental methods used to study sensory processing (From [Gegenfurtner, 1997]). Green boxes indicate non-invasive methods. Red boxes indicate invasive methods. Blue shaded area indicates a time slice of major interest, between 100ms and 10s. Studying the functional activity of the response across different visual areas (from neuron to brain and at diverse temporal and spatial resolutions), and correlating the signals to single-cell responses in these areas as well as to psychophysical responses is a challenging prospect.

2.5.3 Chromaticity-selective cortical cells

The type of chromaticity-selective neuronal responses in the following Section 2.5.4 is the one correlating with *ratios of cone excitations*. The early studies of primary visual cortex adopted a strict criterion. Cells responding only to luminance were classified as *luminance cells*. The few cells responding exclusively to chromatic stimuli were classified as *chromatic cells*. In this way, the proportion of chromatic cells was estimated to be less then 10% [Gegenfurtner, 2003]. However, the definition of chromatic cells that is most frequently adopted in the current literature lies in between the two. Cells that *add* L- and M-cone inputs are called luminance cells, and cells that *subtract* L-, M-, or S-cone inputs are called chromatic cells.

[3]Functional Magnetic Resonance Imaging is based on bloodoxygen- level- dependent (*BOLD*) changes in the magnetic resonance signal. The *bold* assumption is that the blood oxygen level is an indicator for local cortical activity.

With this definition, many luminance cells would also give differential responses to chromaticity, and many chromatic cells would respond to luminance. Thus, there might be a whole continuum of cells from strict chromatic-opponency to strict luminance.

2.5.4 Chromatic properties of V1 and V2 cells

Chromatic cells in V1

Many of the *luminance* cells in the V1 region have highly complex receptive-field properties. Their responses are determined by many conjoined properties of the stimulus, including orientation, spatial frequency, temporal frequency, direction and size. However, about a third of all neurons responds equally strongly to chromaticity and luminance, called *chromaticity + luminance* cells [Johnson et al., 2001]. This finding agrees with the fMRI results of Engel and colleagues showing equal sensitivity to luminance and chromatic contrast in human V1 [Engel et al., 1997]. Spatial properties of these cells seem to be quite different from those of cells which respond only to chromaticity, without any spatial structure. These cells show tuning to spatial frequency that was identical for luminance and chromatic stimuli. Because these neurons were also tuned for stimulus orientation, they are indeed suitable for extracting spatial features. Moreover, most of them have chromatic-opponent receptive field. Until now, most investigators assumed that double-opponent cells are non-oriented and not responsive to luminance. The luminance + chromaticity neurons respond both to chromaticity and to luminance, and they are orientation selective [Schluppeck and Engel, 2002]. An hypothesis might be that information about color and lightness is to extract visual form and to achieve a unitary and stable representation of the visual world [Gegenfurtner, 2001].

Chromatic cells in V2

V2 is at least as large as V1, and is a conduit of essentially all visual cortical information. Most neurons in V2 are orientation-selective but in many respects, the chromatic properties in V2 are very similar to those of V1. Like V1, about 50% of the cell population is selective to chromaticity (According to the Section 2.5.3 definition). Some neurons in V2 are tuned to certain chromatic directions with a narrow bandwidth (See Figure 2.16). Moreover, it has been recently found that V2 contains chromaticity-selective neurons organized into maps in which the chromaticity of a stimulus is represented by the location of the peak response to the stimulus [Xiao et al., 2003]. Thus, these chromatic-selective neurons are organized to form a systematic representation of chromatic space.

2.5.5 Neurons in V4

A first physiological exploration showed a high chromatic selectivity of cells in monkey V4 [Zeki, 1973], claiming to have found the *color center* in the cortex. Zeki [Zeki, 1983] described two populations of chromaticity-selective cells in this area: neurons responding to colored stimuli by the way of wavelength composition of the stimulus, and neurons responding to color appearance, as defined by the human observer. These *chromaticity-coded* cells were thought to provide the basis for *color constancy* (See definition in Section 2.6.4) and were reported absent in earlier stages of the visual pathways, including area V2 [Moutoussis and Zeki, 2002], which provides a major input to V4. However, significant numbers of opponent cells have been found in V1, chromatic-opponent to luminant and equiluminant stimuli [Lennie et al., 1990; Johnson et al., 2001] (See also Section 2.5.4). Moreover, many psychophysical experiments show that there is no single mechanism leading to color constancy, and that it depends on a number of computations, from retina to cortex (See Section 2.6.4). In addition, lesions in monkey V4 produced impairment in shape discrimination, object recognition, texture discrimination and disability of focusing attention (For a review, see [Gegenfurtner and Kiper, 2003]). Thus, the results suggest that the experience of color may depend on the activity of neurons in several cortical areas.

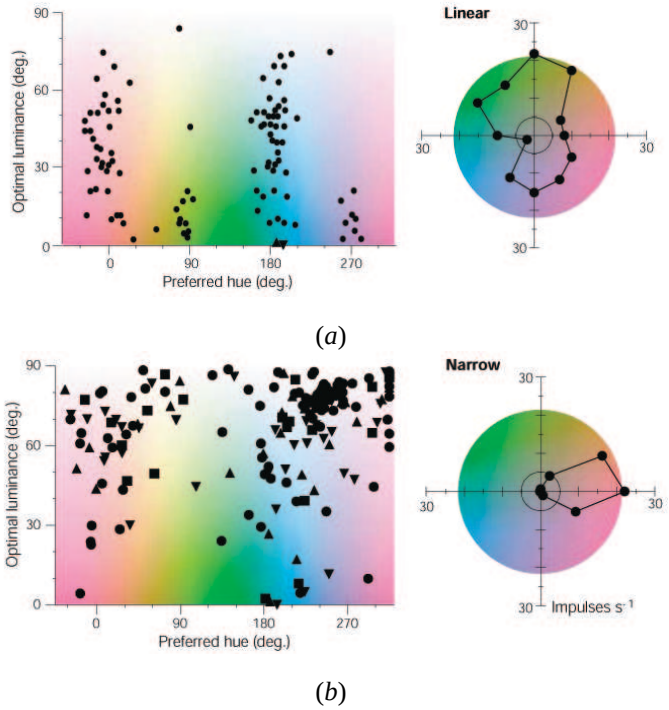

Figure 2.16: Color tuning in LGN and cortex (See review in [Gegenfurtner, 2003]). (*a*) Distribution of optimal chromatic directions for LGN cells [Derrington et al., 1984] and chromatic tuning of *linear* cells found in the LGN and in all areas of visual cortex [Kiper et al., 1997]. (*b*) Distribution of optimal chromatic directions for a sample of V2 cells (triangles and squares) and V3 cells (circles). The *x-axis* gives the cell's preferred hue and the *y-axis* the luminance required for the optimal stimulus. *Narrow* tuning of cell from V2. The magnitude of the response (in impulse per second) to different chromaticities is indicated by the distance from the origin.

To color appearance

Finally, color is a perception, rather than a physical property of a stimulus. When embedded in different surrounding stimuli, the same local pattern can lead to the perception of different colors: this is called *chromatic induction*. On the other hand, the same color pattern under different light sources can look the same (or be *metameric*) or be identified as being the same object (*color constancy*). For the moment, no physiological study has completely explained these phenomena. This leads us to consider theories of color appearance in Section 2.6.

2.6 Color appearance

2.6.1 First theories on color appearance

To the theory of trichromacy

According to *Young*, it is impossible to attribute an infinite number of receptors to the retina for an infinite number of particles [Young, 1802]. He concluded that there are three classes of receptors, with different spectral sensitivities, based on three principal colors. This is the *theory of trichromacy*. However, Young refers to hue sensations, and more recent physiological and psychophysical studies have shown that color

sensation does not occur in photoreceptors [Knoblauch and Shevell, 2001] (See also Section 2.3.2). This notion of mixtures is retained later by *Helmholtz* in 1852 and *Maxwell* in 1855: three classes of retinal receptors share equitably and symmetrically the spectrum [Helmholtz, 1867; Maxwell, 1855] while cone properties differ slightly from these statements (Section 2.3.2). However, Maxwell's experiments about mixtures of colors with spinning discs are the foundation of the modern *colorimetry*, the science to specify colors (See appendix *Colorimetry* for description).

To the theory of antagonistic colors

The physiologist *Hering* proposed an alternative theory to account for better perceptive aspects of colors [Hering, 1964]. He remarked that six hues (red, green, blue, yellow, white and black) can not be decomposed into finer hues. He also noted that some of these hues never appear together: a color can't be green and red, or yellow and blue. He suggested that there exist three channels coding colors in an *antagonistic* way. This model shows qualitative consistency with retinal ganglion center-surround receptive fields and opponent channels (See Section 2.3.2). Those two main theories evoke the retina as if it was alone capable of rendering color sensation. It has been shown in Section 2.5 that the cortex is highly involved in color perception. However, color sensation mechanisms, in which context plays an important role, are still not well understood.

2.6.2 Diverse color phenomena

This Section describes different color phenomena related to transparency perception. The link found with perceptual transparency is developed in Section 3.3.2.

The McCollough effect

The *McCollough effect* refers to the phenomenon that, after an exposure of a few minutes to gratings differing in both orientation and color, subjects perceive similar oriented achromatic gratings as if they were tinted with the complementary hues (See Figure 2.17).

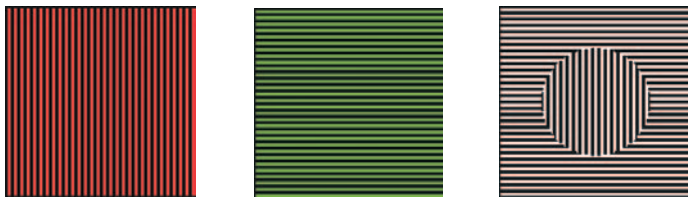

(*a*) (*b*) (*c*)

Figure 2.17: The McCollough effect. If one fixates the red (*a*) and green (*b*) patterns successively, over a few minutes one perceives complementary hues when fixating the white pattern (*c*).

Neon color spreading

The phenomenon of *neon color spreading* is an illusion that owes its name to the apparent diffusion of color (See Figure 2.18). A classic neon color spreading stimulus consists of an incomplete black pattern where the parts of the lines that are missing have been replaced by colored segments. Before the segments are put in the right places, the illusory figure looks white, compact, opaque and sharply outlined. Once the segments bridge the gaps, the illusory figure becomes colored, tenuous, transparent and fuzzy (See Figure 2.19). A recent study showed that the neon color generated around segments embedded in a lattice is an additive

mixture of the color of the segments and the color complementary to the lattice [Pos and Bressan, 2003]. The authors have found that the illusory color is significantly more saturated in the neon effect than without black patterns. They also showed that the external lines need to have a higher contrast than the segments in terms of luminance or hue saturation.

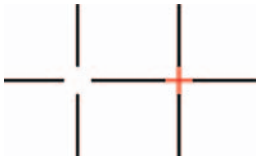

Figure 2.18: Neon color spreading effect: Ehrenstein's figure [Ehrenstein, 1941/1987]. Four black radial lines are separated by a central gap. A clearly delineated bright illusory disk is perceived, but if the inner endpoints of the lines are connected by a colored cross, the disk becomes translucent.

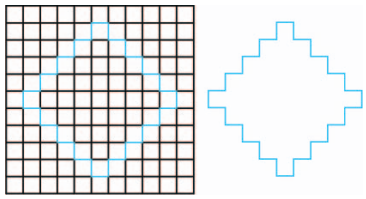

Figure 2.19: Neon color spreading as it was presented by [van Tuijl, 1975]. This configuration consists of a black and blue grid on a white background. Note that the blue color on the left and on the right is physically the same. However, the background close to the blue parts of the grid looks bluish. Moreover, the embedded part seems to be desaturated compared to the same part viewed in isolation, and that one has the impression of a transparent layer covering the region of the subjective color spread.

Watercolor phenomenon

The *watercolor effect* is perceived when a dark contour is flanked by a lighter chromatic contour [Pinna et al., 2001] (See Figure 2.20). Under these conditions, the lighter color will assimilate over the entire enclosed area. It has been shown that the spatial assimilation of the lighter chromatic contour is different from the neon spreading effect because of the figural effect and the spatial extent of the spreading. A possible function of this effect might be grouping parts together by their edge-induced color [Pinna et al., 2003].

2.6.3 Simultaneous color contrast

It has been seen in Section 2.1 (Figure 2.1) that a target's color appearance is influenced by the colors in its surrounding. This phenomenon is known as *chromatic induction* or *simultaneous color contrast* and is related to *color constancy* (See Section 2.6.4). Figure 2.21 illustrates this effect. Ekroll and colleagues presented evidence which strongly suggests that uniform surrounds evoke induction effects of a very peculiar nature, not representative of color induction effects in varied surrounds [Ekroll et al., 2004] (See Figure 2.22). Results from asymmetric color-matching experiments are quite different when simple versus

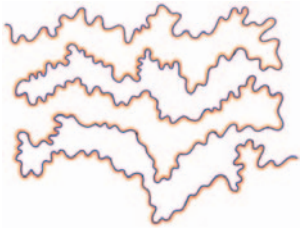

Figure 2.20: The watercolor effect as an example of surface color arising from its boundaries [Pinna et al., 2001]. This Figure shows a purple border delineating an enclosed white area. On the inside of the purple border runs an orange flanking line. However, an area needs to be flanked at least on two sides to produce such an effect.

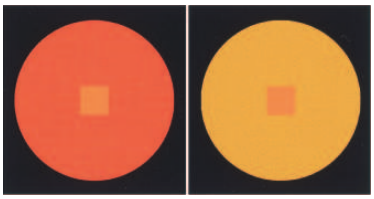

Figure 2.21: Examples of simultaneous color contrast [Ekroll et al., 2004]. The spectral characteristics of the square targets in the centers of the red and yellow circular surrounds are identical. The color elicited by the same targets on differently chromatic backgrounds are different.

complex surrounds are used. Another study shows that chromatic induction from a surround is attenuated by chromatic contrast *within* a remote region outside of the surround and reports that this attenuation depends on the magnitude, spatial frequency and chromaticity of remote chromatic contrast [C. S. Barnes and Shevell, 1999]. Lotto and colleagues have investigated the relationship between the reflectance of objects and their illumination to explain such phenomena [Lotto and Purves, 2000]. The color appearance of the target in a stimulus should change in a predictable manner as the spectral characteristics from the scene are manipulated so as to make the stimulus more or less consistent with different combinations of reflectances and illuminants (See Figure 2.23). The effect of contrast is high because each target seems to share the same reflective surfaces properties as its surrounding squares but under two different illuminants. However, this effect is low when the target shares the same reflective properties as its surround but under the same illumination. Thus, to the authors, what distinguishes constancy from contrast is simply the similarity or difference of the empirical significance of the targets in the stimulus, not their physical attributes. In another study, Brown and Macleod studied the effects on color perception of surrounds that had identical space-averaged means, but *different variances* [Brown and MacLeod, 1997]. They found that color appearance of their targets was dramatically affected by the variance of surround colors, even when the space-averaged light from the surround was constant. These results lead to theories on the *chromatic variability* and *contrast gain control* of the surrounds.

Chromatic variability

Information at the border is critical to determine the perceived color. However, more distant surfaces can also influence it [Lennie and D'Zmura, 1988]. One hypothesis is focused on the *amount of chromatic variability* in the scene (supported by many authors such as [Shevell and Wei, 1998]). More variability in the scene makes it less saturated and color induction weaker. Brenner and colleagues examined whether

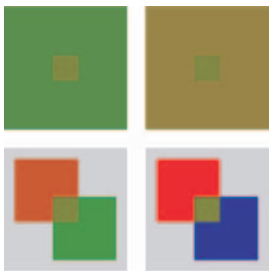

Figure 2.22: Top: Simultaneous color contrast, from [Ekroll et al., 2004]. The two central squares are physically identical, but since they are embedded in different surrounds, they appear rather different. **Bottom**: Another example of the influence of context on perceived color. Again, the central squares are physically equal. Beyond the difference in perceived color, a difference in the perceived opacity of the central squares is notable. In the left configuration one has the impression of seeing a red square behind a green transparent layer, or the converse. The color in the region of the central square appears to be split into two components, one belonging to a transparent layer, and the other to the background. In contrast, the central square in the right configuration appears opaque.

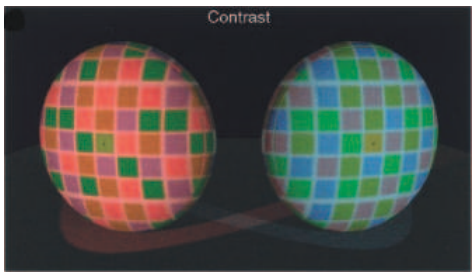

(*a*)

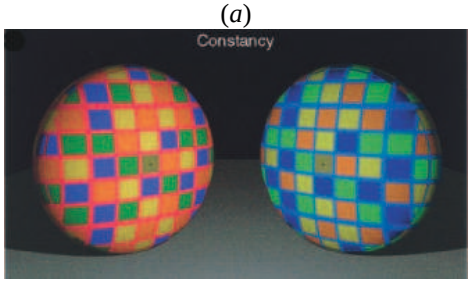

(*b*)

Figure 2.23: The similar empirical basis of color contrast (*a*) and constancy (*b*) (from [Lotto and Purves, 2000]). (*a*) Although the spectral information returns from the central squares (indicated by the black dots) are identical, they elicit different sensations of color because the stimuli increase the probability that the two originate from *differently reflective surfaces under different illuminants*. (*b*) When, however, the spectral information in the scene increases the probability that the returns from the targets originate from *similarly reflective surfaces under similar illumination*, the central squares (indicated by black dots) elicit relatively similar sensations of color.

the reduced chromatic induction in scenes with more chromatic variability depends on the layout of the colors within the scene [Brenner et al., 2003]. They created stimuli in which the chromatic variability was restricted to certain regions (See Figure 2.24). They found no significant result related to where the chromatic variability was located in the scene. The apparent color of the target seems to depend on the *average* chromatic variability of the whole scene. At the same time, Hurlbert and Wolf tested the hypothesis

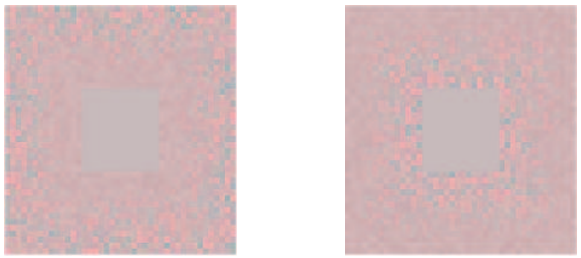

(*a*) (*b*)

Figure 2.24: Example of stimuli used by [Brenner et al., 2003]. Chromatic modulations where located either far (*a*) or close (*b*) to the grey target. No significant responses were found for each condition: the grey target looks the same.

that color contrast is weakened by differences between surfaces, which indicate that they may be under distinct illuminants [Hurlbert and Wolf, 2004]. They tested the effects of relative motion, relative depth and texture differences on simultaneous chromatic contrast. Of these factors, only *texture differences between surfaces* weaken chromatic contrast induction. These results support the chromatic variability theory. They also considered neurophysiological and neuropsychological evidence and concluded that the mechanisms of chromatic contrast effects are located at low levels in the visual system, in primary visual cortex (V1) or below, prior to image segmentation mechanisms which require computation of relative depth or motion. Earlier, Singer and D'Zmura studied the effect of remote chromatic contrast [Singer and D'Zmura, 1994, 1995; D'Zmura and Singer, 1996, 1999] on perceived chromatic contrast at a central position, similar to that reported by Chubb and colleagues for achromatic stimuli [Chubb et al., 1989] and to the contrast gain control developed by Heeger in physiological modeling [Heeger, 1992]. Their results showed that contrast induction is mediated by *binocular visual mechanisms* [Singer and D'Zmura, 1994]. Later, Shevell and Wei considered the locus of the neural mechanism mediating the attenuation caused by the remote chromatic contrast and found a central binocular system as well [Shevell and Wei, 2000]. There is no simple relationship between the color surrounding an object and its perceived color. In another study, Wachtler and colleagues separated non-local from local chromatic interactions and quantified their spatial and temporal properties, to better understand the role of these interactions in color perception [Wachtler et al., 2001]. Stimuli were composed of homogeneous square color fields on a homogeneous background. Chromatic changes were concentrated either on remote fields, either on the background, or on both. They found that remote inducers showed a significant inducing effect only when the color of the background changes. The authors interpreted this as rapid chromatic interactions that support robustness of color vision under changing viewing conditions. Another study has recently shown that when the saturation of a color decreases, its color does not become achromatic but tends toward the color of its surround [Ekroll et al., 2002]. The authors suggest that the center of the three-dimensional standard color space is not always achromatic. This last result has been interpreted as suggested that more than three dimensions are necessary to represent the perceived brightness and color of the illumination that is cast on a surface [MacLeod, 2003].

Color contrast to color adaptation

Recently, Long and Purves used natural scenes to show that color contrast, constancy, and assimilation are all predicted by the *statistical organization* of spectral returns from *natural visual environments* [Long and Purves, 2003]. A large number of natural image samples was collected by using criteria that copied the spatial complexity and contextual color of the standard color contrast, constancy, and assimilation stimuli illustrated in Figure 2.25. They found that as the spatial complexity of the sample increases, the observed

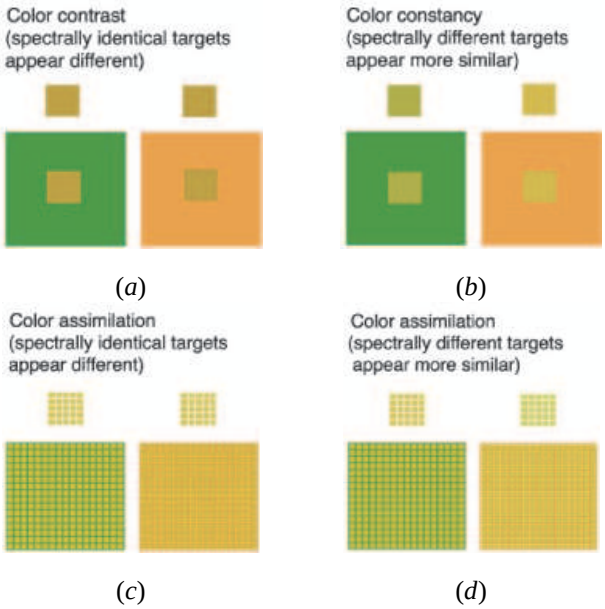

Figure 2.25: Color context effects (from [Long and Purves, 2003]). (*a*) Color contrast. The two spectrally identical central targets appear different when placed in different chromatic contexts. (*b*) Color constancy. Two spectrally different central targets appear more similar when embedded in different chromatic contexts. (*c*) Color assimilation (spectrally identical targets). Spectrally identical targets (the small squares) appear different in the context of the greenish lines on the left vs. the reddish lines on the right. (*d*) Color assimilation (spectrally different targets). Iteration of the stimulus elements can also make spectrally different targets appear more similar. Note that the contexts in *a* and *b* make the color appearance of the targets shift away from that of the contexts; the contexts in *c* and *d*, however, shift the color appearance of the targets toward that of the contexts.

color of the target tends to change from a value *opposite* that of the context to a value *similar* to that of the context. To the authors, when only one or a few target elements are identified in a spectrally homogeneous surround (as in a color contrast and constancy stimuli), the real-world sources of target and context tend to be physically different surfaces in the same illumination; on the other hand, when many target elements are found in a spectrally homogeneous surround, the sources of the target and context are likely to be physically similar surfaces.

2.6.4 Color constancy

A light which is reflected from an illuminated object depends on object surface and illuminant. The illuminant can vary hugely during a day, and these changes can have a considerable impact on the light reflected from an object (See example in Figure 2.26). The light that is reflected from an illuminated object depends

partly on the object's surface and partly on the illumination in the scene. Our visual system must compensate for these illuminant variations, in assigning constant colors to the objects [Lennie and D'Zmura, 1988; Bäuml, 1999b; Gegenfurtner, 1999]. This phenomenon is well known as *color constancy*. Sections 2.2

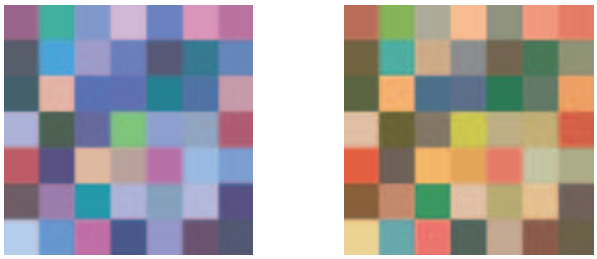

(*a*) (*b*)

Figure 2.26: Matching colored patterns under different lights (Figure from [Foster, 2003]). The patterns on the left and right consist of the same *Munsell* papers illuminated by blue sky (*a*) and the setting sun (*b*).

and 2.3.2 have shown that the perceived color of a surface depends on its spectral reflectance properties mediated by the three cone receptors of the eye (See also [Wandell, 1993, 1995; Kaiser and Boynton, 1996]). An interesting question [Knoblauch and Shevell, 2003] would be *how can color perception depend on the light absorbed by photoreceptors, and at the same time color constancy results in the stable color appearance of objects despite changes in the light stimulating these photoreceptors*? Color constancy depends on different spectral distributions of light from more than one region of the visual field: color constancy fails if there is only a single isolated surface. If a surface is uniform and presented in isolation in a dark field, it is impossible to tell whether its perceived color is due to its own reflecting properties or to the spectrum of the illuminating light: a blue paper under white light can look the same as a white paper in blue light. When several surfaces are present, the task becomes feasible.

Light source and reflected light changes

In order to understand the underlying mechanisms of color constancy, it is useful to consider the physical processes that produce changes in the illumination of a scene. One is a change in the spectrum of the light source that provides the scene illumination: a *light source change*. This change typically affects many object locations in a correlated way. The light incident on objects' surfaces can also change even if the light source is maintained fixed. For example, if the illumination has a certain direction, changing the position of an object can change its illumination. This effect is called *reflected light change*. It is important to distinguish between measurements of constancy with respect to various physical processes, since there is reason to suppose that different visual mechanisms may mediate constancy in the various cases [Delahunt and Brainard, 2004a].

Light source changes Light source changes have been extensively studied and it is now well known that the human visual system shows excellent constancy with respect to such changes, particularly when the stimuli are naturalistic. Recently, some studies have used more natural viewing conditions [Brainard, 1998; Delahunt and Brainard, 2004b] to model observers' responses that characterize the effect of the illuminant on color appearance. Relation to light changes and object position within a scene [Brainard et al., 1997; Bäuml, 1999b] and object pose [Boyaci et al., 2003, 2004; Ripamonti et al., 2004] have also recently been investigated and display constancy.

Reflected light changes Human vision can exhibit constancy with respect to a reflected light change. A study compared the appearance of a test region under two conditions [Bloj et al., 1999]: in the first, the perceived geometry supported the possibility that light from a nearby surface reflected onto the test; in the second, a *pseudoscope*[4] was used to alter the perceived geometry and eliminate the perceptual possibility that light reflected from the nearby surface onto the test, without otherwise changing the stimulus (See Figure 2.27). The color of the test region appeared different in the two conditions, in a manner indicating

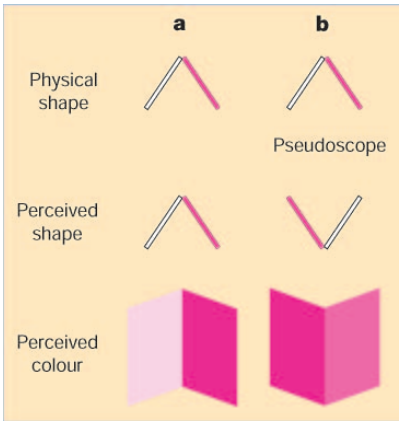

Figure 2.27: The experiment done by [Bloj et al., 1999] (Schema from [Gegenfurtner, 1999]). Observers viewed a folded card opening towards them. **a**: Under normal viewing, observers discount the effect of inter-reflections. **b**: When seen through a *pseudoscope*, the inter-reflections are interpreted as a change in surface color because they are incompatible with the percept of the bent-away card. The magnitude of the effect has been emphasized for clarity.

that the visual system discounted the reflected light in the first condition. The authors suggest that the human visual system incorporates knowledge of mutual illumination (the physics of light reflection between surfaces) at an early stage in color perception. Another study with three-dimensional scenes showed that the degree of constancy varied with the color direction of the illuminant change, and the variation was similar for reflected light and light source changes [Delahunt and Brainard, 2004a]. The overall level of constancy was lower for reflected light changes than for light source changes.

Influence of scene statistics

A recent study has shown that the human visual system may exploit a *higher order scene statistics* to estimate the illuminant, and gives it a weight that is statistically appropriate for the natural environment [Golz and MacLeod, 2002]. According to the grey world hypothesis, an average chromaticity of the image from the retina is proposed as used by the visual system to estimate the illumination. To the authors, this measure is not efficient: with this average, it is impossible to distinguish a reddish scene under a white illumination or a neutral scene under a red light. In their experiment, they analyzed images of natural scenes to find out how effective higher order statistics are as information about the chromaticity of surfaces and illuminants in the natural environment. They generated stimuli in which various statistics varied independently (means, variances, correlations) of the distribution of color and lightness. They found that only the luminance-redness correlation was useful to estimate the illumination color. Thus, reddish scenes but not reddish illuminants generate images with negative luminance-redness correlations. To the authors, an observer can

[4] A *pseudoscope* is a binocular viewing stand fitted with prisms that invert the image in each eye from left to right, thereby reversing binocular stereo disparities and thus, the depths at which objects appear the image.

estimate two unknowns by evaluating both mean and correlation: the predominant color of the scene (in this experiment, the degree of redness), and the redness of the light source that illuminates the scene. In this way, the ambiguity when considering mean chromaticity alone can be resolved. However, Ciurea and Funt used their findings in a color constancy algorithm and showed that the assumptions of Golz and MacLeod did not hold true for a larger image set [Ciurea and Funt, 2004].

Simultaneous and successive color constancy

The visual system has also to manage quite different situations: one type is often referred to as *successive color constancy*, a scene is uniformly illuminated by a light source, and illuminant changes are gradual over time and space. In the other type of situation, multiple light sources are present within the image, and the illuminant variation is abrupt (for example, one part of a scene under the sunlight and the other part cast in shadow). This situation is often referred to as *simultaneous color constancy*. A well-known task to measure perceived surface under different lights is the *asymmetric color matching* task. The scenes usually comprise multiple reflecting surfaces which are presented simultaneously, side by side, or sequentially.

Simultaneous color constancy Asymmetric matching provides a convenient and natural experimental method for studying simultaneous color constancy. Bäuml presented to subjects two identical *Mondrians*, in which one of them was rendered under the standard illuminant and the other was rendered under one of four test illuminants [Bäuml, 1999b,a]. He found that in simultaneous color constancy, image surfaces do not have a major impact on the illuminant adjustment. This provides support for a hypothesis that color appearance and surface color differ quantitatively and not qualitatively.

Successive color constancy Fast illuminant changes can improve estimates of color constancy in the unadapted eye. To test it, Foster and colleagues made surface-color matches across two *Mondrian* patterns (colored rectangular fields) illuminated by different daylights [Foster et al., 2001]. The patterns were presented either in the same position in an alternating sequence or, as a control, simultaneously side-by-side. They found that color constancy is significantly higher with *sequential* stimulus presentation than with simultaneous presentation; this suggests that the visual system has mechanisms which are probably derived from a low-level signal based on spatial ratios of cone excitations. Such signals, which do not require adaptation to the illuminated scene nor knowledge of the illuminant could be generated early in the visual pathway. Rinner and Gegenfurtner determined the temporal characteristics of chromatic adaptation for appearance and discrimination along different color directions [Rinner and Gegenfurtner, 2000]. Their subjects were adapted to a large uniform background illuminated by lamps. In changing the background color along a red-green or blue-yellow color axis, they identified several components of adaptation by their temporal characteristics. They found that color appearance, and thus color constancy, is strongly influenced by an extremely fast mechanism (10ms). To them, this instantaneous process would be situated at a later processing stage, due to cortical computations. Nieves and colleagues have also used the asymmetric color-matching experiment to investigate the role of opponent mechanisms in successive color constancy [Nieves et al., 2000]. They found that L- and M-cones tend to adapt so as to support color constancy, whereas S-cones are strongly influenced by the illuminant changes.

Color constancy in context

Recently, Smithson and Zaidi tested color constancy under a change in illuminant from sunlight to skylight [Smithson and Zaidi, 2004]. They used a square test patch on a varied background of randomly oriented elliptical patches (See Figure 2.28). Under prolonged adaptation to each illuminant, observers demonstrated a high degree of appearance-based color constancy. In a second experiment, they used two illuminants (sunlight and skylight) and two biased sets of reflectances for the background (red-blue biased, and green-yellow biased). Their results showed only a small effect of the chromatic bias of the background on color constancy. These data confirm that the color appearance of the test-materials is not set by the mean

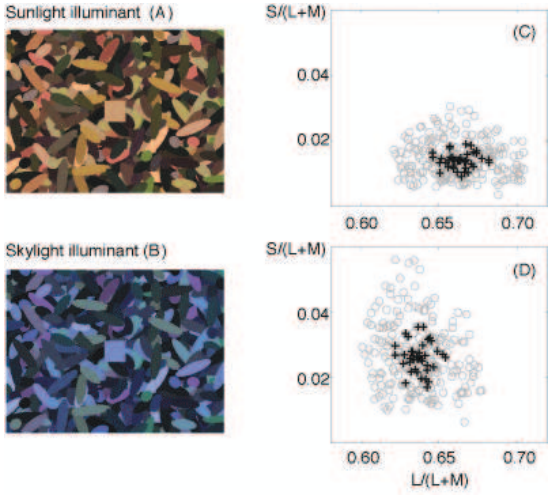

Figure 2.28: (A, B): Example of stimuli used in [Smithson and Zaidi, 2004] (First experiment). On each trial, a square test patch was presented on a varied background of randomly oriented elliptical patches. (C, D): the MacLeod-Boynton chromaticity coordinates of the stimuli, rendered under sunlight (C) and skylight (D). Open circles show the complete set of 280 test-materials. The materials indicated with black plus-symbols were used to generate chromatically *balanced* backgrounds.

chromaticity of the global scene, as suggested by studies such as [Golz and MacLeod, 2002]. In two last experiments, they showed the same stimuli as in their first experiment, but with conflicting backgrounds (where sunlight square test was set on skylight background, and skylight square test was laid on a sunlight background). Observers continued to demonstrate reasonable color constancy. They then reduced the duration of exposure to the test compared to exposure to the background. The results suggest that mechanisms that preserve information across *successive* test-presentations are key determinants of the stability of color appearance, and that observers' judgements are consistent with the hypothesis that the test-materials have a different illuminant from the background.

2.7 Summary

Two main approaches were presented in this Chapter to understand color vision, such as neurophysiological and psychophysical studies. The first part described how light is absorbed by the retina and how it is processed in the cortex (Sections 2.2 to 2.5). These Sections underline the fact that color perception and neural correlates are not evident to bind. Moreover, we perceive color in a context, and different color phenomena result from it. The second part enumerated some of these color phenomena occurring in the world, and related studies trying to characterize their properties via psychophysical experiments (Section 2.6). However, more studies are needed to understand them. A similar phenomenon is transparency perception. Each of the listed color phenomena, such as McCollough effect, neon color spreading, watercolor phenomenon, simultaneous color contrast and color constancy have a corresponding effect on transparency perception (See **Chapter 3**, Section 3.3.2). This effect may help for a better appreciation of the underlying mechanisms of color appearance. This knowledge is thus helpful to understand the following **Chapter 3**, devoted to the perception of transparency.

Chapter 3

Transparency Perception

3.1 Introduction

Transparency perception investigation has a long history. When we look at something through a transparent filter, the colors of the surfaces under the filter might appear different from colors of surfaces seen in plain view, depending on the physical properties of this object. Section 3.2 defines physical transparency models, based on subtractive and additive mixtures properties. However, physical characteristics are not a sufficient condition for transparency perception. Thus, Section 3.3 reviews the main studies and models on perceptual transparency, defining conditions where this phenomenon occurs. These conditions are configural and are related to different color phenomena. Luminance plays an important role in transparency perception and many perceptual models result from it, as well as from chromatic properties. Many of these models can be generalized into the *General Convergence Model*, described in Section 3.4. A series of stimuli has been generated to test it and its relation to color constancy is shown.

3.2 Physical transparency

This section describes physical models of transparency, derived from additive and subtractive color mixtures. These models are *physical* because they only take into account the relationship between physical properties of light and a filter (See Section 3.2.1) or of an *episcotister* (See Section 3.2.2).

3.2.1 Subtractive Model: the Filter Model

It was shown in Section 2.2 that light can be reflected by surfaces. However, some objects do not only reflect light but absorb and transmit it. These objects are called *absorption filters*, and a physical filter model can be formulated [Wyszecki and Stiles, 1982; Nakauchi et al., 1999; Faul and Ekroll, 2002]. The radiant energy $E_i(\lambda)$ incident on the first surface of the filter propagates through the filter and emerges from the second surface as energy $E_t(\lambda)$ (See schema in Figure 3.1). Portions of the radiant flux arriving at the first and second surfaces are lost by reflection of energy $E_r(\lambda)$, whereas the remaining portions are transmitted but reduced because of absorption within the filter. It is possible to formulate an homogeneous absorption filter by *Bouguer's law*

$$\theta(\lambda) = 10^{-dm(\lambda)} \tag{3.1}$$

where d is the path length of the radiant flux in the filter and $m(\lambda)$ the spectral absorption. At normal incidence, d is equal to the thickness of the filter. The quantity $\theta(\lambda)$ is named the internal spectral transmittance of the filter and is defined as the ratio of the radiant flux reaching the back surface of the filter to the flux that enters the filter at its front surface. Now that the inner reflections of the filter is taken into account, the

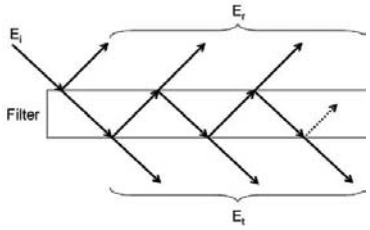

Figure 3.1: Pattern of *internal* reflections and transmissions of a filter medium.

filter transmittance $t(\lambda)$ is given by

$$t(\lambda) = \frac{(1-k)^2\theta(\lambda)}{1-k^2\theta^2(\lambda)} \tag{3.2}$$

where k is the proportion of light reflected by the filter[1]. Similarly, the *filter reflectance* $r(\lambda)$, i.e. the relative amount of incident light of wavelength λ that is eventually reflected from the filter surface, is given by

$$r(\lambda) = k + \frac{k(1-k)^2\theta^2(\lambda)}{1-k^2\theta^2(\lambda)} \tag{3.3}$$

Note that if $n = 1$ and so $k = 0$, then the total transmittance $t(\lambda)$ is equal to the inner transmittance $\theta(\lambda)$ and the total reflection $r(\lambda)$ vanishes. An opaque surface under the filter makes the transmitted light $t(\lambda)$ incident on it and reflected back to the bottom of the filter surface, resulting in a new incident light at the bottom of the filter (See Figure 3.1). The *virtual reflectance* $s(\lambda)$ of the surface covered by the filter can thus be denoted by

$$s(\lambda) = \frac{t^2(\lambda)\upsilon(\lambda)}{1-r(\lambda)\upsilon(\lambda)} + r(\lambda) \tag{3.4}$$

with $\upsilon(\lambda)$ the assumed opaque surface reflectance.

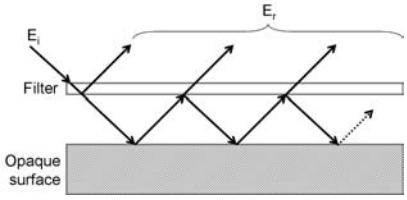

Figure 3.2: Pattern of *external* reflections and transmissions of a filter medium.

3.2.2 Additive Model: the Episcotister Model

Metelli formulated his model of achromatic transparency based on the experimental context of an *episcotister* (a rotating disk with open sectors, see Section 3.3) based on Talbot's law of color fusion[2] [Wyszecki

[1]When a filter has a refractive index (n) different from that of air ($n_{air} \approx 1$), each time the light crosses the filter boundary, the incident light k does not pass the boundary but is reflected. If we assume a normal angle of incidence and an unpolarized light, then $k = (n-1)^2/(n+1)^2$.

[2]Talbot's law states that the brightness of an object examined through a slatted disc, rotating above a critical frequency, is proportional to the angular aperture divided by the opaque sectors.

and Stiles, 1982; Metelli, 1974]. Nakauchi and colleagues extended it to the chromatic case with functions of wavelength [Nakauchi et al., 1999]: the virtual reflectance $s(\lambda)$ is then described as

$$s(\lambda) = \alpha v(\lambda) + (1 - \alpha) f(\lambda) \tag{3.5}$$

with α the degree of transparency (corresponding to the thickness d of the filter compared to a subtractive model) and $f(\lambda)$ the filter reflectance for additive color mixture, corresponding to $r(\lambda)$ and $t(\lambda)$ for subtractive color mixture.

To perceptual transparency

However, systems that are physically transparent may not give rise to perceptual transparency. For example, take a square of colored transparent plastic glued on a uniform cardboard [Metelli, 1974]. The plastic is no longer seen as transparent, it appears to be opaque. Moreover, systems that are not physically transparent may give the perception of transparency. For example, Figure 3.3 contains four opaque surfaces assembled to give the perception of two opaque large rectangles seen behind a transparent filter (two small rectangles). Therefore, physical transparency is neither a necessary nor a sufficient condition for the perception of

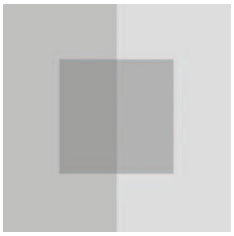

Figure 3.3: Schema illustrating perceptual transparency.

transparency [Metelli, 1974]. The following Section 3.3 introduces perceptual theories of this phenomenon.

3.3 Perceptual transparency

The first studies on perceptual transparency were *qualitative* [Helmholtz, 1867; Koffka, 1935; Hering, 1964], and related to physically transparent systems. Helmholtz described the perception of transparency as *seeing through*; Koffka stated that it is possible to perceive both the color of the filter and of the opaque surface under it. On the other hand, Hering stated that the light reflected by filter and surface under leads to the perception of only one color: the *color fusion*. The first quantitative model was Metelli's *episcotister* model (See Subsection 3.2.2) [Metelli, 1974]. However, chromatic constraints are necessary but not sufficient conditions to perceive transparency. Configuration laws must also be respected and are discussed in Section 3.3.1.

3.3.1 Figural constraints

Transparency depends on form as well on color [Metelli, 1974]. According to Metelli, three conditions are needed to perceive transparency with overlapping surfaces: the *uniformity* of the transparent layer and an *adequate stratification*. To both Metelli and Kanizsa [Kanizsa, 1979], the *continuity* of its boundaries is necessary as well (Figure 3.4). Later, Singh and Hoffman considered the case of discontinuity of the filter [Singh and Hoffman, 1998]. They refined the Gestalt figural conditions in using the *genericity principle*[3]

[3]The genericity principle says to reject *unstable* interpretations of visual stimuli. An unstable interpretation is one which would lead to a qualitative change (e.g., a topological change) in the image

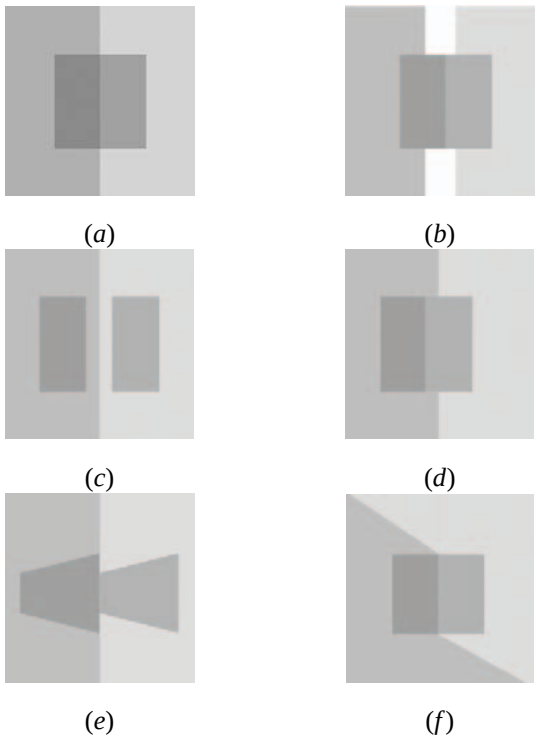

Figure 3.4: Figural constraints for perceptual transparency. (*a*) Adequate configuration to see transparency. (*b*) *Stratification* of surfaces: the underlying surfaces must meet under the small rectangles region. (*c*, d) *Uniformity* of the transparent layer and the *continuity* of its boundaries: The two gray regions that form the transparent surface must be in contact with each other, and each must make contact with only one of the two background regions. (*e*, f) Kanizsa gave Figure (*e*) as an example where transparency is blocked (discontinuity of the contour of filter) [Kanizsa, 1979], and Figure (*f*) as an example where transparency is not blocked (discontinuity in the direction of the line dividing the background).

and the *minima rule*[4]. They set two experiments, each following one of these conditions (See Figure 3.5). Their experimental results showed an effect of each of these rules, and then suggest that the formation of visual objects and their parts can precede the representation of transparency.

The role of X-junctions

Other recent studies have proposed some general constraints for the perception of transparency. For example, the presence of *X-junctions* formed by the junction of borders of surfaces and filter at the overlapping region is a necessary element of the image [Metelli, 1974; Kanizsa, 1979; Beck et al., 1984; Adelson and Anandan, 1990; Adelson, 1993]. Then, a minimum of three or four areas is required to form an X-junction [Masin, 1984] (See Figure 3.6). Watanabe and Cavanagh also demonstrated a special case where *T-junctions* (usually known to indicate occlusion by an opaque surface) can support the perception of transparent surfaces [Watanabe and Cavanagh, 1993b]. In this case, the T-junction is perceived as having an

[4]The human vision represents the shapes of objects in terms of component parts, and the spatial relationships between these parts. The *minima rules* defines part boundaries and is expressed solely in the language of differential geometry. For more explanations, see [Singh and Hoffman, 1998]

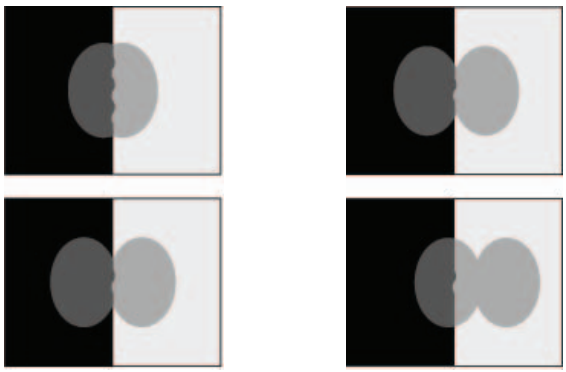

(*a*) (*b*)

Figure 3.5: Example of stimuli used in Experiment 1 (*a*) and in Experiment 2 (*b*) of [Singh and Hoffman, 1998]. (*a*) These figures aim to investigate the role of genericity in the perception of transparency. (*b*) These figures were used to investigate the role of minima rule in the perception of transparency.

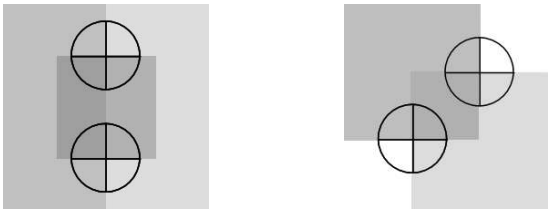

(*a*) (*b*)

Figure 3.6: Example of X-junction with four (*a*) and three areas (*b*).

additional contour that renders it as an *implicit* X-junction. They also suggest that is the same processing for X-junctions and implicit X-junctions to help forming transparent surfaces. Authors like Adelson and Anderson have added luminance rules to these figural constraints [Adelson, 1993; Anderson, 1997] (See Section 3.3.2). In addition, other studies have shown that the perception of transparent surfaces interacts with subjective contours, neon color spreading and stereo depth (See Section 3.3.2).

3.3.2 Relation to depth, neon color spreading and other visual phenomena

To Nakayama and colleagues, the perception of transparency is highly correlated to the perception of *depth*, to the *neon color spreading* and to *subjective contours* [Nakayama et al., 1990].

Relation to depth

The perception of transparency in binocular vision presents a challenge for any model of stereopsis [Wallace and Mamassian, 2004]. For example, Howard and Duke have found an effect that depends on transparency rather than occlusion: monocular zones[5] adjacent to depth steps can create an impression of depth in the absence of binocular disparity [Howard and Duke, 2003]. They showed that the magnitude of depth created by

[5]A monocular zone is a region where a faraway surface is only visible to one eye and lies next to a vertical edge of an opaque object seen by both eyes. A region visible only to the left eye is a *left eye monocular zone* and a region visible only to the right eye is a *right eye monocular zone*.

monocular occlusion fell short of that created by monocular transparency (See Figure 3.7 for explanations).

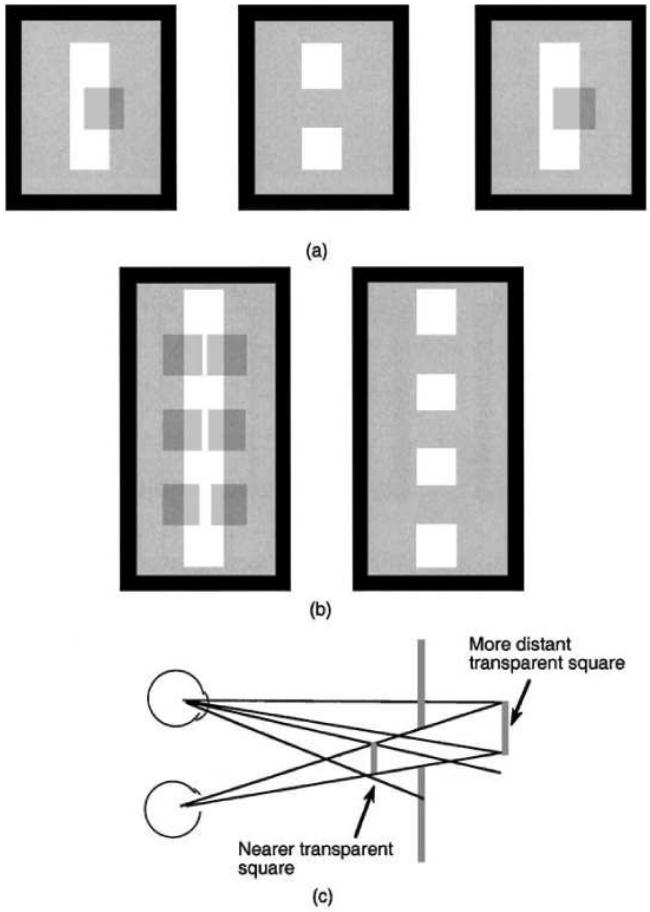

Figure 3.7: Schema of stereogram used in [Howard and Duke, 2003]. (*a*) Crossed or uncrossed fusion creates an impression of a square beyond a transparent surface in one fused image and of a transparent square in front of a surface in the other fused image. (*b*) Fusion creates a set of squares beyond a transparent surface and set of transparent squares in front of a surface. In both cases, the magnitude of depth increases with the extent of displacement of the square relative to the vertical bar in the image of one eye. (*c*) The physical arrangement that would create these depth effects. To the author, these effects do not arise from monocular occlusion because nothing is occluded. They arise because one eye's image contains information that either the square or the surface is transparent.

Relation to the McCollough effect

Other studies also investigated relationships between transparency and different visual phenomena. It has been shown that the orientation-contingent color aftereffect, or *McCollough effect* (See definition in Section 2.6.2) can be mediated by the subjective spatial organization that accompanies the perception of transparency [Watanabe et al., 1992; Watanabe and Cavanagh, 1993a]. Horizontal and vertical bars were com-

bined in three different ways: one condition where bars were overlapped with a luminance combination to give rise to the perception of transparent overlays; one condition where bars overlapped in a way where transparency was not perceived; one last condition when bars did not overlapp. The McCollough effect seen in standard condition is stronger than in any other condition, but they still found that this effect interacted with the valid transparent condition opposite to the invalid transparent condition. To the authors, this effect can be mediated by the subjective spatial organization (representation of vertical and horizontal bars) that accompanies the perception of transparency in their stimulus.

Relation to neon color spreading

Some studies have shown that with the perception of transparency, neon color spreading becomes apparent and depth changes and robust subjective contours can be abolished [Nakayama et al., 1990; Watanabe and Cavanagh, 1992; Ekroll and Faul, 2002]. For example, Nakayama and colleagues found that the perception of transparency always occurs whenever color spreading occurs but the opposite is not true [Nakayama et al., 1990] (See definition in Section 2.6.2). Transparency can occur without neon color spreading. Thus, transparency perception is a necessary condition for the emergence of neon color spreading, but not vice versa. A more recent study investigated the color conditions for the perception of transparency in such neon spreading displays [Ekroll and Faul, 2002]. The authors adapted an existing model of balanced perceptual transparency, which was originally formulated for patterns consisting of four color regions, to configurations in which *only three differently colored regions* could be identified (See Figure 3.8). The predictions of the model concerning the color conditions for perceptual transparency in such configurations were tested in two experiments using dynamic neon color spreading displays. They found that the data are very well accounted by an additive model correctly predicting optimal impressions of transparency. Color combinations deviating slightly from the additive model also looked transparent, but less convincingly so.

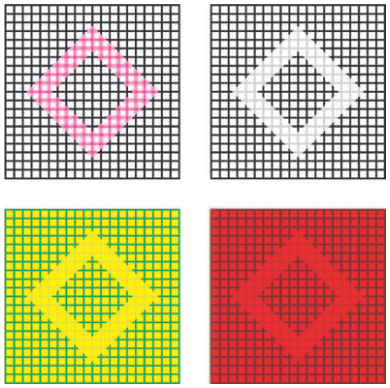

Figure 3.8: Neon color spreading and perceptual transparency. Four neon color spreading stimuli used in [Ekroll and Faul, 2002]. The luminance of the inner elements was intermediate between the two other luminances in the display. The upper left configuration has a combination of colors that is often used for demonstrations of the neon color spreading effect. This color combination does not fit the strict additive model. Still, the impression of transparency is still perceived. However, the impression is rather vague. The other three color combinations fit the strict additive model as far as reproduction allows it. In these configurations the impression of transparency is more convincing and balanced.

Flank transparency

Other studies have found relationships with perceptual transparency and watercolor [Wollschlager et al., 2001, 2002] (See also Section 2.6.2 for a definition). The authors defined *flank transparency* as the perception of a colored transparent filter evoked by apparent-motion or static displays containing as few as two colors. Displays of flank transparency contain a random array of line segments placed on a uniform background and small flanks are added to the line segments (See an example in Figure 3.9). This leads to the perception of a colored transparent pattern with well-defined boundaries moving or not over the array of lines. According to them, current models of perceptual transparency do not account for flank transparency as they require displays containing at least three different colors [Wollschlager et al., 2001]. They also analyzed the properties of a dynamic color-spreading display created by adding narrow colored flanks to rigidly moving black lines. They performed three experiments to study influence of apparent motion, the degrading effect of gaps between lines and flanks and the spatial extent of the color spreading [Wollschlager et al., 2002].

Figure 3.9: Static flank transparency [Wollschlager et al., 2001]. Displays are made of a random array of line segments where small flanks are added.

Relation to luminance contrast

Robilotto and colleagues compared characteristics of perceived transparency versus perceived contrast to determine mechanisms of perceptual transparency [Robilotto et al., 2002]. They simulated pairs of physically different neutral density filters and asked observers to match their perceived transparency. Subjects had to adjust either *reflectivity* of the filter, either its *inner transmittance*, previously determined by physical models (See Section 3.2 for physical transparency properties). Their results showed that observers can make reliable matches through a linear trade-off of these two properties. Similar results with opaque patches (containing the same physical values except that filters' X-junctions were replaced by T-junctions) also suggested that perceived image contrast is the sensory determinant of perceived transparency. In a second experiment, Robilotto and Zaidi examined how contrast in luminance affects the perception of transparency [Robilotto and Zaidi, 2004]. The same pairs of physically density filters as in [Robilotto et al., 2002] were matched by the observers. These filters laid on different backgrounds in luminance and contrast (Figure 3.10). They found identical observers' linear trade-off between reflectivity and inner transmittance of the filters as in [Robilotto et al., 2002]. Reducing luminance or contrast of the background decreased perceived transparency of the overlaying filter. Finally, in a second experiment, observers' also equated perceived contrast with opaque disks (filters with T-junctions abolishing the transparency perception) as they did with filters, showing that perceived transparency corresponds closely to the perceived contrast of the overlaid regions.

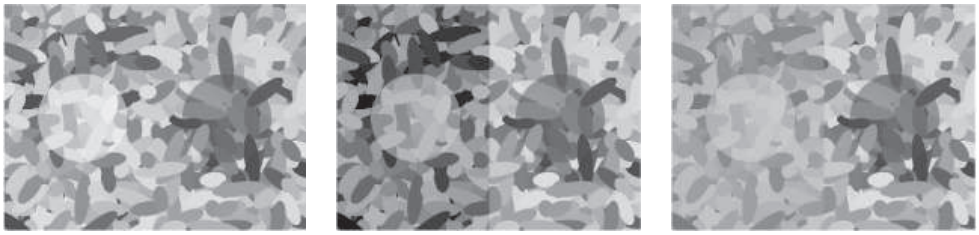

(*a*) (*b*) (*c*)

Figure 3.10: Examples of stimuli used in [Robilotto and Zaidi, 2004]. The left side of each display contained the standard filter specified by fixed β and θ values. The right side of each display contained the matched filter, which had one of its properties fixed while the other was adjusted by the observer. The standard was presented over one of three background conditions, *uniform* background (*a*), *lower luminance* background (*b*), or *lower contrast* background (*c*). Notice the X-junctions around the edges of the filters leading to transparency cues.

Relation to color constancy

Perceptual scission and junctions Khang and Zaidi examined the effects of perceptual scission[6], image junctions, color adaptation, and color correlations on identification [Khang and Zaidi, 2002b]. They used simulations of natural illuminants, materials, and filters in a forced-choice procedure to simultaneously measure thresholds for identifying filters and objects across illuminants, and discrimination thresholds within illuminants. Their stimuli were similar to those of [Smithson and Zaidi, 2004] (See Section 2.6.4 **Color constancy in context**), except that test patches were either colored filters or opaque patches (that were in fact filtered regions rotated at $180°$, which destroyed figural unity) (See Figure 3.11). Observers had to

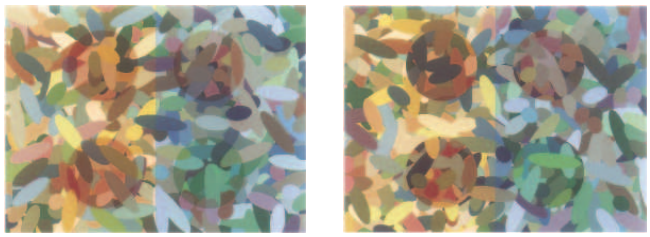

(*a*) (*b*)

Figure 3.11: Stimulus configurations used in the experiments of [Khang and Zaidi, 2002b]. (*a*) Two red filters under direct sunlight (left) and one red filter under zenith skylight (top right), and green test filter (bottom right). (*b*) Filtered regions were rotated $180°$, which destroyed figural unity and color relations between filtered and unfiltered parts of materials on the boundary (same filters as above).

identify the color of the filters or of the opaque regions. The local color relations across the borders of the filters did not play a role in identification performance. In the vast majority of the cases, they could discriminate within illuminants as well as they could identify across illuminants. They showed that geometrical and color scission can enable an observer to identify similar overlays across different illuminants on the basis of

[6]When surfaces are overlaid by a transparent filter, *color scission* refers to the perceptual separation of the colors of the image into the colors of the underlying surface and the color of the overlaying layer.

spectral properties. Since results were similar for identical color distributions, whether transparency cues like X-junctions were present or not, the primary cues for color identification were assumed to be systematic color shifts across illuminants. They conclude that the accuracy of inferred color constancy for ensembles of objects requires color scission between material reflectances and illuminant spectra.

Restricted conditions The authors have also found that transparent layer constancy exists only under restricted conditions [Khang and Zaidi, 2002a]. In their experiments, filters were placed on various sets of chromatic materials and match filters on achromatic materials. In the majority of cases, filter matching was close to veridical. However, filter matching was not possible in cases where the transmittance of the filter was highly dissimilar in shape to the reflectance of the background materials. They thus suggest that the accuracy of color scission in the perception of transparency depends on the color composition of background materials.

Filtered spotlights In a recent study, the authors have also measured illuminant color estimation by human observers for moving, spectrally filtered spotlights [Khang and Zaidi, 2004] (See Figure 3.12). Their

(*a*) (*b*) (*c*)

Figure 3.12: Stimuli used in the experiments of [Khang and Zaidi, 2004]. (*a*) Experiment 1: Red spotlight cast on green-yellow materials (left) and the same red spotlight on gray materials (right). Observers were asked to estimate the color of the spotlight on chromatic materials and to match it by adjusting the color of the spotlight on gray materials. (*b*) Experiment 2: The same red spotlights on the same materials in the presence of dim illumination on the surround. (*c*) Experiment 3: The same red spotlights on the same materials in the presence of brighter illumination on the surround.

results show that when only one illuminant is in the field of view, estimates of illuminant color are seriously biased by the chromaticities of the illuminated surfaces. The results of the second and third experiments show that when the surround of a spotlight is illuminated by a second light, spotlight matching is more accurate in most conditions for bright surrounds. They presented models based on illuminant colors estimations: when the spotlight is brighter than the surrounding illuminant, the discounting is done through an additive model; whereas, for the case where the surrounding illuminant is brighter than the spotlight, the discounting is done through a multiplicative model.

Relation to motion

Another related phenomenon is *motion transparency*: the situation in which two overlapping surfaces move transparently over each other [Snowden and Verstraten, 1999]. Examples are drops of rain running down a car window in a different direction to the background scene, or a cast shadow on a moving surface. In that case, two motions have to be assigned to the same retinal location. Several researchers have tried to solve this problem in using different types of stimuli such as *random-dot patterns* or *plaid patterns*.

Random-dot patterns This type of pattern is used by many researchers with the underlying idea that transparency in motion is based on multiple measures at a point (for a review, see [Snowden and Verstraten, 1999]). It has been found that overlapping dots moving in opposite directions eliminate motion transparency perception [Qian et al., 1994]. Moreover, the velocity field must be sufficiently low to allow grouping and thus, to see transparency [McOwan and Johnston, 1996]. Braddick and colleagues tested the information that is simultaneously represented for one random-dot pattern that moves jointly with another one [Braddick et al., 2002]. They mainly observed that transparency was neither affected by variations of dot density nor by direction of motions. A recent study showed that perceptual segregation of visual entities based on a transparency cue precedes and affects perceptual binding of attributes [Moradi and Shimojo, 2004]. The authors tested whether explicit surface segregation (motion transparency) facilitates binding[7]. They found that when they add an irrelevant transparency cue, the pairing of color and motion paradoxically improved for rapidly alternating surfaces (See illustration in Figure 3.13). They concluded that surface segregation precedes binding of color and motion, and combinations of visual attributes can be segregated almost effortlessly based on motion or depth transparency.

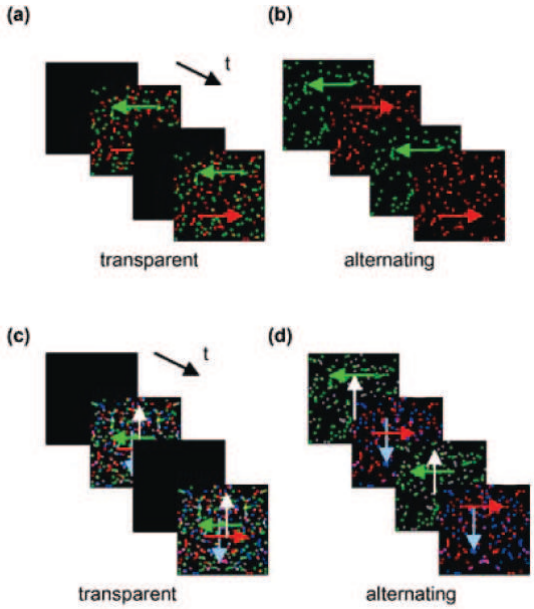

Figure 3.13: Color-motion binding and motion transparency after [Moradi and Shimojo, 2004]. Color-motion binding for transparent (a) and alternating (b) surfaces. In a first experiment, observers were asked to report the direction of the red dots. (c, d) The two additional surfaces (gray, blue) are irrelevant to the task. In a second experiment, participants were asked to report the direction of the red dots. (c) All four surfaces were superimposed (transparent), (d) two superimposed surfaces were alternated.

Plaid patterns Plaids are ambiguous stimuli that can be perceived either as a *coherent* pattern moving rigidly or as two gratings *transparently sliding over each other*. A recent study showed that the global direction of motion of the plaid strongly influences the effect of coherency versus transparency [Hupe

[7] Feature-binding is a term to describe how the visual system determines which combination of attributes (color, etc.) is associated with each entity.

and Rubin, 2004]. The results mainly showed that plaids moving in oblique directions are perceived as sliding more frequently than plaids moving in cardinal directions, and plaids moving in horizontal directions cohered more than plaids moving in vertical directions. They thus imposed new constraints on models of motion integration and transparency.

3.3.3 Achromatic luminance constraints

It has been shown that transparency perception is only possible with some figural constraints and is related to certain types of visual phenomena, such as color constancy. But the most extensively studied conditions for perceptual transparency are those involving achromatic luminance and chromatic constraints (See Sections 3.3.3 and 3.3.4 respectively). The first quantitative Model of transparency perception is Metelli's *Episcotister Model* [Metelli, 1974], based on additive color mixture.

The Episcotister Model

The *episcotister* is a wheel with an open sector rotating in front of two opaque surfaces (Figure 3.14) [Metelli, 1974]. During its rotation the episcotister color is perceived to be a *fusion color* between its sector color and the background color. Metelli described this color in terms of Talbot's law (See Section 3.2.2) of color

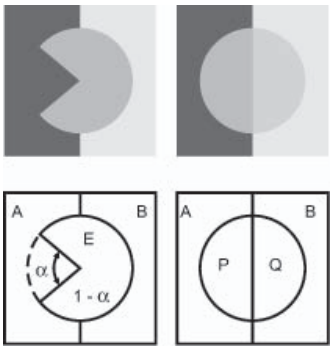

Figure 3.14: Schema of an episcotister from [Metelli, 1974]. On the left side, the episcotister is depicted, on the right side, the perceptual impression resulting from the rotation of the episcotister.

fusion: the fusion of two achromatic color reflectance x and y generates a third color reflectance z[8], where

$$z = \alpha x + (1 - \alpha)y \tag{3.6}$$

with α the proportion in which the two colors are mixed, or, in other words, the open sector relative to the entire disk, i.e. $0 < \alpha < 1$. Consider an episcotister U with reflectance u rotating quickly in front of a bipartite field consisting of two regions A and B. This leads to the perception of two regions P and Q. The reflectances of these regions are given by a, p, q and b respectively:

$$p = \alpha a + (1 - \alpha)u \tag{3.7}$$

$$q = \alpha b + (1 - \alpha)u \tag{3.8}$$

Then solving for α and u results in

$$\alpha = \frac{p - u}{a - u} = \frac{q - u}{b - u} = \frac{p - q}{a - b} \tag{3.9}$$

[8]Note that reflectance clue (λ) ($x(\lambda), y(\lambda), z(\lambda)$, etc.) has been removed in this section for clarity.

$$u = \frac{aq - bp}{(a + q) - (b + p)} \tag{3.10}$$

Since the degree of transparency α is subject to the natural restrictions $0 < \alpha < 1$ it follows

$$p < q \Leftrightarrow a < b \tag{3.11}$$

and

$$|p - q| \quad < \quad |a - b| \tag{3.12}$$

respectively. According to the Episcotister Model, perceptual transparency should be then observed whenever these two conditions of preservation of contrast direction (Equation 3.11) and reduction of contrast (Equation 3.12) are met. Later, Tommasi has found that the model that gives the best prediction of α is Equation 3.9 [Tommasi, 1999]. To him, when $|p - q| = 0$, the regions P and Q are opaque, and when $|p - q| = |a - b|$, the regions P and Q are transparent.

Extension to a Ratio-of-contrasts Model More recently, Singh [Singh, 2004] observed that when matching the lightness of surfaces seen through a filter, observers' matches are consistent with Metelli's equations and with Metelli's α. Metelli's model successfully predicts lightness through transparency, but systematically fails to predict perceived transmittance. According to the author, this can be explained by a model based on the *ratio-of-contrasts*. This suggestion is relevant with recent results of Robilotto and Zaidi who found that transparency corresponds closely to the perceived contrast of the filter [Robilotto and Zaidi, 2004] (See Section 3.3.2). To some other researchers, perceptual transparency implies the encoding of the *luminance* of these regions. For example, Gerbino and colleagues proposed an alternative model saying that the visual systems computations might be in terms of luminance values rather than reflectance values [Gerbino et al., 1990].

Luminance conditions for perceptual transparency

Section 3.3.1 has shown that figural constraints as junctions, and more precisely X-junctions (implicit or not) are necessary for transparency perception. Some researchers have classified X-junctions on the basis of the ordinal relations that can occur between the four luminance values, in taking into account the two qualitative constraints of Metelli to predict when the central region will be seen as transparent. These constraints stipulate that the two halves of the central region must have the same contrast polarity as the two halves of the surround (the *polarity constraint*) and must have a lower luminance difference as well (the *magnitude constraint*).

Polarity constraint Adelson and Anandan directly used the polarity constraint to classify the X-junctions into *non-reversing*, *single-reversing* and *double-reversing* [Adelson and Anandan, 1990; Adelson, 2000] (See Figure 3.15 for explanations) .

Magnitude constraint However, the schemes in Figure 3.15 do not take into account Metelli's magnitude constraint. Anderson proposed a qualitative rule that articulates a sufficient local image condition to initiate *perceptual scission*: when two aligned contours have discontinuities in *contrast magnitude*, but preserve contrast polarity, the lower contrast region is decomposed into two causal layers [Anderson, 1997] (See Figure 3.16 for example). To resume, the Episcotister-based approach has been adopted more or less in its original formulation by most of the researchers investigating perceptual transparency. This model has also been extended to chromaticities (See Section 3.3.4) and to achromatic and chromatic *translucency* [Brill, 1984, 1994; Singh and Anderson, 2002b,a]. However, Beck has proposed an alternative model based on subtractive color mixture [Beck, 1978; Beck et al., 1984].

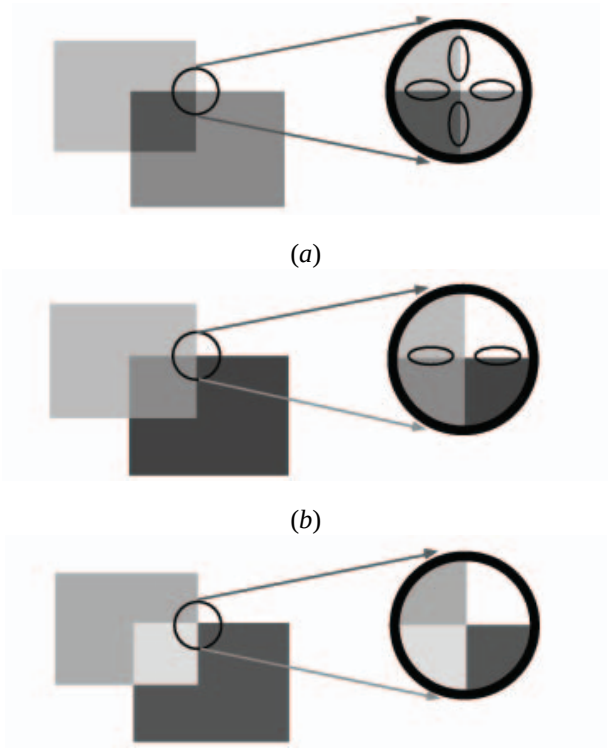

Figure 3.15: Junction classification schemes based on Metelli's polarity constraints (Schema from [Anderson, 1997]). The elliptic apertures are included to indicate contours that preserve contrast polarity and contours that do not. In (*a*), both sets of aligned contours preserve contrast polarity (*Non-reversing junction*). This implies that either contour may be overlaid with a transparent surface, which generates a bistability in the perceived depth of the two layers. In (*b*), a pattern with only a single set of contours preserves polarity, and hence, only this contour is consistent with an overlaying transparent surface (*Single-reversing junction*). In (*c*), neither pair of aligned contours preserve polarity, and hence, this pattern does not support the percept of transparency (*Double-reversing junction*).

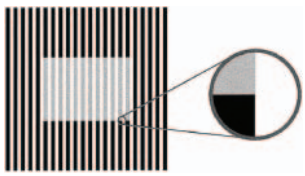

Figure 3.16: An example demonstrating Anderson's qualitative rule for initiating *perceptual scission* into multiple layers (Schema from [Singh and Anderson, 2002b]). The two aligned vertical contours of the enlarged T-junction preserve contrast polarity, and the upper half has lower contrast. As a result, the upper half scissions into two layers: a light-colored transparent layer and an underlying layer with black and white stripes.

Alternative model of the episcotister

Subtractive color mixture is possible when light is selectively absorbed. The model takes into account the percentage of transmission of each absorbing material as a function of the wavelength of the spectral energy power distribution of the light source [Beck, 1978]. According to the author, many common occurrences of transparency are in terms of subtractive rather than additive color mixture [Beck et al., 1984]. When an object is viewed through a liquid or a glass, subtractive color mixture occurs. Considering again two surfaces A and B, with P and Q their regions under the filter, their apparent reflectances p and q in a subtractive model would be equal to

$$p = \frac{r + (t^2 a)}{1 - ra} \tag{3.13}$$

$$q = \frac{r + (t^2 b)}{1 - rb} \tag{3.14}$$

with r and t the reflectance and the transmittance of the filter, respectively. Solving Equations 3.13 and 3.14 for t nd r yields

$$t = \sqrt{\frac{(c - bcd + bd^2 - d)(b - a - abc + a^2 c)}{(b - a + abd - abc)^2}} \tag{3.15}$$

$$r = \frac{bd - ac}{b(1 + ad) - a(1 + bc)} \tag{3.16}$$

To the author, the perception of transparency is then the result of encoding the *lightness* of regions p and q as lightness of underlying regions a and b modified by the lightness of the filter.

3.3.4 Chromatic constraints

Chromatic properties, as well as figural and achromatic luminance constraints, have a strong effect on perceptual transparency. Variants of Metelli's Episcotister Model, based on *additive color mixture*, have been extended by many other researchers in chromatic space. However, according to Faul and Ekroll, the findings in the chromatic domain are not as clear-cut, since there are chromatic stimuli that conform to the additive model that do not appear transparent [Faul and Ekroll, 2002]. They, thus, propose an alternative psychophysical model based on *subtractive color mixture*.

Subtractive models

Psychophysical models of subtractive transparency refer to situations in which a structured opaque surface in seen through a light-transmitting object, for example, a glass filter [Beck et al., 1984; Nakauchi et al., 1999; Faul and Ekroll, 2002]. In these cases, subtractive color mixture is involved. Faul and Ekroll have created two psychophysical experiments with chromatic stimuli, in which they compared predictions of the *General Convergence Model* of [D'Zmura et al., 1997] (derived from Metelli's Model, see Section 3.4) and their subtractive Scaling Model [Faul and Ekroll, 2002].

The Scaling Model They proposed a novel psychophysical model of color transparency derived from physical subtractive filter model (See Section 3.2.1 for definition) and from cone fundamentals L, M and S. Given four regions A, B, P and Q at an X-junction, an illumination spectrum $I(\lambda)$ and cone fundamentals $\phi_i(\lambda)$ with $i = L, M, S$, it is possible to calculate the four cone excitations A_i, B_i, P_i and Q_i from (virtual)

reflectance spectra $a(\lambda)$, $b(\lambda)$, $p(\lambda)$ and $q(\lambda)$. Then,

$$A_i = \int a(\lambda)I(\lambda)\phi_i(\lambda)\,d\lambda \tag{3.17}$$

$$B_i = \int b(\lambda)I(\lambda)\phi_i(\lambda)\,d\lambda \tag{3.18}$$

$$P_i = \int p(\lambda)I(\lambda)\phi_i(\lambda)\,d\lambda \tag{3.19}$$

$$Q_i = \int q(\lambda)I(\lambda)\phi_i(\lambda)\,d\lambda \tag{3.20}$$

The Scaling Model states that the four cone excitations A_i, B_i, P_i and Q_i at an X-junction should be optimal for an impression of transparency if the following relations hold:

$$P_i = \delta_i(A_i + \kappa I_i) \tag{3.21}$$

$$Q_i = \delta_i(B_i + \kappa I_i) \tag{3.22}$$

with the illumination factor $I_i = (A_i + B_i)/2$, the transmittance factor $0 < \delta_i < 1$ and $\kappa \geqslant 0$. If the cone excitations A_i, B_i, P_i and Q_i are given, then the unknown parameters δ_i and κ can be calculated in the following way

$$\delta_i = \frac{P_i - Q_i}{A_i - B_i} \tag{3.23}$$

$$\kappa = \frac{2(Q_iA_i - P_iB_i)}{(P_i - Q_i)(A_i + B_i)} \tag{3.24}$$

This Scaling Model approximately describes the changes in color that occur when a physical filter lays on a bipartite background. The authors' observations indicate that the parameters of the model relate to the perceived quality of the filter. For example, the ratio of δ_i is correlated with the perceived color of the filter and with its perceived thickness. The parameter κ is related to the perceived *haziness* of the filter (for example, for $\kappa = 0$, the filter looks like clear colored glass). After a numerical experiment, they found that the predictions of the additive model and the Scaling Model are very similar. They thus designed psychophysical experiments to investigate distinctive different predictions of both models.

The Scaling Model predictions In their experiments, they used two different types of stimuli (one type is described in Figure 3.17). They found that the observers' responses conform very closely to the predictions of the Scaling Model and deviate systematically from the predictions of the additive model.

Computational theory

The work of Faul and Ekroll was inspired by those of Beck [Beck et al., 1984] and Nakauchi [Nakauchi et al., 1999]. Beck and colleagues extended Metelli's Model to both additive and subtractive mixtures (See subtractive version in Section 3.3.3). Nakauchi and collaborators proposed a computational theory of perceptual transparency based on both additive and subtractive color mixtures as well. They described physical models and Sections 3.2.1 and 3.2.2 mainly relates their ideas. They then reformulated these physical models with the use of sensory responses to color surrounding an X-junction. They reformulated Equations 3.19 and 3.20

$$P_i = \int \phi_i(\lambda)I(\lambda)p(\lambda)\,d\lambda \tag{3.25}$$

$$Q_i = \int \phi_i(\lambda)I(\lambda)q(\lambda)\,d\lambda \tag{3.26}$$

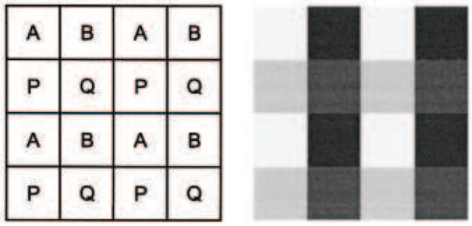

Figure 3.17: Achromatic version of the stimulus configuration used by [Faul and Ekroll, 2002] in their first experiment. Note that the experimental stimuli were chromatic. They identified tristimulus vectors A, B and P, such that the additive and the subtractive model predict unique and distinctly different settings Q_a and Q_s, respectively, for the remaining tristimulus vector Q. The task of the subjects was to find the position on the line through Q_a and Q_s that optimizes the impression of transparency. Thus the two models could be compared according to a clear criterion: if the conditions for optimal perceptual transparency are described by the additive model, then it is to be expected that the subjects will choose point Q_a . If they are instead described by the Scaling Model, then the subjects should choose Q_s.

to

$$\mathbf{r_p} = \mathbf{\Phi_I p} \tag{3.27}$$

$$\mathbf{r_q} = \mathbf{\Phi_I q} \tag{3.28}$$

where the vector $\mathbf{r}$ contains the sensory responses, Φ_I is the matrix whose ith row is $\phi_i(\lambda)I(\lambda)$, and the vector $\mathbf{p}$ or $\mathbf{q}$ represents surface reflectances. They used their equation for physical model of additive color mixture, as

$$\mathbf{r_p} = \mathbf{\Phi_I}[\alpha\mathbf{a} + (1-\alpha)\mathbf{f}] = \alpha\mathbf{r_a} + (1-\alpha)\mathbf{r_f} \tag{3.29}$$

$$\mathbf{r_q} = \mathbf{\Phi_I}[\alpha\mathbf{b} + (1-\alpha)\mathbf{f}] = \alpha\mathbf{r_b} + (1-\alpha)\mathbf{r_f} \tag{3.30}$$

where $\mathbf{f}$ is the reflectance of the filter itself, and for physical model of subtractive color mixture:

$$\mathbf{r_p} = \mathbf{\Phi_I}(\mathbf{f} + \mathbf{Ma}) \tag{3.31}$$

$$\mathbf{r_q} = \mathbf{\Phi_I}(\mathbf{f} + \mathbf{Mb}) \tag{3.32}$$

where $\mathbf{M}$ represents a diagonal matrix representing the filter effect:

$$\mathbf{M}_{k,k} = \frac{t^2(\lambda_k)}{1 - \mathbf{f}(\lambda_k)\mathbf{X}(\lambda_k)} \tag{3.33}$$

with $\mathbf{X} = \mathbf{a}, \mathbf{b}$. These models address the question of the role of color signals involved in perceptual transparency.

Cone-excitation ratios

Westland and Ripamonti investigated the relationships between color signals and surfaces covered by a filter [Westland and Ripamonti, 2000; Ripamonti and Westland, 2001, 2003; Westland et al., in press]. They recall that *cone-excitation ratios* are almost constant when surfaces are seen under a certain illuminant and under another illuminant (color constancy) [Westland and Ripamonti, 2000; Ripamonti and Westland, 2003]. They found the same phenomenon for perceptual transparency: cone-excitation ratios between surfaces illuminated directly and cone-excitation ratios between the same surfaces seen through a transparent filter were almost invariant. They suggested that cone-excitations ratios may be useful to define the stimulus conditions necessary for the perception of transparency.

The principle The principle of cone-excitation ratios states that the ratio of the cone excitations between two opaque surfaces (say A and B) and the ratio between the same surfaces covered by a filter are almost statistically invariant within each cone class. They formulated it by the equation

$$\epsilon_{i,A}/\epsilon_{i,B} = \epsilon'_{i,A}/\epsilon'_{i,B} \tag{3.34}$$

where the cone excitation is given by $\epsilon_{i,j}$ for cone class i ($i \in \{L, M, S\}$) and a surface j seen directly or under a filter ($\epsilon'_{i,j}$).

Predictions In a series of experiments [Westland and Ripamonti, 2000], the authors have shown that cone-excitation ratios are almost invariant in some cases from a set of physically transparent filters and for a wide range of simulated filters. For the physical sets, they found that the invariance is weakest when the transmittance of the filter is low at some wavelengths (when the spectral transmittance of filters approaches zero) and cone-excitations can't be invariant. Thus they found that the invariance is weaker for the colored filters (which allowed little transmittance at certain wavelengths) than for achromatic filters. In other experiments [Ripamonti and Westland, 2003], the observers were asked to select the stimulus containing an homogeneous transparent filter that covered a Mondrian pattern. In the simulation, each Mondrian was partially covered by a transparent filter that could be either a physically plausible filter or one simulated in which cone-excitation ratios were perfectly invariant. Other control and noise simulations were added. They found that observers' performances were the same for the two conditions presented above. They also added another condition where the physically transparent filter was compared with a simulation in which cone-excitations ratios for *all three* cone classes were perturbed, or for a *single* cone class was perturbed, or for *pairs* of cone classes were perturbed (See Figure 3.18). They found that the invariance of the S-

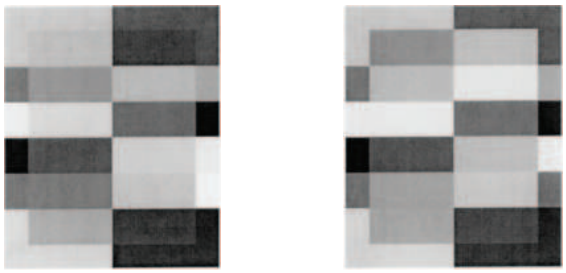

(*a*) (*b*)

Figure 3.18: Two Mondrian displays covered by a transparent filter [Ripamonti and Westland, 2003]. (*a*) The spatial cone-excitation ratios were invariant. (*b*) The cone excitations were systematically perturbed.

cone excitations is less useful for the prediction of perceptual transparency than that of the L- and M-cone classes.

Comparisons In other recent experiments [Westland et al., in press], Westland and colleagues showed that the Invariant-ratio Model is a special case of the General Convergence Model of [D'Zmura et al., 1997] (See Section 3.4 for a definition). They compared the Invariant-ratio Model with the Convergence Model (Figure 3.19) (that is also a special case of the General Convergence Model) and found that in most cases, observers preferred the stimulus defined by the Invariance-ratio Model: when the difference between the two stimuli increased, the observers increasingly preferred the invariant stimulus they use, suggesting that there are stimuli that are better predicted by the Convergence Model and other stimuli that are better predicted by the Invariant-ratio Model.

(*a*) (*b*)

Figure 3.19: Two Mondrian displays covered by a transparent filter [Westland et al., in press]. (*a*) Filter defined by the Convergence Model. (*b*) Filter defined by the Invariant-ratios Model.

Additive models

Da Pos extended the Episcotister Model of Metelli in the chromatic domain [Pos, 1989, 1999]. This extension refers to the *tristimulus values* determined in the chromatic domain (See **Appendix A** for explanation). He pointed out the fact that Metelli's model only considers the lightness value Y; thus, the reflectances a, p, q and b described in Section3.3.3 can be rewritten as

$$Yp = \alpha Ya + (1-\alpha)Yu \tag{3.35}$$

$$Yq = \alpha Yb + (1-\alpha)Yu \tag{3.36}$$

in which Y refers to the lightness of any color taken into account. Then it is possible to write the two other variables, which in fact are automatically determined:

$$Xp = \alpha Xa + (1-\alpha)Xu \tag{3.37}$$

$$Xq = \alpha Xb + (1-\alpha)Xu \tag{3.38}$$

$$Zp = \alpha Za + (1-\alpha)Zu \tag{3.39}$$

$$Zq = \alpha Zb + (1-\alpha)Zu \tag{3.40}$$

The value α should still be in a range between 0 and 1, Xu, Yu and Zu values cannot result in less than 0 or cannot be larger than the X, Y, Z of the perfect white. Da Pos and colleagues did a series of experiments reported in [Pos, 1989] showing that the structure of Metelli's Model is adequate (although more studies are needed and this Model is a necessary but not sufficient condition to explain this phenomenon) to offer a good description of chromatic perceptual transparency. A series of studies of D'Zmura's group generalized Da Pos's approaches as well as those implying chromatic constraints (Section 3.3.4) and relation to color constancy (Section 2.6.4), in the *General Convergence Model*. D'Zmura and colleagues [D'Zmura et al., 1997] suggested that perceptual transparent filters may be created via chromatic changes in any linear color space. They defined these systematic changes as *translation*, *convergence* or composition of both: the *General Convergence Model* (GCM) (Section 3.4), that corresponds to subtractive as well as additive color mixtures, and recent models can be viewed as special cases of it (See Section3.3.4). This Model has been tested (Section 3.4.2) and is related to color constancy (Sections 3.4.3 and 3.4.4). A recent research focuses on brain activity linked to the vision of color filters (Section 3.4.5). These filters are made from translations defined by the Model. One part of this thesis was interested in comparing systematic color changes consistent and inconsistent with the GCM (See **Chapter 4**).

3.4 The General Convergence Model (GCM)

3.4.1 Presentation

D'Zmura and colleagues developed a model on color transparency perception, combining additive and subtractive color mixtures [D'Zmura et al., 1997]. They observed that translation and convergence (or a combination of both) in a linear color space lead to the perception of transparency, while other systematic changes in color space, including rotation and shear, do not.

Examples The authors plotted changes in the chromaticities of the lights from color patches seen under and around a square of transparent yellow plastic sheet (Figure 3.20). One notes a decrease[9] in luminance when surfaces are seen under the filter; thus, luminance seems to be crucial for perceptual transparency. However, they also produced translations along the equiluminant plane of the *DKL* color space [Derrington

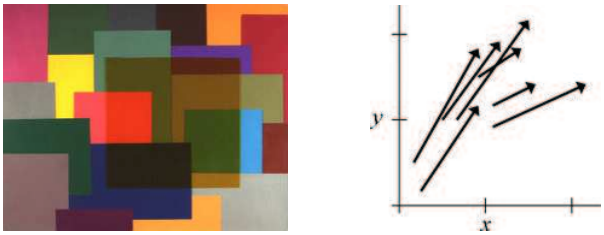

(*a*) (*b*)

Figure 3.20: (*a*) A flat array of papers on which a small square sheet of transparent yellow plastic laid on [D'Zmura et al., 1997]. (*b*) Illustration of plots of the changes in the chromaticities of the lights of papers in the *CIE* 1931 xy chromaticity diagram (See **Appendix A**). Each vector represents each of these papers: the vector's basis represents chromatic properties of a surface seen in plain view, the vector's head represents chromatic properties seen under the filter.

et al., 1984] and observed transparency. Figure 3.21 shows an example of the equiluminant filter obtained. Inspired by previous work of Metelli [Metelli, 1974] and Da Pos [Pos, 1989], the authors created system-

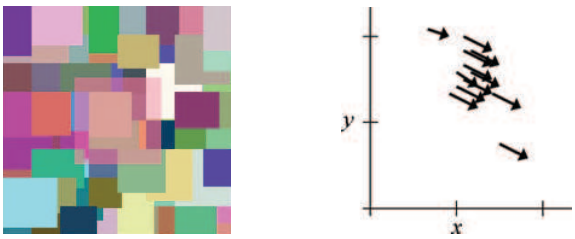

(*a*) (*b*)

Figure 3.21: (*a*) Pink filter obtained by a translation towards the L cardinal point of the L-M-cone axes [D'Zmura et al., 1997]. (*b*) Illustration of plots in the *CIE* 1931 xy chromaticity diagram of the equiluminant translations.

atic changes as convergences. They showed that equiluminant convergences, as well as those that are not equiluminant, give rise to the perception of transparency (Figure 3.22).

[9] An increase of luminance can give rise to perceptual transparency as well, as shown in **Chapter 3** with the Episcotister Model.

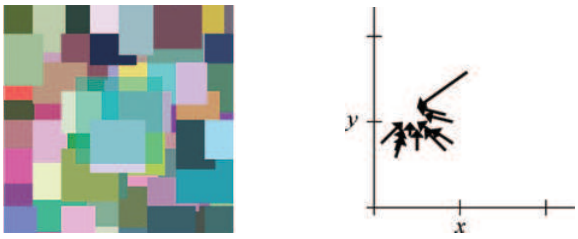

(*a*) (*b*)

Figure 3.22: (*a*) Filter obtained by a convergence towards the M cardinal point of the L-M-cone axes [D'Zmura et al., 1997]. (*b*) Illustration of plots in the *CIE* 1931 xy chromaticity diagram of the equiluminant convergences.

Formulation of the translation

The translation is formulated in the *CIE* XYZ color space [Wyszecki and Stiles, 1982; Pos, 1989] (See **Appendix A**). If a surface reflects a light that is represented by a vector of tristimulus values $\mathbf{a} = (X_a Y_a Z_a)$, a translation is a vector of tristimulus values $\mathbf{t} = (X_t Y_t Z_t)$, that is added to the tristimulus values of a surface $\mathbf{a}$ to provide new tristimulus values as $\mathbf{b} = (X_b Y_b Z_b)$:

$$\mathbf{b} = \mathbf{a} + \mathbf{t} \tag{3.41}$$

The authors conducted experiments to measure the strength of perceptual transparency created from equiluminant translations. Their results showed that observers were all able to match the perceived strength transparency to an achromatic standard: the perception of transparency is possible with equiluminant translations. Their experiments showed that luminance is not necessary for perceptual transparency and that equiluminant translations are readily interpreted by the visual system. They assume that translations in any direction in any linear color space would lead to perceptual transparency.

Formulation of the convergence

Convergence is formulated as a surface color, which is represented by a vector $\mathbf{a}$ of tristimulus values. The target of convergence is represented by vector $\mathbf{g}$. For example, considering the tristimulus values from two surfaces A and B given by vectors $\mathbf{a_A}$ and $\mathbf{a_B}$: these vectors lie on lines that joins the vector $\mathbf{g}$, which defines the tristimulus values of the convergence point. The results are the vectors $\mathbf{b_A}$ and $\mathbf{b_B}$ and can be written as:

$$\mathbf{b_{A,B}} = (1-\alpha)\mathbf{a_{A,B}} + \alpha\mathbf{g}, \quad with \quad 0 \leq \alpha \leq 1 \tag{3.42}$$

The parameter α represents the length of $\mathbf{b}$ from $\mathbf{a}(\alpha = 0)$ to $\mathbf{g}(\alpha + 1)$ in convergence motion. The authors underline the fact that convergence provides a systemic chromatic change that is interpreted by the visual system as a transparent overlay.

Formulation of both convergence and translation

A uniform systematic color change can be created by combining both translation and convergence. An translation $\mathbf{t}$ can be added to a convergence, and a new convergence can be described in the following way:

$$\mathbf{b} = (1-\alpha)\mathbf{a} + \alpha\mathbf{g}', \quad with \quad 0 \leq \alpha \leq 1 \tag{3.43}$$

with

$$\mathbf{g}' = \mathbf{g} + \frac{1}{\alpha}\mathbf{t} \tag{3.44}$$

3.4.2 Test of the Convergence Model

A psychophysical examination of the conditions under which color transparency is perceived has been performed [Chen and D'Zmura, 1998]. To test the Convergence Model (a special case of the GCM), the authors prepared a series of stimuli created in a color space and predicted that the observers responses will fit to this Model.

Stimulus configuration The authors presented stimuli as shown in Figure 3.23. Colors of each stimulus were set in the *DKL* color space [Derrington et al., 1984]. The authors used three planes in the color space, the equiluminant plane (LM and S axis), and the luminant planes (the achromatic axis combined with either LM, or S axis).

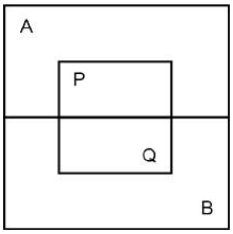

Figure 3.23: Stimulus configuration in [Chen and D'Zmura, 1998]: a bipartite comprising areas A and B. The observer had to set the color of region Q, given prior colors of regions P, A and B so that the central square appeared transparent.

Model's prediction They applied the Convergence Model (See Equations 3.42 and 3.41) to the colors of the stimulus regions, arguing that if the central square appears transparent, then, colors $\mathbf{b}$ of regions P and Q will follow

$$\mathbf{b_P} = (1-\alpha)\mathbf{a_A} + \alpha\mathbf{g} \tag{3.45}$$

and

$$\mathbf{b_Q} = (1-\alpha)\mathbf{a_B} + \alpha\mathbf{g} \tag{3.46}$$

Then, the values of color in region Q (the one that observers adjust) would be

$$\mathbf{b_Q} = \mathbf{a_B} + (1-\alpha)(\mathbf{b_P} - \mathbf{a_A}), \quad for \quad \alpha \in [0,1) \tag{3.47}$$

For $\alpha = 0$, then $\mathbf{b_Q}$ describes a translation as

$$\mathbf{b_Q} = \mathbf{a_B} + (\mathbf{b_P} - \mathbf{a_A}), \quad for \quad \alpha = 0 \tag{3.48}$$

Thus, stimuli presented to the subjects followed either translations or convergences in the color space (See examples in Figure 3.24).

Fitting of the Model Observers' responses agreed well with the model. Transparency is perceived with convergences, and translations at certain limits, even in the equiluminant plane. According to the authors, these results are a strong argument to consider perceptual models rather than physical models based on filter models or the Episcotister Model, since these models can't produce equiluminant transparent surfaces. However, while this Model is necessary, it is not a sufficient condition for transparency perception: when the two parts of the central square have opposite hues or lightnesses, transparency is not observed. The authors recalled that the color of the transparent overlay must share hue characteristics with both underlying surfaces, as suggested Da Pos [Pos, 1989], and thus, complementary hues appearing in the central square can't be perceived as transparent.

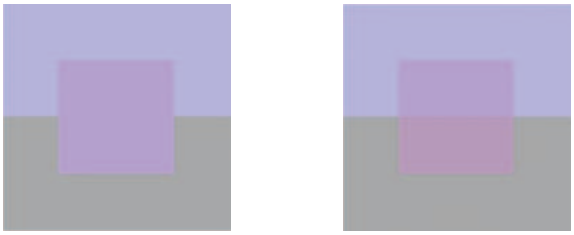

(*a*) (*b*)

Figure 3.24: Examples of stimuli used in the experiment [Chen and D'Zmura, 1998]. (*a*) A pure convergence. Since $\alpha = 1$, the central square is opaque. When $\alpha < 1$, the central square appears transparent. (*b*) A pure translation, when $\alpha = 0$.

3.4.3 Relation to color constancy

D'Zmura and colleagues [D'Zmura et al., 2000] also examined whether the Convergence Model describes the color appearance of surfaces seen *behind* transparent filters. The aim of this study is to find how the colors and lightnesses of surfaces seen to lie behind a transparent filter depend on the color of this filter.

Stimulus configuration Several color pseudo-squares, overlaid by a simulated moving color filter, were shown to the subjects. Color properties of each stimulus were defined in the *DKL* color space [Derrington et al., 1984]. Color filters were defined by the Convergence Model, following either Equation 3.42 or Equation 3.41. Three planes in the color space were used, the equiluminant plane (LM and S axis), and the luminant planes (the achromatic axis combined with either LM, or S axis), either positive (lighter filter) or negative (darker filter). The authors used an asymmetric color-matching technique to measure surface

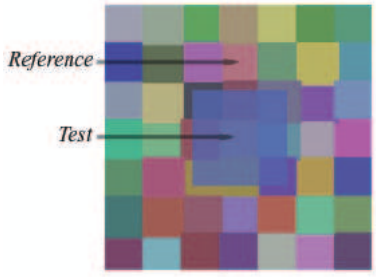

Figure 3.25: Stimulus configuration in [D'Zmura et al., 2000]: color pseudo-squares were overlaid by a color moving filter. The observers' task was either to judge or to adjust the color of this filter (*Test*) to the color of a reference color square (*Reference*).

color. In this way, they compared the chromatic properties of test surfaces (seen behind a transparent filter) to properties of surfaces seen in plain view. Their results revealed how well observers discount the chromatic properties of the transparent filter when judging the color of surfaces. However, they found that observers are only partially color-constant, and they fitted these degrees of constancy to several Models.

Models The authors applied eleven Models in total: six in the *DKL* color space (Affine, Convergence, General Convergence, Linear, Diagonal and Translation Models), five in the *LMS* cone excitation space [Smith and Pokorny, 1975] (Affine, Convergence, Linear, Translation and von Kries Scaling Models).

Affine Model This Model is applied in both the *DKL* color space and in the *LMS* space of cone-excitations, and is described in the following Equation

$$\mathbf{b} = \mathbf{M}\mathbf{a} + \mathbf{t} \tag{3.49}$$

where $\mathbf{a}$ is the vector of *reference-color* coordinates, $\mathbf{M}$ is a $3x3$ matrix describing the linear transformation, $\mathbf{t}$ the translation vector, and $\mathbf{b}$ the predicted vector of *test-color* coordinates.

Convergence Model This Model is described in Equation 3.42. To the authors, this is a special case of the Affine Model.

General Convergence Model This Model has six parameters (three for describing a color change and three for describing change of contrast) and is defined by

$$\mathbf{b} = \mathbf{D}\mathbf{a} + \mathbf{t} \tag{3.50}$$

where

$$\mathbf{D} = \begin{bmatrix} d_{1,1} & 0 & 0 \\ 0 & d_{2,2} & 0 \\ 0 & 0 & d_{3,3} \end{bmatrix} \tag{3.51}$$

in which elements of the diagonal matrix $\mathbf{D}$ may be used to describe changes of contrast only in the three axes in color space. To the authors, the Convergence Model is a special case of the General Convergence Model which is a special case of the Affine Model.

Linear Model This Model is a special case of the Affine Model and is defined by

$$\mathbf{b} = \mathbf{M}\mathbf{a} \tag{3.52}$$

Translation Model This is a special case of the Affine Model as well, but has no contrast-reduction parameter (compared to the Convergence Model). It can be written with three parameters (describing chromatic change) by

$$\mathbf{b} = \mathbf{a} + \mathbf{t} \tag{3.53}$$

Diagonal Model This Model can be expressed by

$$\mathbf{b} = \mathbf{D}\mathbf{a} \tag{3.54}$$

in which $\mathbf{a}$ is a vector of *reference-color* coordinates and $\mathbf{D}$ a diagonal matrix producing the scaled *test-color* coordinates $\mathbf{b}$, in the *DKL* space. The same transformation in the LMS space corresponds to the von Kries Model.

Von Kries Scaling Model This Model can be described by the following Equation

$$\mathbf{b} = \mathbf{D}\mathbf{a} \tag{3.55}$$

where $\mathbf{a}$ is a vector *reference-color LMS* cone excitations, and $\mathbf{D}$ a diagonal matrix that scales the cone-excitations to produce the scaled cone-excitations $\mathbf{b}$.

Fitting of the Models For *color condition* and for all observers, the Affine Model fits the data best, in both *DKL* and *LMS* color spaces. In the *DKL* color space, Convergence and General Convergence Models fit almost as well the data than the Affine Model. In the *LMS* color space, these are the Convergence and Linear Models that fit almost as well as the Affine. The fits also showed that results do not depend on a special filter hue. However, the contrast-reduction parameter α is needed to fit the color-matching data. Thus, they conclude that observers take contrast variation into account when they judge surface colors. The same results were found for *lightness condition*. Thus, this study reported that observers exhibit color constancy when they see surfaces under a transparent overlay.

3.4.4 Tests in more complex scenes

Hagedorn and D'Zmura investigated color constancy in the case when surfaces are seen with fog [Hagedorn and D'Zmura, 2000]. They showed that the Convergence Model describes well their data, because it takes into account both changes in color and in contrast.

Stimulus configuration A Mondrian placard was set in two texture-mapped rooms 3.26. Placards and rooms were identical, except that one room contained fog and the other room did not. Observers performed an asymmetric matching task by matching the color appearance of a central square of the Mondrian in the fogged room to the central square of the Mondrian in the reference room (no fog). The fog was simulated

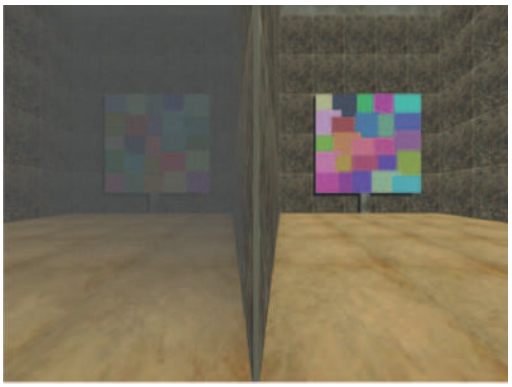

Figure 3.26: Stimulus configuration in [Hagedorn and D'Zmura, 2000]: Example of the two texture-mapped rooms, one containing fog and one being the reference room. Observers had to match the color appearance of a central square of the Mondrian in the fogged room (left) to the central square of the Mondrian in the reference room (right).

with the Convergence Model (See referred Equation 3.42). The authors set various fog conditions, with different intensities. Chromatic properties of each Mondrian and also fog were created in the *DKL* color space [Derrington et al., 1984]. They varied fog color, fog intensity and tested placard position in depth.

Fitting of the Model The authors applied five of the Models tested in [D'Zmura et al., 2000]: the Affine, Convergence, Linear, Translation and von Kries Models. For the *color condition*, the Affine Model fitted the data best (since the all other Models are instances of the Affine Model, this should be this way), and the Convergence Model fitted the data nearly as well. However, the other Models fitted the data not so well. The same good fits were found with the same Models for the *fog-intensity condition*. Finally, observers show almost a complete color constancy. Thus, subjects take into account chromatic properties of the fog, and discount reduction of contrast and changes in colors of lights from surfaces when matching. In all

cases, the Convergence Model, which has only four parameters, fits the data almost as well as the Affine Model that has twelve parameters. Fog and a transparent filter share common properties as the perceived layering in depth of the visual field in chromatic processes. It also may be interesting to find which brain's areas treat such processes (Section 3.4.5).

3.4.5 Brain activity and color transparent filters

The interpretation of surface cues leading to transparency perception requires a global integration of the local color differences in the image. It may be helpful to locate neurons or brain areas involved in this integration. It has been shown in Section 2.5.4 that neurons in V1 have small receptive fields; however, to integrate these local color differences, larger receptive fields are needed. Such neurons may be located in visual areas out of V1. To test this hypothesis, Knoblauch and Dojat designed an fMRI study (See Section 2.5.2 for definition) to identify areas involved in perceptual transparency [Knoblauch and Dojat, 2003]. The authors compared signals detected from two types of stimuli: a Mondrian pattern on which a transparent color filter is applied, created from translations in a *RGB* color space (See **Appendix A** for a definition); a Mondrian on which no transparent filter is perceived, built from shears in the same color space (See Figure 3.27). Their results showed that area V4 is activated when color stimuli are presented

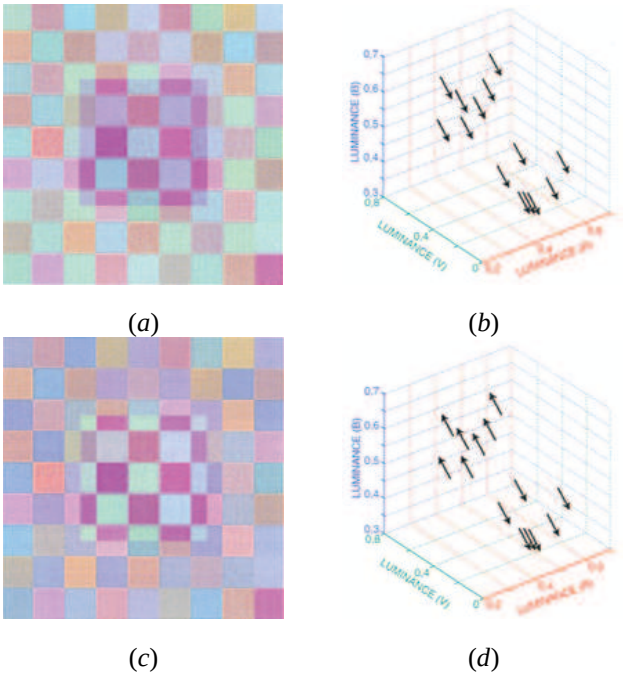

(*a*) (*b*)

(*c*) (*d*)

Figure 3.27: Examples of similar stimuli used in the experiment [Knoblauch and Dojat, 2003]. (*a*) A Mondrian pattern overlaid by a transparent color filter. (*b*) Translations created in a *RGB* color space. Vector's heads represent colors of surfaces seen under the filter. (*c*) A Mondrian pattern with no transparent color filter. (*d*) Shears in a *RGB* color space. These chromatic changes do not lead to the perception of transparency.

to subjects. They also showed that specific areas are active when transparent filters appear. Further studies are needed, but these first results can lead to the conclusion that visual areas beyond V1 are necessary for transparency perception.

3.5 Summary

This Chapter presented physical and perceptual approaches of the perception of transparency. It allowed us to make the link between perceptual transparency and diverse phenomena such as color constancy or motion (See Section 3.3.2). Different models have been shown, as additive (Section 3.2.2) and subtractive (Section 3.2.1) physical models, and perceptual models as the Episcotister Model of Metelli (Section 3.3.3) and its extension to chromatic domain by Da Pos, the Scaling Model based on subtractive color mixture, the Computational Model of Nakauchi and his colleagues, and the Invariant-ratio Model based on the invariant cone-excitations ratios (Section 3.3.4). All these models refer or compare their characteristics and predictions to the *General Convergence Model* (GCM). Several studies have concentrated on conditions within the scope of the GCM, as shown in Section 3.4. The GCM includes convergence and translation, or the combination of both. This Model has been tested (Section 3.4.2) and is highly related to color constancy (Section 3.4.3) and colors seen through fog (Section 3.4.4). Recent studies try to link brain activity and perceptual transparency, by the way of filters created via translations (Section 3.4.5). However, incidental observations suggest that chromatic changes outside of this model, such as shearing transformations, do not appear transparent [Knoblauch and Dojat, 2003], but systematic observations of such stimuli were not reported. In fact, physical transparency can occur in situations that would be described as neither additive nor subtractive, for example, when either the filter or the underlying surfaces are fluorescent. A first approach is to study the effect of a variety of chromatic changes on the appearance of transparency and to observe their consistency with the GCM. This first experiment is described in **Chapter 4**.

Chapter 4

Systematic Chromatic Changes underlying the Perception of Transparency

4.1 Introduction

As described in **Chapter 3**, the observations of D'Zmura and colleagues suggest that chromatic changes such as translations and convergences in a linear color space give the impression of transparency, but other transformations, such as shear and rotation, do not [D'Zmura et al., 1997]. The model was tested psychophysically by Chen and D'Zmura, and a second psychophysical study examined whether the convergence model describes the color appearance of surfaces seen to lie behind transparent filters [Chen and D'Zmura, 1998]. Hagedorn and D'Zmura have also found that the Convergence Model describes well the color appearance of surfaces seen through fog, since it takes into account color shift and change in contrast [Hagedorn and D'Zmura, 2000]. However, all of the studies discussed above have concentrated on conditions within the scope of the GCM.

The purpose of our study is to generate systematic chromatic changes consistent or not with the GCM. This Chapter is organized as follows: an overview is given in Section 4.2, the experimental method is shown in Section 4.3, results are presented in Section 4.4, and discussed in Section 4.5.

4.2 Overview of the study

To explore the limits of systematic chromatic changes, stimuli consistent and inconsistent with the GCM of transparency perception were generated [Gerardin et al., 2003a,b]. The magnitude of the chromatic change, as well as its elevation from the equiluminant plane were also manipulated. The stimulus consisted of a bipartite field partially overlaid by a square. Observers classified each stimulus as to whether the overlaying square appeared transparent or not. The relation between the classification judgments and the stimulus categories was evaluated using a log-linear model (See **Appendix B** for explanation). The main results support the GCM in showing that convergence and translation (except when equiluminant) lead to the perception of transparency, while shear and divergence do not. Large equiluminant translations were less often judged as transparent, consistent with observations reported by Chen and D'Zmura with respect to color changes that cross hue boundaries [Chen and D'Zmura, 1998] (See Section 3.4.2). Surprisingly, we found that small shears and divergences were also classified as transparent, in contradiction with the model. The results question the generality of the Convergence Model.

4.3 Method

4.3.1 Equipment

The stimuli were displayed on a BARCO monitor connected to a DELL (Precision 6.1.0) PC (the resolution was 1280x1024, 256 colors per channel, and the frame rate was 75Hz). After the monitor calibration (GretagMacbeth Eye-One Monitor), the spectral radiance of the monitor was measured with a Minolta CS-1000 spectroradiometer to obtain the gamma of the monitor and then to find the best correspondence between linearized monitor RGB and CIE-1931 XYZ.

4.3.2 Stimulus configuration

The experimental stimuli were created with Matlab v.6.0.088 R12 (Mathworks, MA., U.S.A.), and displayed with Winvis (Neurometrics, CA., U.S.A.). The stimulus consisted of a bipartite field (5x5 deg) embedded in a bipartite surround (10x10 deg) (See Figures 4.1 and 4.2), displayed in the center of the monitor. The bipartite surround was fixed at 25 cd/m^2 for all conditions. Four types of color change were

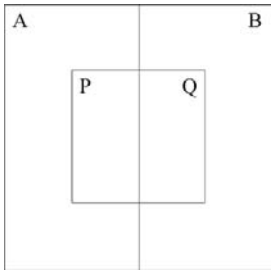

Figure 4.1: Stimulus configuration in [Gerardin et al., 2003a,b]: Example of the bipartite field embedded in a bipartite surround.

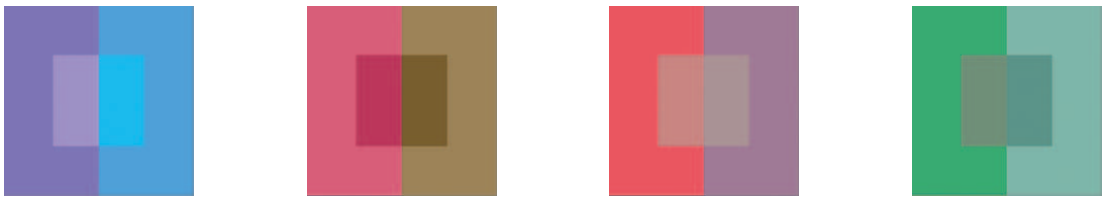

(*a*) (*b*) (*c*) (*d*)

Figure 4.2: Examples of stimuli used in the experiment [Gerardin et al., 2003a,b]. (*a*) Filter created from translations pointing to higher luminance. (*b*) Filter created from translations pointing to lower luminance. (*c*) Filter from convergences directed to higher luminance. (*d*) Filter from convergences directed in the equiluminant plane.

tested: pure translation (See Equation 4.1), pure convergence (See Equation 4.2), shear (Equation 4.3), and divergence (Equation 4.4) in the CIE-1931 XYZ space created as follows, respectively, for two regions A and B overlaid by a transparent filter (See also Figure 4.3 for an illustration):

$$\mathbf{b_{P,Q}} = \mathbf{a_{A,B}} + \mathbf{t} \tag{4.1}$$

$$\mathbf{b_{P,Q}} = (1-\alpha)\mathbf{a_{A,B}} + \alpha\mathbf{g}, \quad with \quad 0 < \alpha < 1 \tag{4.2}$$

$$\mathbf{b_P} = \mathbf{a_A} + \mathbf{t} \quad and \quad \mathbf{b_Q} = \mathbf{a_B} - \mathbf{t} \tag{4.3}$$

$$\mathbf{b_{P,Q}} = (1-\alpha)\mathbf{a_{A,B}} - \alpha\mathbf{g}, \quad with \quad 0 < \alpha < 1 \tag{4.4}$$

Three conditions accounted for luminance elevation (the CIE Y tristimulus value): vectors in the equilu-

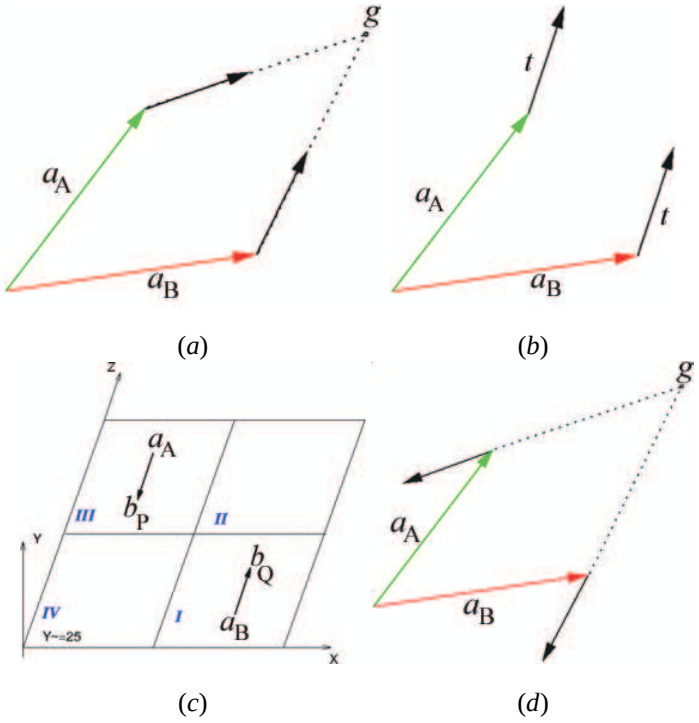

Figure 4.3: Systematic chromatic shifts used in the experiment [Gerardin et al., 2003a,b]. (*a*) Convergence: vectors point to the same convergence point. (*b*) Translation: vectors point to the same direction. (*c*) Shear: vectors point to opposite directions. (*d*) Divergence: vectors point to divergent directions.

minant plane, vectors that point to a lower luminance (filter) and vectors directed to a higher luminance (illumination). Ten different vector lengths were assigned to these conditions, with $\parallel \mathbf{t} \parallel = \{1, 2, ..., 10\}$ for translations, shears, and divergences, and $\alpha = \{0.1, 0.2, ..., 1\}$ for convergences. In the case of non-equiluminant changes, the maximum luminance deviation was $10cd/m^2$.

4.3.3 Procedure

Six (two female and four male) observers were selected for their normal or corrected-to-normal visual acuity and normal color vision, according to the *Farnsworth-Munsell 100-Hue-Test*. A total of 240 stimuli were selected: 60 per each chromatic change, 20 per each luminance level and 2 per each vector length. The psychophysical experiments took place in a completely dark room. Subjects sat in front of the monitor at 50cm from the screen. The set of all patches was presented in a randomized sequence. The observer classified the central patch of each stimulus as either transparent, opaque or unable to decide. Each observer repeated the experiment four times. A training set was presented before each session and discarded. No feedback was provided during the experiment.

4.3.4 Statistics

Log-Linear Models [Knoke and Burke, 1980] were fit to the data, where response classification (RC) was treated as a response variable and chromatic variation (CV), luminance elevation type (LE) and vector length (VL) as explanatory variables. VL was considered an ordinal variable. Fitting was performed using a Generalized Linear Model assuming the data to follow a *Poisson* distribution and using a logarithmic link function. Significance was evaluated with χ^2 statistics. All calculations were performed within the R statistical environment [R, 2004]. In the simplest model, the response variable, RC, will be independent of the explanatory variables. The rejection of this model implies that there is at least one significant interaction between RC and an explanatory variable and that the explanatory variable, thus, differentially affects the perception of transparency. Subsequently, interaction terms are added to the model, starting with the most significant, until further additions no longer produce a significant change in χ^2. The modeling process is termed hierarchical because the exclusion of a factor or an interaction term results in the exclusion of all higher order interactions in which it participates [Bishop et al., 1975]. The model with the minimum number of significant terms is considered to describe the data best.

4.4 Results

Figures 4.5 to 4.8 show the total number of responses of the observers for each type of chromatic variation as a function of vector length and for each of the three luminance elevation conditions. The model with no interactions between RC and the explanatory variables was rejected ($\chi^2 = 4672$, df = 238, $p < 0.001$). The minimum model that describes the data well includes interactions of RC with CV ($\chi^2 = 2134$, df = 6, $p < 0.001$) and with VL ($\chi^2 = 928$, df = 18, $p < 0.001$). These interactions are evident in the different pattern of responses across the four sets of Figures and confirm that the four types of chromatic variation do differentially affect whether or not the central region appears transparent.

4.4.1 Convergence and Translation

Figure 4.5 shows that except for the longest vector length, convergences appear transparent for all types of luminance elevation. Translations (Figure 4.6) show a similar pattern when there is a non-zero luminance elevation. Longer vector lengths do not systematically appear transparent at equiluminance, however.

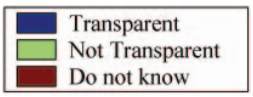

Figure 4.4: Legend of results.

4.4.2 Shear and Divergence

Shear and Divergence (Figures 4.7 and 4.8) show a different pattern in which the shorter vector lengths are classified as being transparent for all luminance elevations, but not the longer ones. The interaction of RC with luminance elevation did not attain significance ($\chi^2 = 8.54$, df = 4, $p = 0.074$), although a comparison between the coefficients for the convergence and translation interaction terms indicates that the differences observed at equiluminance are significant ($p < 0.001$). As the above description suggests, one three-way interaction (CVxVLxRC, $\chi^2 = 940$, df = 54, $p < 0.001$) also needed to be included in the minimal model, reflecting the different pattern of responses as a function of vector length for different types of chromatic variation across the central square patch.

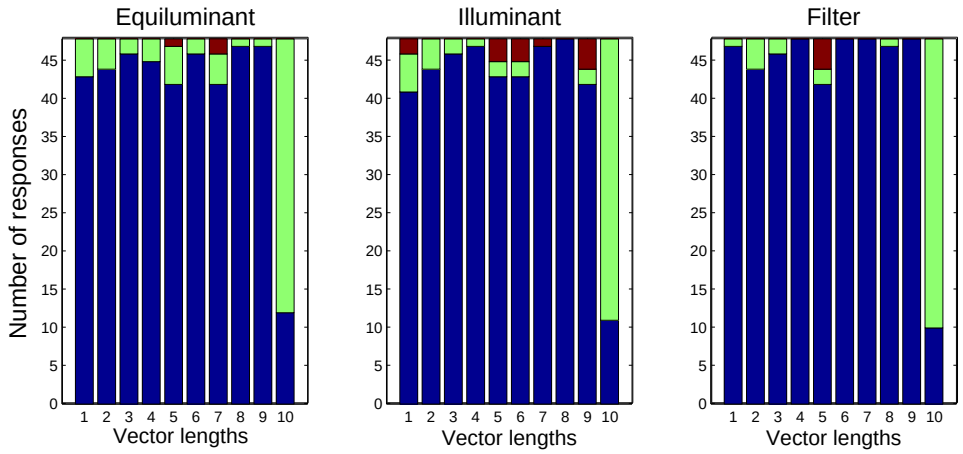

Figure 4.5: Results for **Convergence** [Gerardin et al., 2003a,b]: Convergences appear to be transparent for all types of luminance elevation and all vector lengths, except the last one expected to appear opaque.

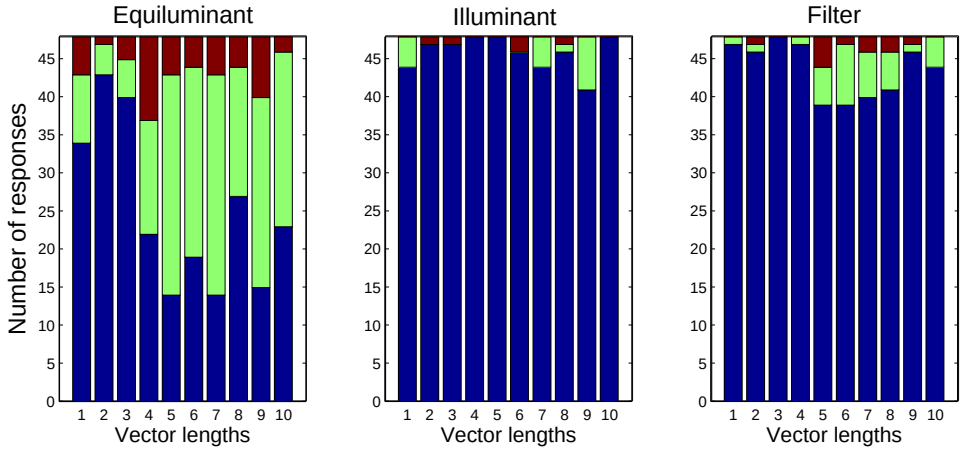

Figure 4.6: Results for **Translation**: Translations appear to be transparent except for equiluminant plane, when vector lengths increase.

4.5 Discussion

Our results confirm some previous findings on the chromatic conditions that lead to the perception of transparency but also reveal puzzling conditions which evoked transparency unexpectedly, that is for small shearing and divergent changes. Convergent chromatic changes provided very robust transparency effects whether the changes were equiluminant or not. Translational changes, however, were most consistently classified as appearing transparent when a luminance component was present. Short equiluminant translations were more frequently classified as transparent than longer ones. Chen and D'Zmura noted that chromatic variations that crossed hue boundaries tended to interfere with transparency perception [Chen and D'Zmura, 1998], and Faul and Ekroll have classified and modeled additional conditions within the

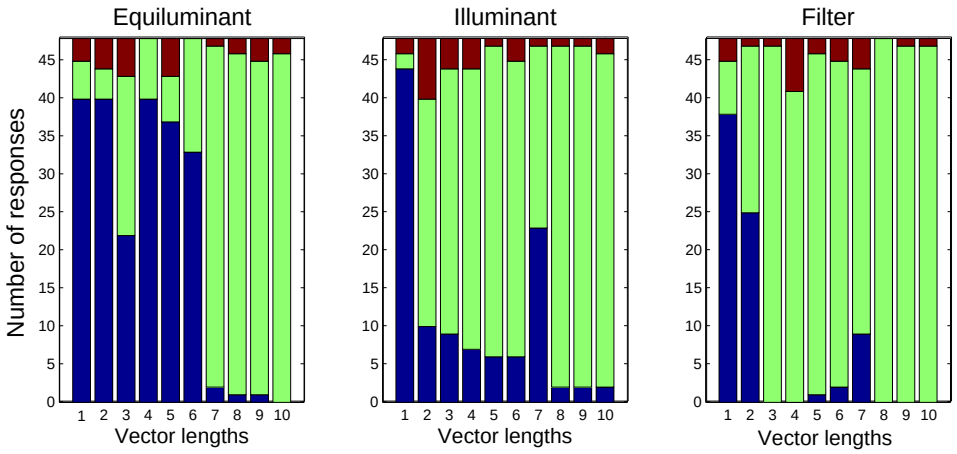

Figure 4.7: Results for **Shear**: Short shears appear to be transparent.

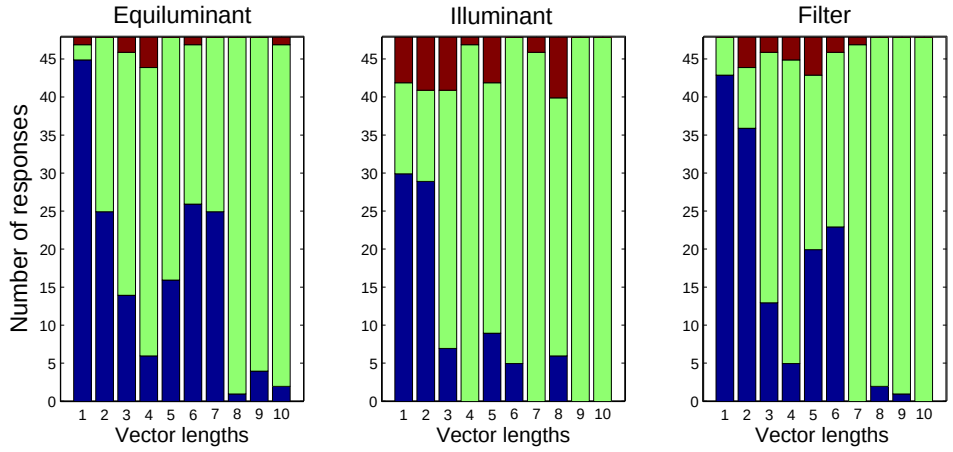

Figure 4.8: Results for **Divergence**: As shears, short divergences appear to be transparent.

GCM that do not appear transparent [Faul and Ekroll, 2002]. Surprisingly, small shears and divergences were consistently judged as transparent which is contrary to the predictions of the GCM and, thus, of the special cases within it, as well. Visually, these conditions appear to resemble the transparency that arises from convergent chromatic variations, that is changes in contrast in the transparent region. In a previous study, shearing chromatic variations were found not to produce transparency [D'Zmura et al., 1997], but the generality of the stimulus conditions related to this situation were not extensively investigated. We do not have an explanation for why small shears evoke transparency. Since physical transparency is not necessarily limited to that resulting simply from additive and subtractive processes (for example, when the transparent medium is fluorescent), however, it is perhaps not unreasonable to suppose that some stimuli that cannot be described as such could evoke an appearance of transparency.

4.6 Summary

We generated stimuli from four systematic chromatic changes, consistent or inconsistent with the GCM. This model usually rejects rotation and shear, and our study showed that this assumption is not clear cut. Our main results support the GCM in showing that convergence and translation (except when equiluminant) lead to the perception of transparency, but some shears (with short vector lengths) and some divergences do as well. Diverse factors have an effect on transparency perception, as vector lengths or luminance plane. Other studies have added motion in their stimuli (See Sections 3.3.4 and 3.4), claiming that this enhances the transparency effect. Section 3.3.2 has shown that motion interacts with this phenomenon. It would be useful to see if motion has an effect on systematic chromatic changes. **Chapter 5** describes experiments showing that configuration complexity and motion play an important role in the perception of transparency.

Chapter 5

Effects of Motion and Configural Complexity on Color Transparency Perception

5.1 Introduction

Some researchers such as Hupé and Rubin have added motion to their stimuli, showing that this enhances the transparency effect [Hupe and Rubin, 2000]. They showed that static non-transparent stimuli may appear transparent in motion. It appears that luminance cues can be overridden by motion cues in transparency. Moreover, segmentation based on motion can override conflicting luminance and color cues. Khang and Zaidi used backgrounds simulating a wide variety of spectral reflectances, spectrally reflective filters and equal energy light [Khang and Zaidi, 2004]. Background materials were simulated as overlaying a circular region and moving along a circle. They pointed out that a moving filter has the advantage of covering a larger sample background of material than a static filter of the same size and noted as well that the movement of filters greatly enhances the perception of a transparent layer. In this Chapter, we investigated whether similar trends in motion transparency can be found with respect to the systematic chromatic changes. Because Hupé and Rubin, Khang and Zaidi have proposed two types of stimuli with different complexities, a simple and a more complex configuration of stimuli were defined.

A preliminary study showed effects of motion and configuration complexity on diverse systematic chromatic changes [Gerardin et al., 2004]. Here, we describe another experiment in which the stimuli were characterized within a more uniform color space CIE LUV. This study is described in the following Section: an overview is given in Section 5.2, the experimental method is shown in Section 5.3, results are presented in Section 5.4, and discussed in Section 5.5.

5.2 Overview of the study

This experiment is designed to test whether motion influences the perception of transparency generated by an overlay created from five different systematic chromatic changes. Bipartite and checkerboard like stimulus configurations were shown to the observers. A variety of chromatic transformations and changes in elevation from the equiluminant plane were studied for static versus motion overlays. The relation between the classification judgments and the stimulus categories was evaluated using a log-linear model (See **Appendix B**). Our main results show that responses for stimuli generated from the five systematic chromatic variations vary according to several variables such as motion, configural complexity, vector length and luminance level. Higher order interactions were found with chromatic variations associated to luminance

elevation, filter type and/or motion that change also quantitatively the observers' responses whatever the configuration or the absence/presence of motion are. These results question the generality of the GCM, but also indicate that adding motion and stimulus complexity are not neutral with respect to the chromatic shifts evoking transparency. Thus, studies have had used motion to enhance transparency may yield different results about the color shifts supporting transparency perception. The same might be supposed for stimulus complexity.

5.3 Method

5.3.1 Equipment

All experiments were conducted with a BARCO PCD-321 monitor connected to a DELL Precision 330. The monitor had a resolution of 1280 x 1024 and ran at 75Hz. After the monitor luminance calibration (GretagMacbeth Eye-One Monitor), the spectral radiance of the monitor was measured with a Minolta $CS1000$ spectroradiometer to find the best correspondence between linearized monitor RGB and the CIE-1931 XYZ space. The stimuli were generated in the CIE LUV space (See **Appendix A**).

5.3.2 Stimulus configuration

The experimental stimuli were created with Matlab v.6.0.088 R12 (Mathworks, MA., U.S.A.), and displayed with OpenGL. The stimuli consisted of a bipartite or a checkerboard configuration (10x10 deg) (See Figure 5.1), displayed in the center of the monitor, with a central static or moving overlay (5x5 deg). The moving overlay kept the same circular movement (2 deg. radius) for all trials, with a speed of 120 deg. per second. The rotation remained clockwise in all cases. Four luminance levels of the surrounding bipartite (for bipartite configuration) and of the surrounding patches (for checkerboard configuration) were defined (40 cd/m^{-2}, 45 cd/m^{-2}, 50 cd/m^{-2} and 55 cd/m^{-2}).

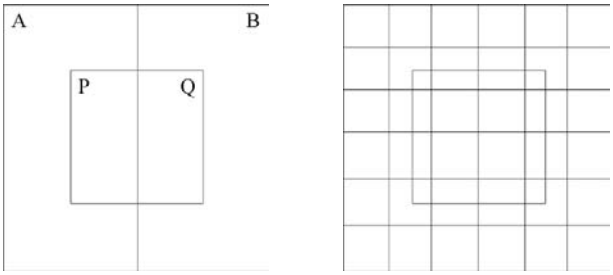

(*a*) (*b*)

Figure 5.1: Stimuli configuration. The test overlay square moved clockwise in motion sessions. (*a*) Bipartite configuration. (*b*) Checkerboard configuration.

Color space

In recent studies on transparency perception, different color spaces were investigated: CIE XYZ [D'Zmura et al., 1997], DKL [Chen and D'Zmura, 1998; D'Zmura et al., 2000; Hagedorn and D'Zmura, 2000] and Munsell [Westland and Ripamonti, 2000; Ripamonti and Westland, 2003; Faul and Ekroll, 2002; Khang and Zaidi, 2002a, 2004]. In our experiment, CIE LUV (a more uniform color space compared to the above cited) was chosen to control $\Delta {E_{uv}}^*$ of each vector length.

Systematic chromatic changes

Five chromatic transformations were considered: pure translation (See Equation 5.1), pure convergence (Equation 5.2), shear (Equation 5.3), divergence (Equation 5.4) and rotation (Equation 5.5) in the CIE LUV space created as followed, respectively, for two regions A and B overlaid by a transparent filter:

$$\mathbf{b_{P,Q}} = \mathbf{a_{A,B}} + \mathbf{t} \tag{5.1}$$

$$\mathbf{b_{P,Q}} = (1-\alpha)\mathbf{a_{A,B}} + \alpha\mathbf{g}, \quad with \quad 0 < \alpha < 1 \tag{5.2}$$

$$\mathbf{b_P} = \mathbf{a_A} + \mathbf{t} \quad and \quad \mathbf{b_Q} = \mathbf{a_B} - \mathbf{t} \tag{5.3}$$

$$\mathbf{b_{P,Q}} = (1-\alpha)\mathbf{a_{A,B}} - \alpha\mathbf{g}, \quad with \quad 0 < \alpha < 1 \tag{5.4}$$

$$\mathbf{b_P} = \mathbf{a_A} + \mathbf{t} \quad and \quad \mathbf{b_Q} = \mathbf{a_A} - \mathbf{a_Q} \tag{5.5}$$

A total of 720 stimuli were presented to the subjects (See Table 5.1 for a summary), including 2 types of configuration (Bipartite field or Checkerboard), with 2 motion conditions (present or absent), 5 systematic color changes, 4 different directions of each color change, 3 arbitrary vector lengths (corresponding to computed $\Delta {E_{uv}}^* = 8, 20, 32$) and 3 luminance levels (vectors point to a higher (+1), equal (0) or lower luminance (-1)). Figure 5.2 shows plots of convergences with three different vector lengths, in the u, v

Total	L^*	$\Delta {E_{uv}}^*$	**Filter**	**Shift**	**Motion**	**Complexity**
	-1	8	Direction 1	Convergence	Absent	Bipartite
	0	20	Direction 2	Translation	Present	Checkerboard
	+1	32	Direction 3	Shear		
			Direction 4	Divergence		
				Rotation		
720	**3**	**3**	**4**	**5**	**2**	**2**

Table 5.1: Conditions of the experiment. See text for explanations.

plane. Other systematic chromatic changes, such as translations, shears, divergences and rotations, are shown in Figure 5.3 to 5.6, respectively. Illustrations of related filters are shown in Figures 5.7 to 5.11 (Prints of Figures may not be representative about their effective appearance on a calibrated monitor).

5.3.3 Procedure

Four color normal observers were tested (Three females and one male). They had normal or corrected-to-normal visual acuity and normal color vision, according to the *Farnsworth-Munsell 100-Hue-Test*. The psychophysical experiments took place in a completely dark room. Subjects sat in front of the monitor at 50cm from the screen. The set of all patches was presented in a randomized sequence. For each patch, the observer judged whether the overlay was transparent or not. Each session was repeated four times. A training set was presented before each session and discarded. No feedback was provided during the experiment.

5.3.4 Statistics

Log-Linear Models [Knoke and Burke, 1980] were fit to the data, where response classification (RC) was treated as a response variable. Explanatory variables were the absence or presence of motion (Static/Motion, (SM)), configural complexity (CC), chromatic variation (CV), filter type (FT), luminance elevation type (LE) and vector length (VL) (See Table 5.1 for a summary). VL was considered as an ordinal variable. Fitting was performed using a Generalized Linear Model assuming the data to follow a *Poisson* distribution

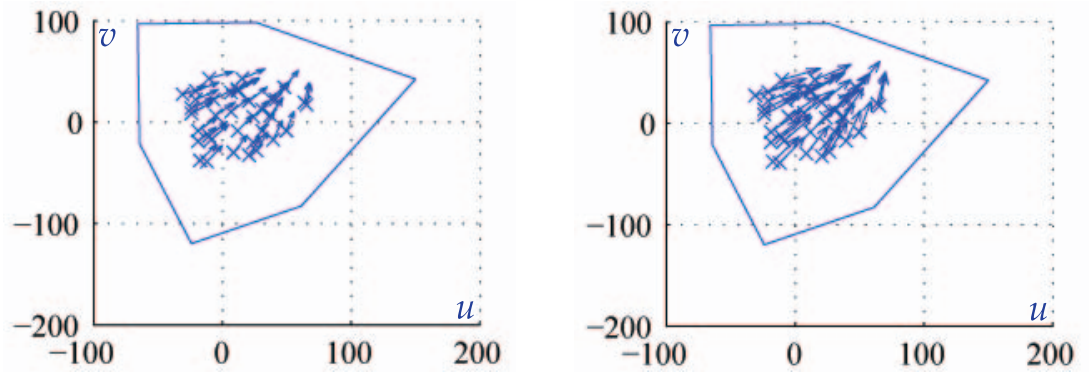

(*a*) (*b*)

Figure 5.2: Plots of **convergences** in the equiluminant u, v plane. (*a*) Convergences with $\Delta {E_{uv}}^* = 20$; (*b*) Convergences with $\Delta {E_{uv}}^* = 32$. Four different directions were generated (only one direction is shown here).

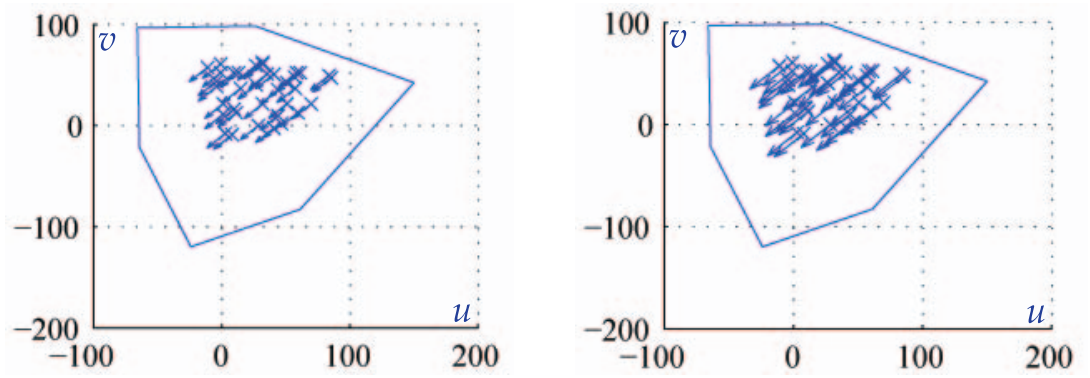

(*a*) (*b*)

Figure 5.3: Plots of **translations** in the equiluminant u, v plane. (*a*) Translations with $\Delta {E_{uv}}^* = 20$; (*b*) Translations with $\Delta {E_{uv}}^* = 32$. Four different directions were generated (only one direction is shown here).

and using a logarithmic link function. Significance was evaluated with χ^2 as well as z-score statistics (See **Appendix B**). All calculations were performed within the R statistical environment [R, 2004]. The model with the minimum number of significant terms is considered to describe the data best.

5.4 Results

Figures 5.12 to 5.16 show the total number of responses of the observers for each type of luminance elevation and for each vector length ($\Delta {E_{uv}}^*$). Each set of responses or graphic (that includes luminance elevation and vector length) is ordered according to four main sub-groups, such as bipartite or checkerboard configuration with static or moving filter each (namely (Static [Bip.]), (Motion [Bip.]), (Static [Check.]), (Motion [Check.])). Interactions between observers' responses classification (RC) and explanatory variables such as Static/Motion condition (SM) are presented in Section 5.4.2. Section 5.4.3 shows interactions between

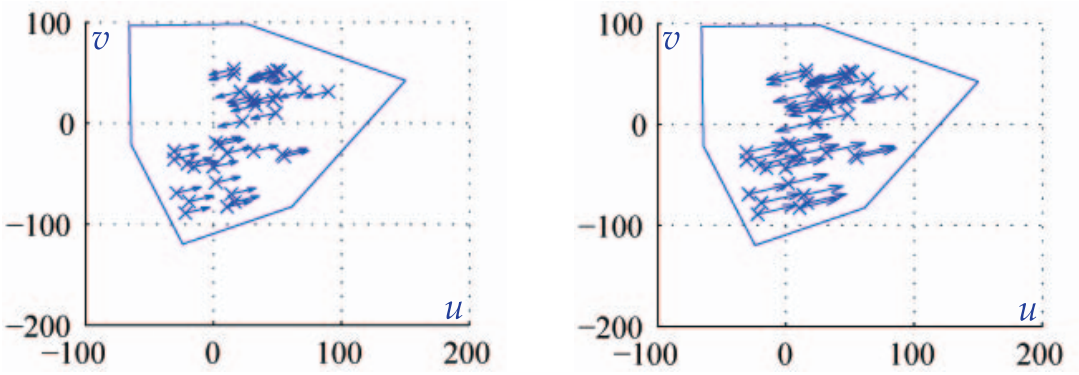

(*a*) (*b*)

Figure 5.4: Plots of **shears** in the equiluminant u, v plane. (*a*) Shears with $\Delta {E_{uv}}^* = 20$; (*b*) Shears with $\Delta {E_{uv}}^* = 32$. Four different directions were generated (only one direction is shown here).

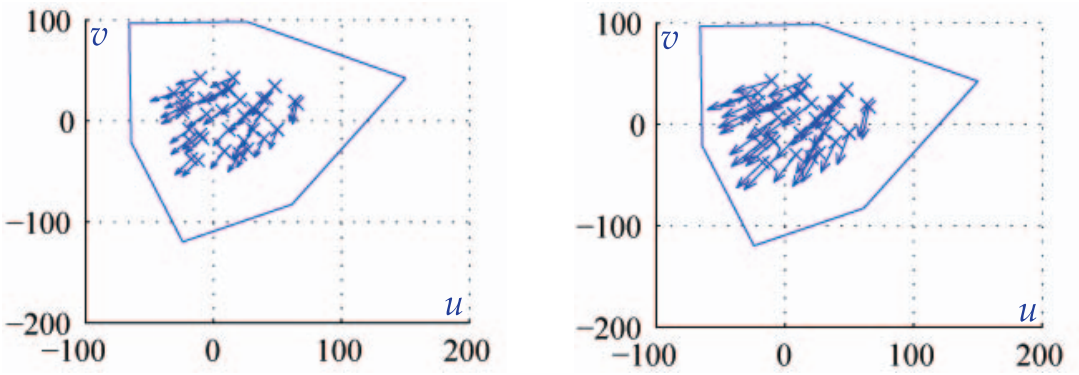

(*a*) (*b*)

Figure 5.5: Plots of **divergences** in the equiluminant u, v plane. (*a*) Divergences with $\Delta {E_{uv}}^* = 20$; (*b*) Divergences with $\Delta {E_{uv}}^* = 32$. Four different directions were generated (only one direction is shown here).

RC and Configural Complexity condition (CC). Section 5.4.4 describes interactions between RC and explanatory variables for each systematic chromatic changes (CV). Variations among observers' responses are discussed in Section 5.4.1. Additional results are listed in **Appendix C**.

5.4.1 Observers

Four observers participated but it was found that one observer's data stood-out as influential. As it was the experimenter, the question as to whether her responses are biased by her expert knowledge of the stimuli and hypotheses can be raised. Analysis with her data indicated some interactions of the variable *Observer* (OB) with some of the experimental factors in some cases, such as CC and VL. Analysis without her data (PG) rendered such interactions non-significant. Thus, the results shown in the following Sections have a total number of three observers. Results for *each* observer (including (PG)) are shown in **Appendix C**.

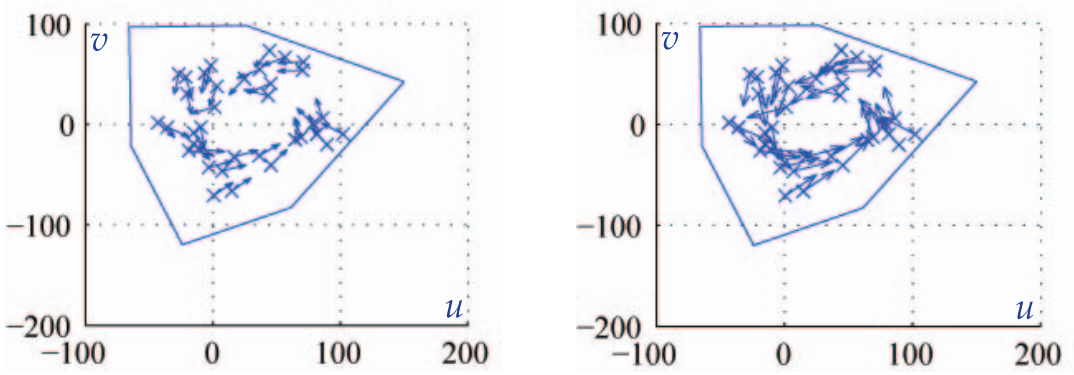

(*a*) (*b*)

Figure 5.6: Plots of **rotations** in the equiluminant u, v plane. (*a*) Rotations with $\Delta {E_{uv}}^* = 20$; (*b*) Rotations with $\Delta {E_{uv}}^* = 32$. Four different directions were generated (only one direction is shown here).

(*a*) (*b*) (*c*)

Figure 5.7: Example of filters created from **convergences** ($\Delta {E_{uv}}^* = 32$ in u, v plane; Checkerboard configuration). (*a*) Resulting filter which vectors point to low luminance level (*filter* condition); (*b*) Resulting filter from *equiluminant* shifts; (*c*) Filter generated from *illuminant* shifts.

(*a*) (*b*) (*c*)

Figure 5.8: Example of filters created from **translations** ($\Delta {E_{uv}}^* = 32$ in u, v plane; Checkerboard configuration). (*a*) Resulting filter which vectors point to low luminance level (*filter* condition); (*b*) Resulting filter from *equiluminant* shifts; (*c*) Filter generated from *illuminant* shifts.

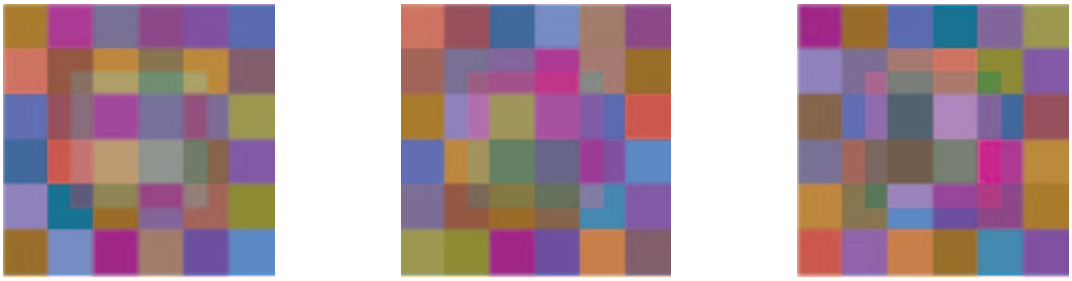

(*a*) (*b*) (*c*)

Figure 5.9: Example of filters created from **shears** ($\Delta {E_{uv}}^* = 32$ in u, v plane; Checkerboard configuration). (*a*) Resulting filter which vectors point to low and to high luminance levels; (*b*) Resulting filter from *equiluminant* shifts; (*c*) Filter generated from *illuminant* combined with *filter* shifts.

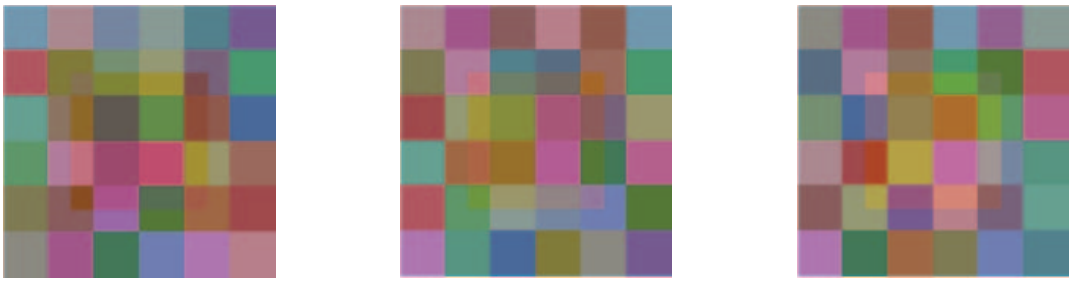

(*a*) (*b*) (*c*)

Figure 5.10: Example of filters created from **divergences** ($\Delta {E_{uv}}^* = 32$ in u, v plane; Checkerboard configuration). (*a*) Resulting filter which vectors point to low luminance level (*filter* condition); (*b*) Resulting filter from *equiluminant* shifts; (*c*) Filter generated from *illuminant* shifts.

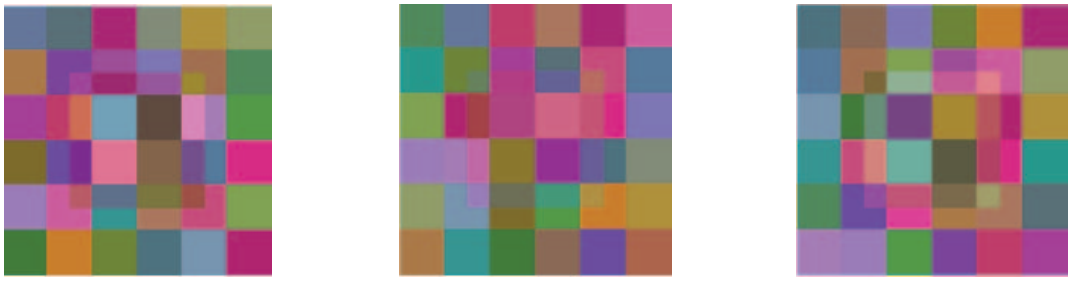

(*a*) (*b*) (*c*)

Figure 5.11: Example of filters created from **rotations** ($\Delta {E_{uv}}^* = 32$ in u, v plane; Checkerboard configuration). (*a*) Resulting filter which vectors point to low and to high luminance levels; (*b*) Resulting filter from *equiluminant* shifts; (*c*) Filter generated from *illuminant* combined with *filter* shifts.

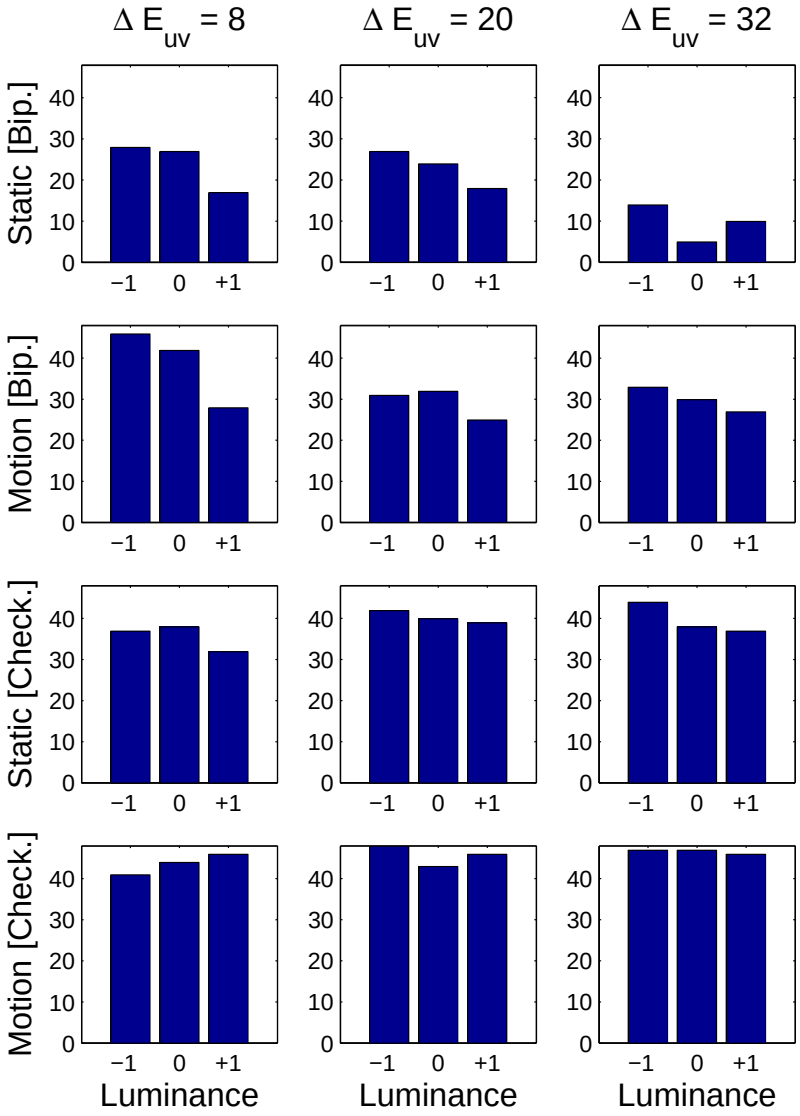

Figure 5.12: Results for **convergences** for all observers. The first row (up) describes observers' cumulated responses for bipartite configuration when filter is static (**Static [Bip.]**). The second row shows observers' cumulated responses when filter moves (**Motion [Bip.]**). The third row shows observers' cumulated responses for checkerboard configuration with static filter (**Static [Check.]**). The last row (down) illustrates observers' cumulated responses for checkerboard configuration when filter moves (**Motion [Check.]**). All observers' responses are distributed as a function of luminance level (**(-1)**: Filter condition; **(0)**: Equiluminant condition; **(+1)**: Illuminant condition). The first column (left) shows observers' responses for $\Delta {E_{uv}}^* = 8$ in u, v plane, the second column depicts responses for $\Delta {E_{uv}}^* = 20$ and the last column (right) shows responses for $\Delta {E_{uv}}^* = 32$.

5.4.2 Static / Motion condition (SM)

Among all data, observers' responses classification (RC) are significantly influenced by the variable SM, with $z = -5.359$, $p < 0.0001$. These interactions are evident in the different pattern of responses across the

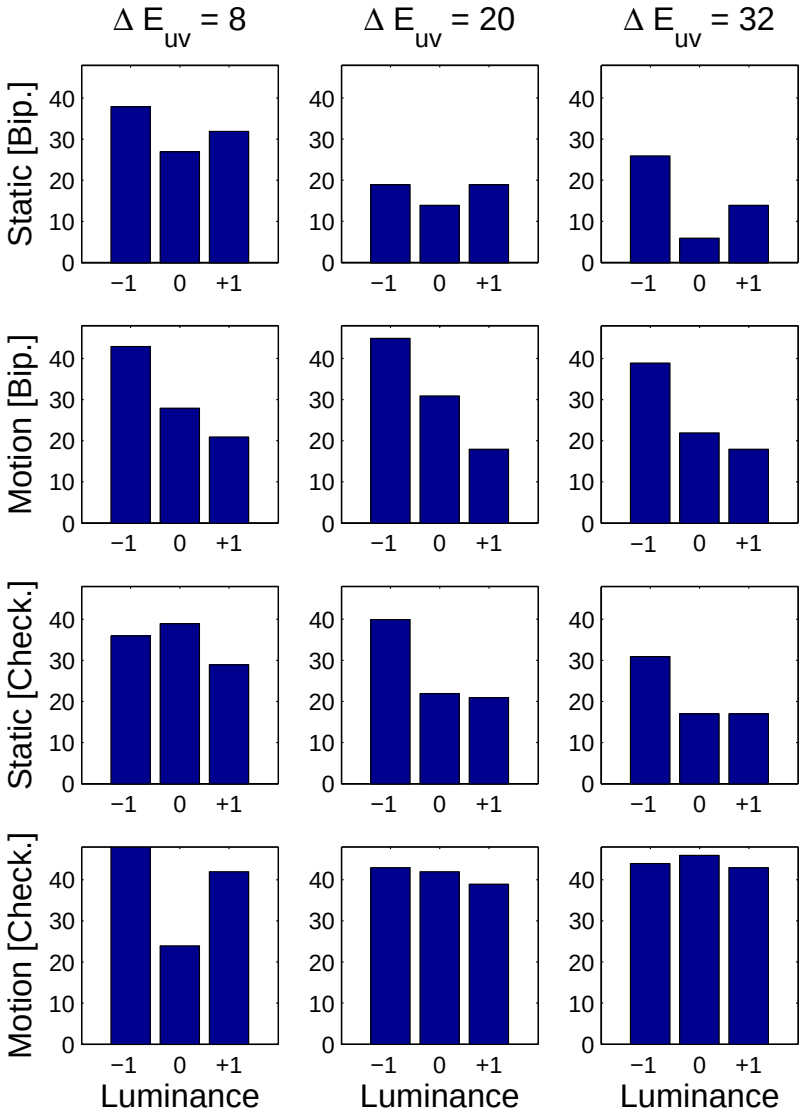

Figure 5.13: Results for **translations** for all observers. The first row (up) describes observers' cumulated responses for bipartite configuration when filter is static (**Static [Bip.]**). The second row shows observers' cumulated responses when filter moves (**Motion [Bip.]**). The third row shows observers' cumulated responses for checkerboard configuration with static filter (**Static [Check.]**). The last row (down) illustrates observers' cumulated responses for checkerboard configuration when filter moves (**Motion [Check.]**). All observers' responses are distributed as a function of luminance level (**(-1)**: Filter condition; **(0)**: Equiluminant condition; **(+1)**: Illuminant condition). The first column (left) shows observers' responses for $\Delta {E_{uv}}^* = 8$ in u, v plane, the second column depicts responses for $\Delta {E_{uv}}^* = 20$ and the last column (right) shows responses for $\Delta {E_{uv}}^* = 32$.

five sets of Figures and confirm that motion affects whether or not the central region appears transparent. This is highly visible for convergences when the configuration is a bipartite field (See Figure 5.12, (Motion

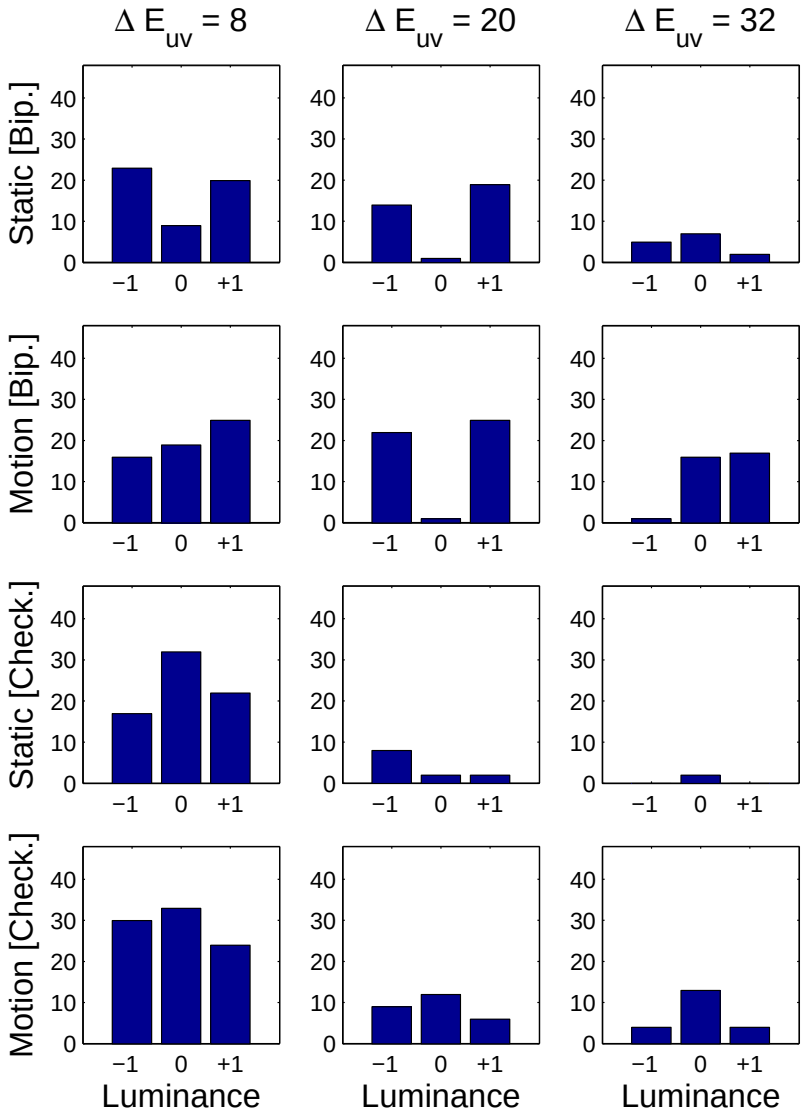

Figure 5.14: Results for **shears** for all observers. The first row (up) describes observers' cumulated responses for bipartite configuration when filter is static (**Static [Bip.]**). The second row shows observers' cumulated responses when filter moves (**Motion [Bip.]**). The third row shows observers' cumulated responses for checkerboard configuration with static filter (**Static [Check.]**). The last row (down) illustrates observers' cumulated responses for checkerboard configuration when filter moves (**Motion [Check.]**). All observers' responses are distributed as a function of luminance level (**(-1)**: Filter condition; **(0)**: Equiluminant condition; **(+1)**: Illuminant condition). The first column (left) shows observers' responses for $\Delta {E_{uv}}^* = 8$ in u, v plane, the second column depicts responses for $\Delta {E_{uv}}^* = 20$ and the last column (right) shows responses for $\Delta {E_{uv}}^* = 32$.

[Bip.])) and for translations and divergences for both configurations (See Figure 5.13 and Figure 5.15 in rows (Motion [Bip.]) and (Motion [Check.])).

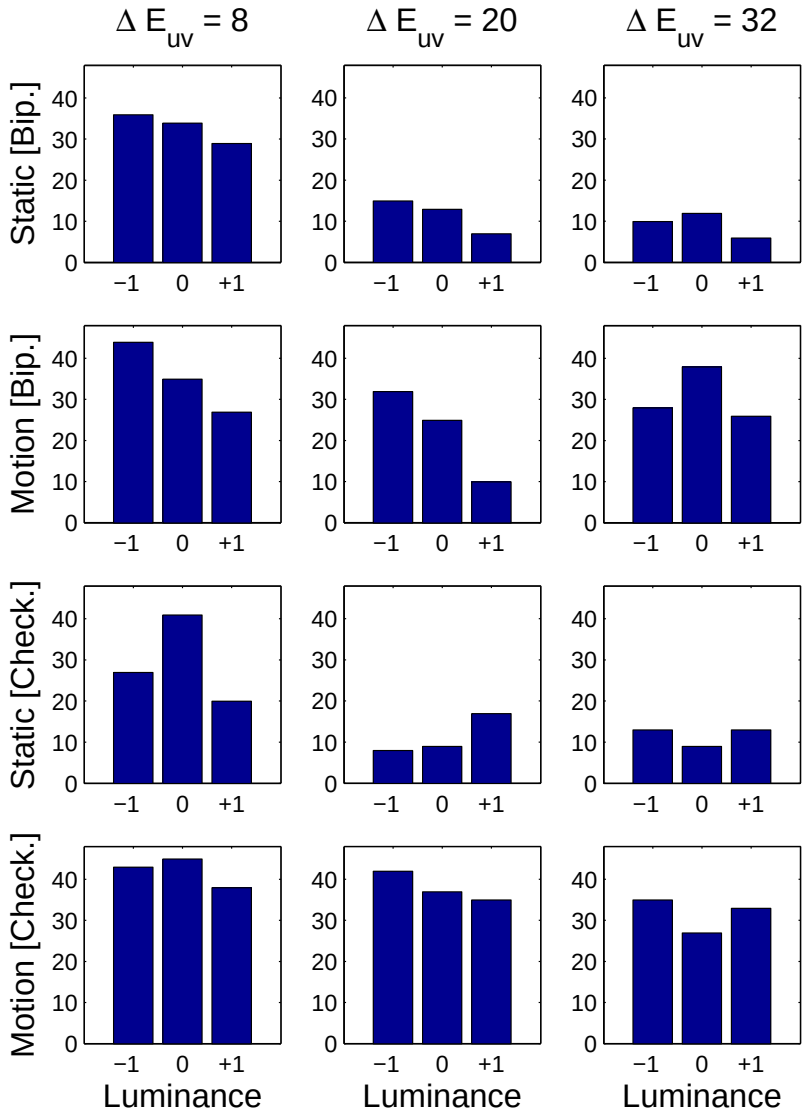

Figure 5.15: Results for **divergences** for all observers. The first row (up) describes observers' cumulated responses for bipartite configuration when filter is static (**Static [Bip.]**). The second row shows observers' cumulated responses when filter moves (**Motion [Bip.]**). The third row shows observers' cumulated responses for checkerboard configuration with static filter (**Static [Check.]**). The last row (down) illustrates observers' cumulated responses for checkerboard configuration when filter moves (**Motion [Check.]**). All observers' responses are distributed as a function of luminance level (**(-1)**: Filter condition; **(0)**: Equiluminant condition; **(+1)**: Illuminant condition). The first column (left) shows observers' responses for $\Delta {E_{uv}}^* = 8$ in u, v plane, the second column depicts responses for $\Delta {E_{uv}}^* = 20$ and the last column (right) shows responses for $\Delta {E_{uv}}^* = 32$.

5.4.3 Simple / Complex configuration (CC)

In general, observers respond differently whether the stimulus is a bipartite field or a checkerboard ($z = 8.974$, $p < 0.0001$). Configural complexity also influences responses differently for each chromatic vari-

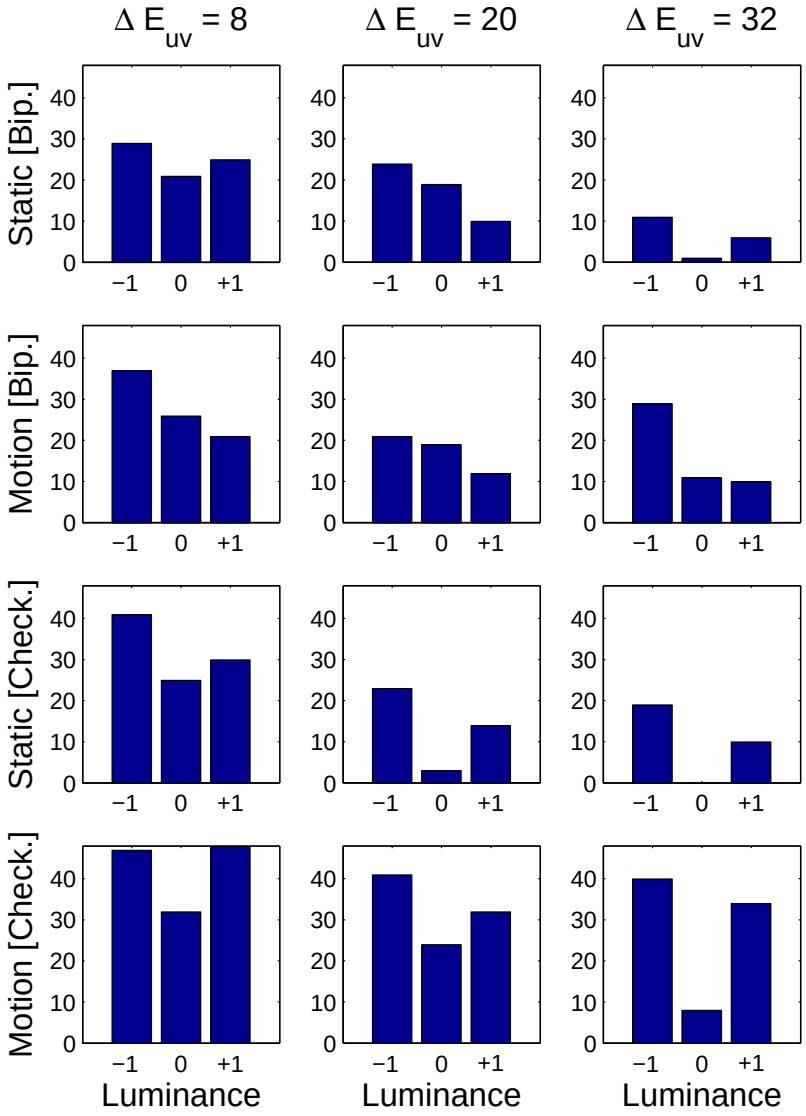

Figure 5.16: Results for **rotations** for all observers. The first row (up) describes observers' cumulated responses for bipartite configuration when filter is static (**Static [Bip.]**). The second row shows observers' cumulated responses when filter moves (**Motion [Bip.]**). The third row shows observers' cumulated responses for checkerboard configuration with static filter (**Static [Check.]**). The last row (down) illustrates observers' cumulated responses for checkerboard configuration when filter moves (**Motion [Check.]**). All observers' responses are distributed as a function of luminance level (**(-1)**: Filter condition; **(0)**: Equiluminant condition; **(+1)**: Illuminant condition). The first column (left) shows observers' responses for $\Delta {E_{uv}}^* = 8$ in u, v plane, the second column depicts responses for $\Delta {E_{uv}}^* = 20$ and the last column (right) shows responses for $\Delta {E_{uv}}^* = 32$.

ation (CV). For example, this effect can be seen for convergences, in which responses for 'Transparent' are significantly larger for filters laid on a checkerboard configuration rather than on a bipartite field (See

Figure 5.12, (Static [Bip.]) and (Static [Check.])). All these effects are described for each chromatic change (CV) in the following section.

5.4.4 Chromatic variations (CV)

Our results confirm that the five types of chromatic variation (CV) differentially affect the perception of transparency. Observers' responses for shears and rotations strongly differ from those for convergences with $z = -3.898$, $p < 0.0001$ and $z = -4.585$, $p < 0.0001$, respectively. Responses for translations slightly differ from those of convergences ($z = -2.364$, $p < 0.01$), and responses for convergences and divergences tend to be similar. However, responses do not significantly vary among different vector lengths (VL), except when this parameter is associated with other explanatory variables, such as motion (SM) and luminance level (LE). For example, luminance elevation, associated with vector length (VL) has an influence on observers' response classification for translations, shears and rotations. Equiluminance also interacts slightly with motion and short vector length to increase the perception of a transparent overlay ($z = -2.08$, $p < 0.01$) for all chromatic variations. Finally, responses for equiluminant condition and filter condition (LE) are slightly different those for the illuminant condition ($z = 2.226$, $p < 0.01$ and $z = 3.263$, $p < 0.001$ respectively).

Convergences Figure 5.12 shows that an overlay generated from convergences leads to perceptual transparency. However, when the configuration is a bipartite field and when the filter is static ((Static [Bip.]) condition in this Figure 5.12), the observers tend to respond 'Not Transparent', especially when vector length increases (overlays are almost seen as opaque when $\Delta {E_{uv}}^* = 32$). This effect tends to be removed when motion is added ((Motion [Bip.]) condition in Figure).

Translations Observers are sensitive whether overlays generated from translations are moving or static ($z = 2.793$, $p < 0.001$). In Figure 5.13, it appears that the overlay is 'Transparent' in motion conditions ((Motion [Bip.]) and (Motion [Check.])), compared to static conditions. The effect of motion is even more significant when ΔE^*_{uv} increases ($z = -3.303$, $p < 0.0001$). Configural complexity (CC) has a weak influence on translations $z = -2.163$, $p < 0.01$. In Figure 5.13, no visible difference is noticed between (Static [Bip.]) and (Static [Check.]). However, motion associated to CC increases the perception of transparency. When the overlay is generated from translations with the filter condition ((**-1**) in Figure 5.13), one can see that observers tend to respond 'Transparent' (with $z = 3.42$, $p < 0.0001$) compared to other luminance conditions (such as equiluminant and illuminant conditions). When overlays are equiluminant, observers tend to respond 'Transparent'for short vector lengths ($z = 2.045$, $p < 0.01$, see first column of Figure 5.13), but this effect decreases when vector lengths increase, except for (Motion [Check.]) condition.

Shears Shears are seen as opaque despite the motion parameter but are slightly influenced by the other variables. Compared to convergences, Simple/Complex configuration (CC) has much less influence on shears ($z = -7.796$, $p < 0.0001$): Figure 5.14 shows that observers see an opaque overlay when laid on a checkerboard configuration. Ambiguities seen in conditions (Static [Bip.]) and (Motion [Bip.]) are removed. However, shears are influenced by luminance combined with vector length. For equiluminant condition and $\Delta E^*_{uv} = 8$ (See first column of Figure 5.14), responses tend to be 'Transparent' compared to other conditions ($z = 3.604$, $p < 0.0001$). One can see in Figure 5.14 that number of responses for 'Transparent' decreases abruptly when $\Delta E^*_{uv} = 20$, whatever the configuration is, or whether the overlay moves or not. Vector length is thus critical for shears, in any condition ($z = -3.653$, $p < 0.0001$).

Divergences Motion (SM) strongly influences divergences ($z = 3.267$, $p < 0.001$). Stimuli generated from divergences and combined with motion (and despite longer vector lengths) lead to the perception of transparency. This is visible in Figure 5.15, in (Motion [Bip.]) and (Motion [Check.]) conditions. Compared to convergences, configural complexity (CC) alone has much less influence on divergences ($z =$

-4.529, $p < 0.0001$) but when added to motion, the overlay tends to appear more transparent ($z = -1.965$, $p < 0.01$). It is also visible in the first column of Figure 5.15 that short vector length ($\Delta E^*_{uv} = 8$) in static conditions influences observers' responses for 'Transparent'.

Rotations Compared to convergences, motion influences rotations as well ($z = 2.236$, $p < 0.01$), but less strongly, probably due to the fact that it is apparent for checkerboard configuration: SM strongly interacts with Simple / Complex configuration (CC) ($z = -2.699$, $p < 0.001$) and interacts with vector length as well. CC alone has a weaker influence on rotations ($z = -2.498$, $p < 0.01$). In Figure 5.16, it is visible in (Motion [Check.]) that, compared to the equiluminant condition, observers tend to respond 'Transparent' when the overlay is generated from filter and illuminant conditions ($z = -3.973$, $p < 0.0001$). Thus, for non-equiluminant conditions, observers see a transparent overlay for rotations when motion interacts with CC. Finally, when $\Delta E^*_{uv} = 8$, observers tend to respond 'Transparent' ($z = -2.656$, $p < 0.001$) (See first column of Figure 5.16). This proportion increases when additional parameters such as CC and motion are present.

5.5 Discussion

Our results reveal different conditions which evoke opacity or transparency, that is when motion is added, or when stimulus configuration is changed. Convergent chromatic changes provided robust transparency effects except for bipartite configuration associated to long vector length parameter. This lack of effect is removed when the filter starts moving. In a previous experiment [Gerardin et al., 2003a,b], we did not notice such 'Not Transparent' responses. One explanation would be that, in this study, observers compare stimuli with two different configurations, and those having a more complex one appear more transparent than those with bipartite configuration. Chen and D'Zmura noted that chromatic variations that crossed hue boundaries tended to not lead to the perception of transparency [Chen and D'Zmura, 1998], and Faul and Ekroll have classified additional conditions within the GCM when the overlay does not appear transparent [Faul and Ekroll, 2002]. Another explanation concerns the positions of the vectors (See Figure 5.17). In bipartite configuration, vectors are randomized, and selected ones might be close or far from each other. Vectors placed side by side may be perceived as more transparent (because their perceived colors are more similar) than when vectors have distant positions. Changes such as translations, however, were most consistently

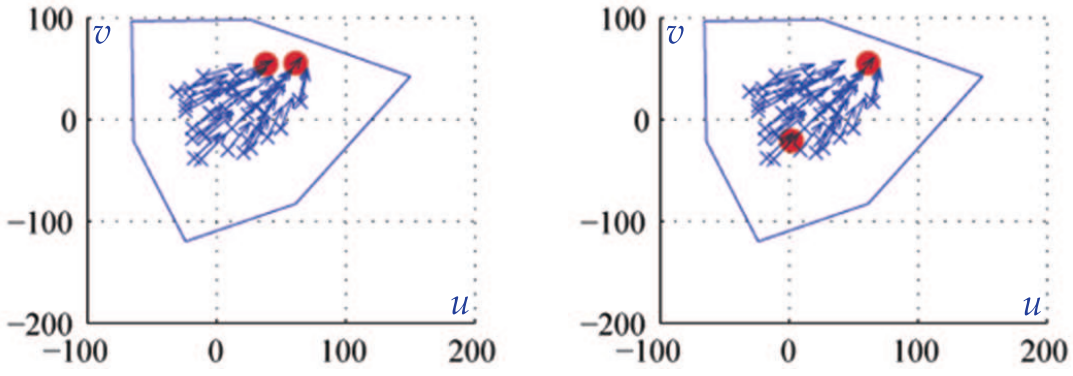

(*a*) (*b*)

Figure 5.17: Position of convergent vectors in a bipartite configuration (red dots). Selected vectors might be close (*a*) or far (*b*) from each other.

classified as appearing transparent when all conditions were included. Our last study showed that short

equiluminant translations were more frequently classified as transparent than longer ones (See **Chapter 4**), and this effect remains constant in our present experiment, but for bipartite field and static filter conditions only. It is clear now that when the filter moves or when the configuration increases in complexity (and thus, the number of translational changes increases), this effect is no longer visible. Our results also show that divergences, shears and rotations tend to appear transparent for short vector length, and especially when motion is added. Moreover, rotations were consistently judged as transparent when variables such as motion and luminance were combined. These results are contrary to the predictions of the GCM. Finally, a necessary condition for divergences to appear transparent is motion associated to configural complexity. A first conclusion may be that several perceptual parameters, different from necessary X-junctions (See **Chapter 3**) and chromatic variations are needed to perceive transparency. We recall that D'Zmura and colleagues, as well as Khang and Zaidi, pointed out that a moving filter has the advantage of covering a larger sample background than a static filter of the same size and noted that filters' movements enhance the perception of a transparent layer [D'Zmura et al., 2000; Khang and Zaidi, 2004]. In our stimuli, the moving filter covers all patches of the background, and in the case of checkerboard configuration, all chromatic variations shown in Figures 5.3 to 5.6 are visible in the stimulus. Thus, any possible ambiguity is removed. This may explain the strong results for the (Motion [Check.]) condition, where convergences and translations appear transparent, while shears do not. But this does not explain why in the same condition, divergences and rotations lead to transparency perception. We expected these two chromatic changes to appear in the 'Not Transparent' classification, such as for shears. Moradi and colleagues tested whether motion transparency facilitates binding and found that the pairing of color and motion paradoxically improved for rapidly alternating surfaces when they added an irrelevant transparency cue [Moradi and Shimojo, 2004]. They concluded that surface segregation precedes binding of color and motion, and combinations of visual attributes can be segregated based on motion or depth transparency. One can be inspired by their conclusion. Divergences and rotations are influenced by perceptual factors such as motion and configural complexity much more than any other chromatic change. One can thus assume that observers segregate the overlay with the help of motion and thus, these chromatic variations appear transparent while they do not when static, and this effect would be less strong for shears. At the same time, X-junctions may have been reinforced since subjective contours are intensified when motion occurs [Chen and Cicerone, 2002].

5.6 Summary

The GCM requires some systematic chromatic changes such as convergences, translations or divergences and excludes rotations or shears. Our results showed that when other perceptual factors such as motion or configural complexity are taken into account, results are less clear cut. Configural complexity helps convergences to appear transparent and interacts with motion to render transparent stimuli generated from rotations. When the overlay created from divergences or translations moves, observers tend to respond 'Transparent' as well, while they respond 'Not Transparent' when static. In general, motion related to vector length lead overlays to appear transparent. Short vector lengths have an effect on transparency perception for shears. This factor associated to luminance elevation influences observers' responses for translations, shears and rotations. A model taking into account these additional factors would be useful to better understand transparency perception. Another parameter is the perception of a transparent overlay in a more realistic scene, that is, surfaces seen behind a filter and its shadow. **Chapter 6** describes such an experiment and discusses the results.

Chapter 6

Effect of Shadow on Transparency Perception

6.1 Introduction

One limitation of models of transparency perception described in **Chapter 3** is that they are not physical models of transparent filters; rather, they are psychophysical models which attempt to describe those changes in surface color which lead to the perception of transparency. The work described below begins an attempt to extend these models to handle transparency perception in complex scenes involving surfaces varying in shape and depth, change in conditions of illumination, and shadow. The work focuses particularly on the effect of shadows on transparency perception.

Shadows in visual scenes can have profound effects on visual perception [Pavani and Castiello, 2004]. They are frequently present when we recognize natural objects, and provide information about illumination and three-dimensional surface shape. Shadows can be classified into two types. An *attached shadow* occurs when a surface turns away from the lighting direction, causing that region to become darker. A *cast shadow* occurs when an object is interposed between a light source and a surface, blocking the illumination from reaching the surface. Cast shadows can be *extrinsic*, i.e. one object casts a shadow onto another; or they can be *intrinsic*, i.e. an object casts a shadow onto itself. All types of shadows tend to be present in real-world scenes, although intrinsic cast shadows are confined to objects with concavities.

Shadows have been shown to be useful for a variety of tasks. Bülthoff and colleagues demonstrated that shadows can cause flat objects to appear three-dimensional, and non-rigid motion to appear rigid [Bülthoff et al., 1994]. Other studies showed that shadows can provide information about three-dimensional shape [Cavanagh and Leclerc, 1989; Norman et al., 2000]. Puerta also showed that they are sufficient to produce stereo depth perception [Puerta, 1989].

We investigate the effects of shadows on transparency in experiments that use simulated displays with both filters and shadows lying in front of surfaces. The shadow is positioned to appear as a shadow cast by the filter onto the surfaces, so signaling the position of a light source. Mamassian and colleagues have shown that shadows were perceptually relevant for the recovery of spatial arrangement (See Figure 6.1) [Mamassian et al., 1998]. We used a similar stimulus configuration to simulate the perception in depth of a transparent filter and the surfaces seen behind it. We varied the properties of filter and shadow systematically in measurements of surface lightness. This study is described in the following Sections: an overview is given in Section 6.2, the experimental method is described in Section 6.3, results are presented in Section 6.4, and discussed in Section 6.5.

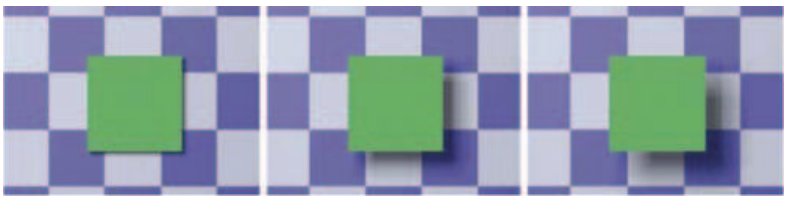

Figure 6.1: Effects of cast shadow position on object location [Kersten et al., 1996]. The square appears farther from the background checkerboard when the cast shadow is detaching from the square. When these images are shown in succession, the square appears to move in depth even though the square is strictly static.

6.2 Overview of the study

This study aims to investigate the effects of shadows on the perception of a transparent filter. A lightness-matching task was proceeded to evaluate how much constancy is shown by the subject among several experimental conditions. Six conditions were tested, in which shadow position, shadow blur, and the blending values of shadow and filter were varied. Comparisons between results for white and black filters were also performed. Our results show that lightness constancy is very high even if surfaces are seen under both filter and shadow. They also show a systematic deviation from perfect constancy in a manner consistent with a perceived additive shift.

6.3 Methods

6.3.1 Display

An asymmetric matching procedure was used to measure the perceived value of surfaces seen to lie through a filter and its shadow. Experiments were performed on a DELL Trinitron monitor connected to a DELL Precision 330. The monitor had a resolution of 1280x960 and ran at 60Hz (brightness setting at 50, and contrast setting at 100). A SpectraScan PR 650 spectroradiometer was used to measure the chromatic properties of the monitor and to measure the non-linear relationship between software input value and monitor output intensity. Gamma correction was used to linearize the input-output relationship. The CIE 1931 standard-observer chromaticities and maximal luminances are presented in Table 6.1. Experimental stimuli were created using OpenGL. True colors were used (32 bits per pixel). All stimuli were displayed in grayscale.

	R	**G**	**B**	**W**
$L_{max}(cd/m^{-2})$	28.9	92.5	15.4	138
x	0.622	0.281	0.151	0.311
y	0.346	0.61	0.066	0.326

Table 6.1: CIE standard observer chromaticity (x, y) and maximum luminance L_{max} of each phosphor R, G and B, and for White.

6.3.2 Stimulus configuration

The stimulus was a square of 22 cm x 22 cm which was viewed at a distance of 57 cm and, so, subtended 22 deg x 22 deg of visual angle. It was made of 121 patches (11 x 11), each of size 2 deg x 2 deg (see Figure 6.2). Patch height and width varied randomly on the interval [2,2.2] deg and were drawn in random order. The resulting occlusion cues minimize the incidence of transparency among the patches themselves, an artifact visible when identically-sized patches of random value are placed in a square array. Each patch had a grayscale value drawn randomly from the interval [0.2, 0.6]. OpenGL was used to transform patch

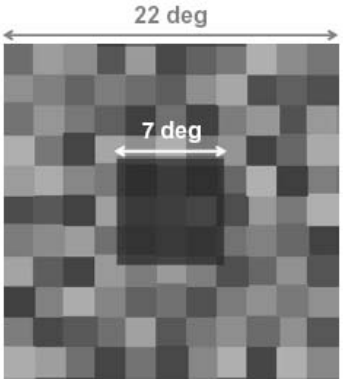

Figure 6.2: Stimulus configuration; see text for details.

intensities to simulate a filter and its shadow; details are provided in the section below. The filter was spatially homogeneous and described a square of size 7 deg x 7 deg. Its position oscillated horizontally at a constant speed, about the center of the display, between position 1.5 deg to the right and 1.5 deg to the left of center. The filter's shadow moved in a similar way; each cycle of oscillation had a duration of 2 sec (0.5 Hz). Shadow position, relative to that of the filter, are described in Section 6.3.4. Subject sat in a dark room.

Filter and Shadow blending

Both filter and shadow were created with OpenGL transparency blending according to the following equations:

$$b_f = \alpha f + (1-\alpha)a, \quad and \quad b_s = \beta s + (1-\beta)a \tag{6.1}$$

where a is the patch's grayscale value, b_f is the grayscale value for the same patch when lying behind the filter, and b_s is the grayscale value for the patch when lying in shadow. The blending of the patch value a with the filter f and the shadow value s is governed by the blending parameters α and β, respectively. When a patch is viewed through both filter and shadow, the displayed value for the patch is given by the following:

$$b_{f,s} = \alpha f + (1-\alpha)(\beta s + (1-\beta)a) \tag{6.2}$$

The shadow was applied in front of surfaces but behind the filter. Thus, two transparent overlays were shown to the subject. A Gaussian taper was applied to the edge of the shadow area to create a penumbra that strengthened the shadow illusion.

6.3.3 Procedure

Asymmetric matching task

An asymmetric matching technique was used to assess the perceived lightness of patches seen to lie behind filter and shadow (Figure 6.3). The display's central patch, which always lay behind the filter, served as the *test square*. The value of the test square was adjusted by observers to match perceived lightness of the patch which served as a *reference square*. The reference square was always seen directly, which neither intervening filter nor shadow; it lays four squares above the test square. In each experimental condition, an observer matched perceived test square lightness to one of six reference square lightnesses. The six possible values for reference square luminance are listed in Table 6.2. Shadow position, shadow blur and shadow

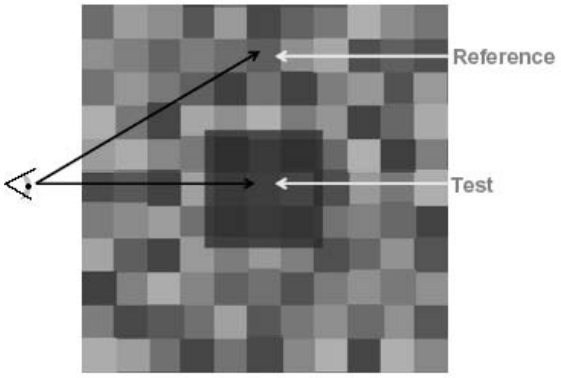

Figure 6.3: Method of adjustment: the observer adjusts lightness of two squares: one under Filter (Test) and one outside the Filter (Reference).

Value	0.2	0.3	0.4	0.5	0.6	0.7
L (cd m^{-2})	27.6	41.4	55.2	69	82.8	96.6

Table 6.2: The six reference values and their luminance.

blending parameter β were varied in the five experimental conditions described in the following section.

6.3.4 Conditions

Condition 1: Compare Filter and Shadow to Filter alone (position a)

In this first condition, filter and shadow lay directly atop one another. Both filter and shadow had sharp borders. This configuration is shown in Figure 6.4 (*a*) and is one of four configurations for filter and shadow that were used in these experiments. The shadow is invisible in this configuration because it is placed directly under the filter. The effect on surface luminance signals of such a combination of filter and shadow is identical physically to that of an equivalent filter - without shadow - of suitably adjusted value and blending parameter.

Condition 2: Compare Filters and Shadows with different positions

In the second condition, two configurations in which the shadow overlays the test surface (Figure 6.4 (*a*, b)) were compared to two in which the shadow did not lie over the test surface (Figure 6.4 (*c*, d)). Shadows

with sharp edges were used. One expects equivalent perceived lightnesses for the two cases in which the shadow lies over the surface (*a*, b) and for the two cases in which it does not (*c*, d).

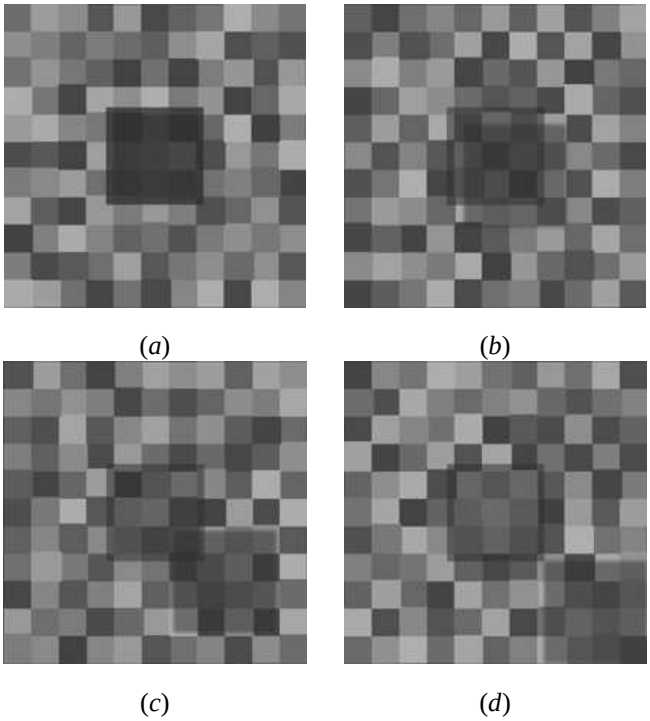

Figure 6.4: Four different shadow positions were tested. (*a*) Shadow and Filter have the same centered position; (*b*) Shadow lies partially under the Filter and covers the test square; (*c*) Shadow lies partially under the Filter but does not cover the test square; (*d*) Shadow and Filter areas do not overlap.

Condition 3: Compare Filters and Shadows to Filter alone (positions b, c)

In the third condition, blurred shadows were used in the configurations shown in Figures 6.4 (*b*) and 6.4 (*c*). In the first, the test surface lies in shadow; in the second, it does not. Differences in perceived lightness should depend on shadow position.

Condition 4: Compare Filters and Shadows with different β

The fourth condition examined lightness constancy in the presence of shadows through a parametric variation a shadow blending value β. Blurred shadows with different β values ($\beta = [0.2, 0.3, 0.4, 0.5, 0.6]$) were displayed under filter. One set shown in Figure 6.4 (*b*) and another set shown in Figure 6.4 (*c*) were presented to the observer.

Condition 5: Compare Filters and Shadows with different blurs

The effect of shadow blur on perceived lightness was examined in the fifth condition. Shadows with three different blurs (*low, medium* or *high* blur) were shown to the observer. One set shown in Figure 6.4 (*b*) and another set shown in Figure 6.4 (*c*) were presented to the observer.

6.4 Results

Lightness-matching data were collected as a function of the luminance of the transparent filter and as a function of the reference luminance. These comparisons provide an estimate of how much constancy is shown by the observer in these tasks. Our results show that lightness constancy is very high even if surfaces are seen under both filter and shadow. They also show a systematic deviation from perfect constancy in a manner consistent with a perceived additive shift.

6.4.1 Results for Condition 1

Our stimulus configuration includes two transparent layers: one filter and one shadow. In condition 1a, we used an invisible shadow with sharp edges that was positioned directly behind the filter (Figure 6.4 (*a*)). In a first experiment, we confirmed that test surface lightness in this configuration is identical to that found with a filter alone, where the filter is chosen to have an equivalent effect on lights from underlying surfaces (See Equation 6.3). The equivalent filter's blending value α' was chosen identical to $\alpha + \beta - \alpha\beta$, which is the blending value in the case where both filter and shadow are present.

$$b_f = \alpha' f + (1 - \alpha')a \tag{6.3}$$

In a second experiment, we used the same invisible shadow configuration (Figure 6.4 (*a*)) to compare lightness perceived through a dark filter and through a light (white) filter. Both experiments help to characterize human lightness constancy for surfaces seen through filter.

Compare Filter and Shadow to Filter alone (position a)

Figure 6.5 shows results for observer PG. Condition parameters are listed in Table 6.3. Constancy is

Positions	**Filter value**	**Filter** α	**Shadow value**	**Shadow** β
(a)	0	0.5	0	0.5
(a)	0	0.75	0	0

Table 6.3: Condition 1a parameters (Shadow position, Filter and Shadow values, Filter and Shadow contrast parameters α and β).

observed for both conditions, with a tendency to overestimate the test value for low reference values (for example, 98% constancy is noted for judging value = 0.2 for both conditions), and to underestimate it for higher reference values (97.7% and 98.7% constancy for judging value = 0.7 for both conditions respectively). 100% constancy is observed for both conditions for reference value = 0.5. We can see that both combinations (Filter + Shadow versus Filter alone) show the same results.

Compare black Filter to white Filter and their Shadows (position a)

Figure 6.6 shows results for observer PG. Condition parameters are listed in Table 6.4. Constancy is observed for Black Filter, with a tendency to overestimate the test value for low reference values and to underestimate it for higher reference values as well. However, if constancy is close to 100% for the first 3 values for White Filter, the observer tends to underestimate the test value, when 95.8% is noted for the reference value 0.7.We can see in Figure 6.6 the influence of the Filter value (Black versus White): the subject has more difficulties to evaluate the test value when the Filter is white and when the reference value is darker. This is possibly due to the high contrast between Filter and Shadow. Best-fit lines through the results in Figures 6.5 and 6.6 have slopes less than unity. This is consistent with observers misestimating the change in contrast caused by the filter, an idea explored more fully below.

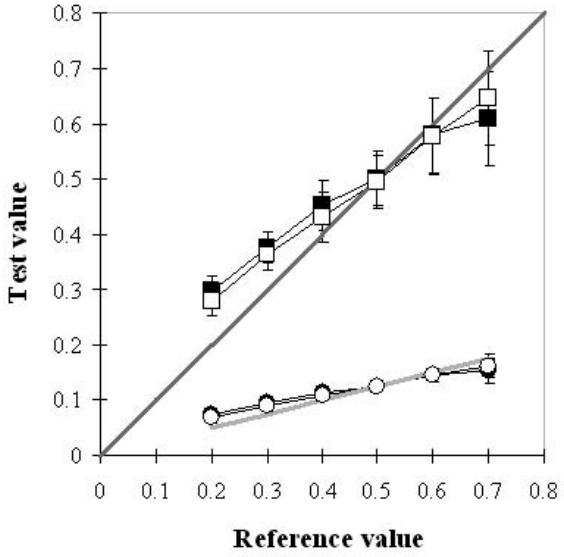

Figure 6.5: Compare Filter and Shadow ($\alpha, \beta = 0.5$; black squares and circles) and Filter ($\alpha = 0.75$; white squares and circles). Results of matching task for PG. Squares represent results in plain view; circles represent results under Filter. A gray diagonal shows the perfect constancy for results in plain view, and a lighter gray line for results under Filter. Ten observations per plotted point were performed.

Positions	Filter value	Filter α	Shadow value	Shadow β
(a)	0	0.5	0	0.5
(a)	0	0.5	0	0.5

Table 6.4: Condition 1b parameters (Shadow position, Filter and Shadow values, Filter and Shadow contrast parameters α and β).

6.4.2 Results for Condition 2

The second condition aims to observe the influence of different Shadow positions on the lightness-matching task. Two experiments were performed. The first examined the effect of shadow position in cases where both filter and shadow covered the test square (Figure 6.4 (*a*, b)). The second examined the effect in cases where the filter but not the shadow lay in front of the test square (Figure 6.4 (*c*, d)).

Compare Filters with different Shadow positions

Two different scenes were presented to the subject: the first scene shows the Shadow with the same position as the Filter (position (*a*)), and the second one shows the Shadow partially under the Filter (position (*b*)), but still covering the test square. Both Shadows had sharp edges. Filter and Shadow blending parameters α, β were identical for both scenes. Figure 6.7 shows results for observer PG. Condition parameters are listed in Table 6.5. Constancy is observed for both conditions, with a tendency to overestimate the test value for low reference values (97.6% constancy is noted for value = 0.2 for position (*a*) and 98.9% for position (*b*)), and to underestimate it for higher reference values (97.7% for both positions). No major difference is noticed

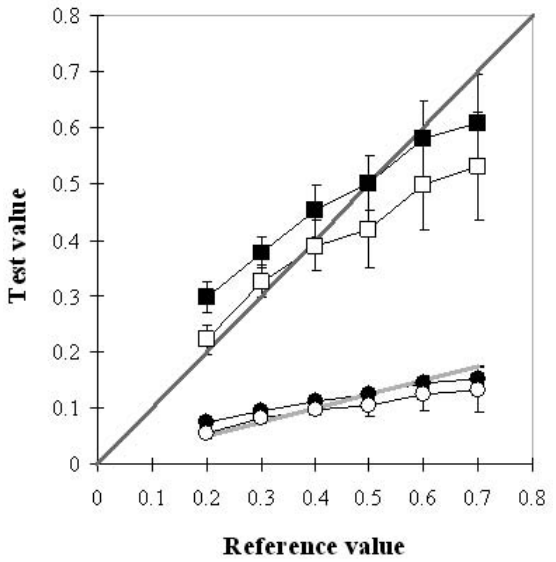

Figure 6.6: Compare Black Filter (black squares and circles) to White Filter (white squares and circles) and their Shadows ($\alpha, \beta = 0.5$). Squares represent results in plain view; circles represent results under Filter. A gray diagonal shows the perfect constancy for results in plain view, and a lighter gray line for results under both Filters. Ten observations per plotted point were performed.

Positions	**Filter value**	**Filter** α	**Shadow value**	**Shadow** β
(a)	0	0.5	0	0.5
(b)	0	0.5	0	0.5

Table 6.5: Condition 2a parameters (Shadow position, Filter and Shadow values, Filter and Shadow contrast parameters α and β).

in subject's answers for these two different Shadow positions. The equivalence of the lightness estimates suggests that the effects of the visible shadow with sharp edges (Figure 6.4 (*b*)) are captured wholly by an equivalent filter.

Compare Filters with different positions of blurred Shadows

This second experiment compared lightness estimates in cases where a shadow was visible but did not lie over the test square (Figure 6.4 (*c*, d)). The shadows in both configurations had blurred edges. Filter and Shadow blending parameters α, β were identical for both scenes. Figure 6.8 shows results for observer PG. Condition parameters are listed in Table 6.6. Constancy is observed for both positions, with a tendency to underestimate the test value for higher reference values (93.9% and 93.3% for both conditions respectively). For this condition, no overestimation of the test value is found for lower reference values, compared to Condition 2a.

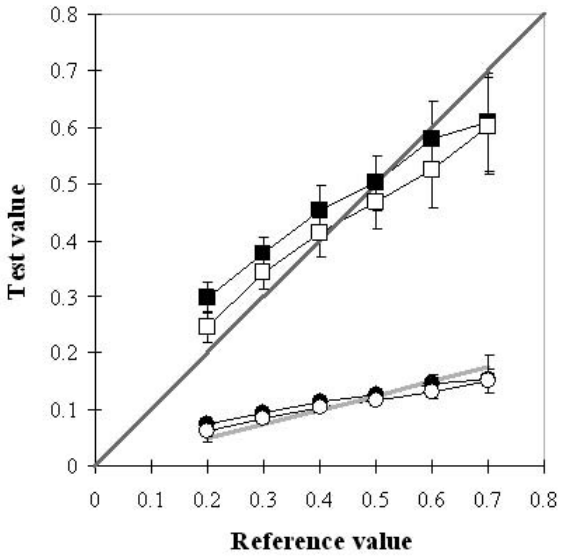

Figure 6.7: Compare Filter with Shadow position (*a*) (black squares and circles) to Filter with Shadow position (*b*) (white squares and circles) ($\alpha, \beta = 0.5$). Results of matching task for PG. Ten observations per plotted point were performed.

Positions	Filter value	Filter α	Shadow value	Shadow β
(c)	0	0.5	0	0.5
(d)	0	0.5	0	0.5

Table 6.6: Condition 2b parameters (Shadow position, Filter and Shadow values, Filter and Shadow contrast parameters α and β). Shadows were equally blurred.

6.4.3 Results for Condition 3

In this condition we compared surface lightness estimates found when filter and visible shadow lie in front of the test surface (Figure 6.4 (*b*)) to those found when the visible shadow was present but only the filter lays in front of the test surface (Figure 6.4 (*c*)). The filter in the latter configuration (*c*) was chosen to provide the same effects on surface values as those found when both filter and shadow overlay the surface (*b*) (See Equation 6.3). A filter with contrast parameter $\alpha = 0.5$ was compared to a filter with $\alpha = 0.75$ using shadow positions (*b*) and (*c*), respectively. Figure 6.9 shows results for observer PG. Condition parameters are listed in Table 6.7. Constancy is observed for both conditions, with a small tendency to overestimate

Positions	Filter value	Filter α	Shadow value	Shadow β
(b)	0	0.5	0	0.5
(c)	0	0.75	0	0.5

Table 6.7: Condition 3 parameters (Shadow position, Filter and Shadow values, Filter and Shadow contrast parameters α and β). Shadows were equally blurred.

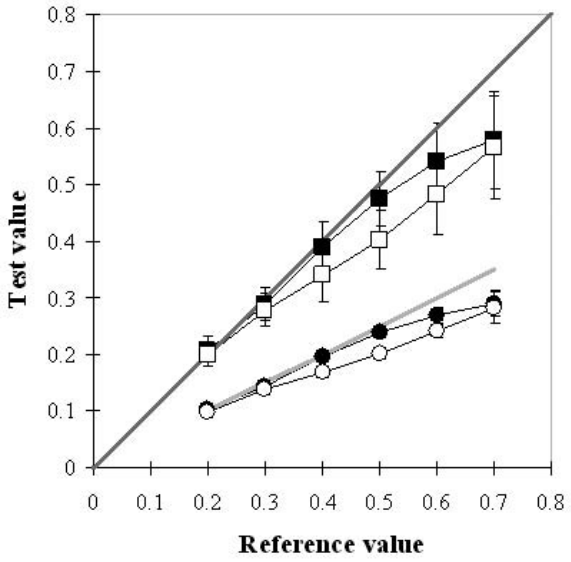

Figure 6.8: Compare Filter with Shadow position (*c*) (black squares and circles) to Filter with Shadow position (*d*) (white squares and circles) ($\alpha, \beta = 0.5$). Results of matching task for PG. Ten observations per plotted point were performed.

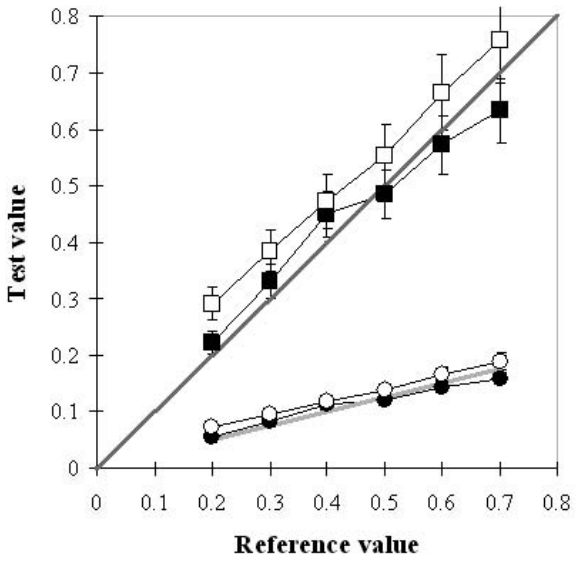

Figure 6.9: Compare Filter with Shadow position (*b*) (black squares and circles; $\alpha, \beta = 0.5$) to Filter with Shadow position (*c*) (white squares and circles; $\alpha = 0.75, \beta = 0.5$). Results of matching task for PG. Ten observations per plotted point were performed.

and underestimate the test value for higher reference values with position (*b*) (99.5% and 98.3% for first and last values). However, the subject always overestimates the test value with Shadow in position (*c*), with

constancy situated in a range of 97.8% to 98.6%. The results suggest that the effect of the blurred shadow on test surface lightness in configuration (*b*) are identical to those of an equivalent filter.

6.4.4 Results for Condition 4

In this condition, we measured the effects of varying filter value (black versus white) and of varying the shadow blending parameter β. Four experiments were performed. The first used a black filter with a shadow of varying blending parameter in configuration (*c*), where the shadow lays under the filter but did not lie atop the test surface. The second used a white filter. The third and fourth experiments used black and white filters, respectively, with the shadow in configuration (*b*), where the shadow lays under the filter and also lays atop the test surface. The results show a high degree of lightness constancy in all cases, with the shadow blending parameter having a small effect. It was found more difficult to estimate lightness when a white filter (but not the shadow) overlays the test surface.

Compare Black Filter with different Shadows (when β varies) in position (*c*)

These first results compare subject's answers according to different Shadow blending values for a Black Filter when Shadow does not lay on the test square. A filter with contrast parameter $\alpha = 0.5$ was compared with different Shadow blending values ($\beta = 0.2, 0.3, 0.4, 0.5, 0.6$). Figure 6.10 shows results for observer PG. Condition parameters are listed in Table 6.8. Constancy is observed for all choices of Shadow blending

Positions	**Filter value**	**Filter α**	**Shadow value**	**Shadow β**
(b, c)	0, 1	0.5	0	0.2
(b, c)	0, 1	0.5	0	0.3
(b, c)	0, 1	0.5	0	0.4
(b, c)	0, 1	0.5	0	0.5
(b, c)	0, 1	0.5	0	0.6

Table 6.8: Condition 4 parameters (Shadow position, Filter and Shadow values, Filter and Shadow contrast parameters α and β). Shadows were equally blurred.

parameter β, with a tendency to overestimate the test value for lower reference values and to underestimate it for higher reference values. See Table 6.9 for an example. This suggests, just as for the results of Condition

β	0.2	0.3	0.4	0.5	0.6
Constancy ($\%$)	96.2	96.3	95.5	93.9	92.7

Table 6.9: $\%$ constancy under Filter for reference value 0.7 according to β parameter. The accuracy gently decreases when β increases.

1 and 2, that observer misestimates the change in contrast caused by the filter. The small effect of shadow blending value is curious, as the shadow does not lie atop the test surface.

Compare White Filter with different Shadows (when β varies) in position (*c*)

These results compare subject's answers according to different Shadow blending values for a White Filter when Shadow does not lay on the test square. Filter with contrast parameter $\alpha = 0.5$ was compared with different Shadow blending values ($\beta = 0.2, 0.3, 0.4, 0.5, 0.6$). Figure 6.11 shows results for observer PG.

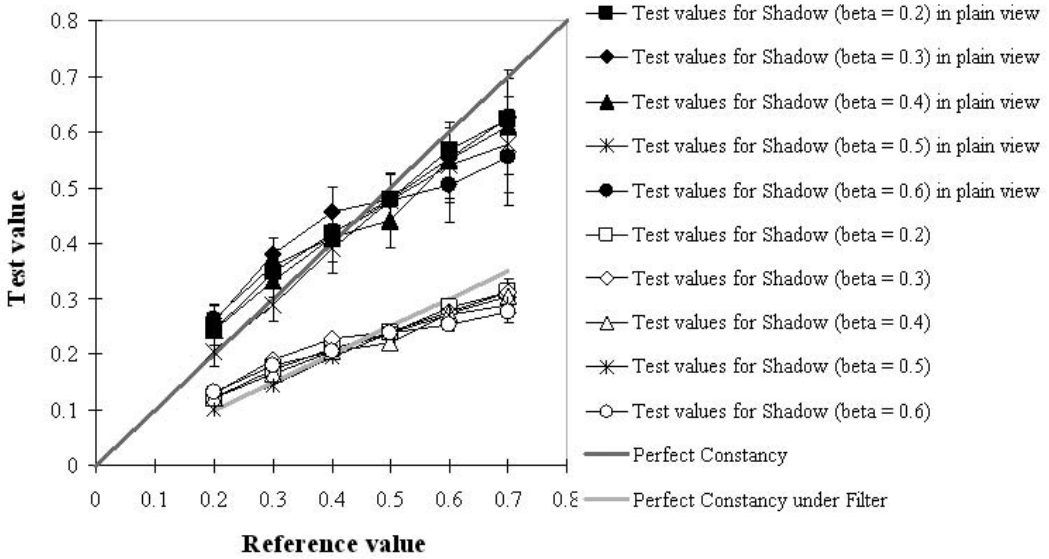

Figure 6.10: Results for Condition 4a. Compare Filter with Shadows with different β in position (c). Results of matching task for PG. Black figures represent results in plain view; white figures represent results under Black Filter. Ten observations per plotted point were performed.

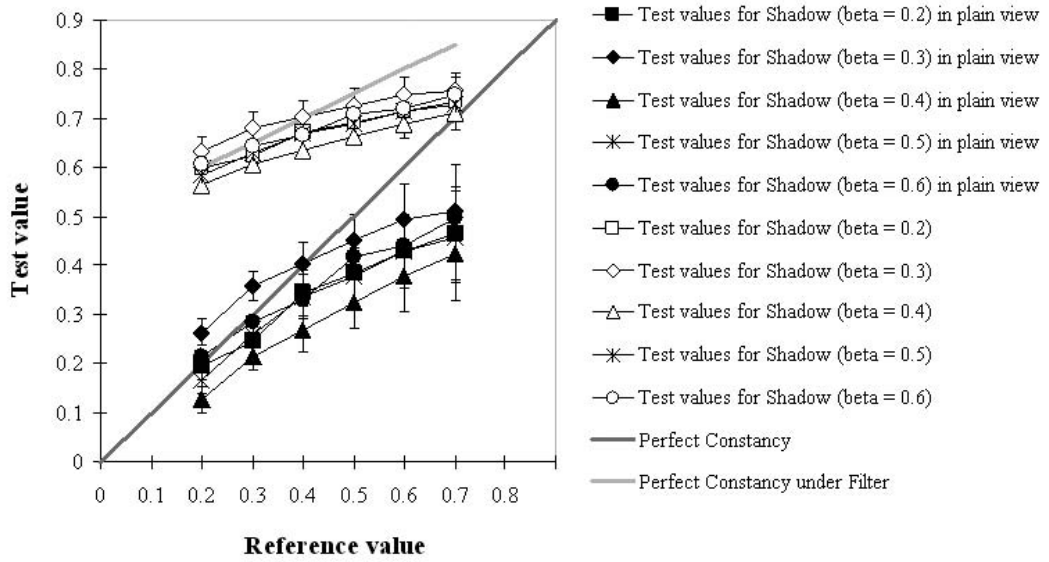

Figure 6.11: Compare Filter with Shadows with different β in position (c). Results of matching task for PG. Black figures represent results in plain view; white figures represent results under White Filter. Ten observations per plotted point were performed.

Condition parameters are listed in previous Table 6.8, with Filter value = 1. Constancy is observed for all choices of Shadow β. The results show a relatively strong tendency to underestimate test value for

lighter reference values and a weak tendency to overestimate test values for darker reference values (See Table 6.10 for examples). This suggests that the observer misestimated the way in which the filter altered

β	0.2	0.3	0.4	0.5	0.6	**Reference value**
Constancy (%)	99.7	96.8	96.3	98.3	99.2	**0.2**
	88.3	90.6	86.1	87.9	89.9	**0.7**

Table 6.10: % constancy under Filter for reference values 0.2 and 0.7 according to β parameter. The accuracy highly decreases when the reference value increases, independently of β parameter.

surface contrast. The spread among results found with different choices for shadow β do not suggest the presence of an effect of β. Figure6.11 shows that the relationship between value and shadow β is not systematic. Rather, the spread among the results seems due more to the increased difficulty found in the asymmetric matching task when a White filter is used.

Compare Black Filter with different Shadows (when β varies) in position (*b*)

In this experiment we compared the dependance of lightness estimates on shadow blending parameter β in configuration (*b*), for which both filter and shadow lie atop the test square (Figure 6.4 (*b*)). A black filter with contrast parameter $\alpha = 0.5$ was compared with different Shadow β ($\beta = 0.2, 0.3, 0.4, 0.5, 0.6$) in configuration (*b*). Figures 6.12 and 6.13 show results for observer PG. Condition parameters are listed in previous Table 6.8, with Filter value = 0.0 (a black filter). In Figure 6.12, we can see that constancy is

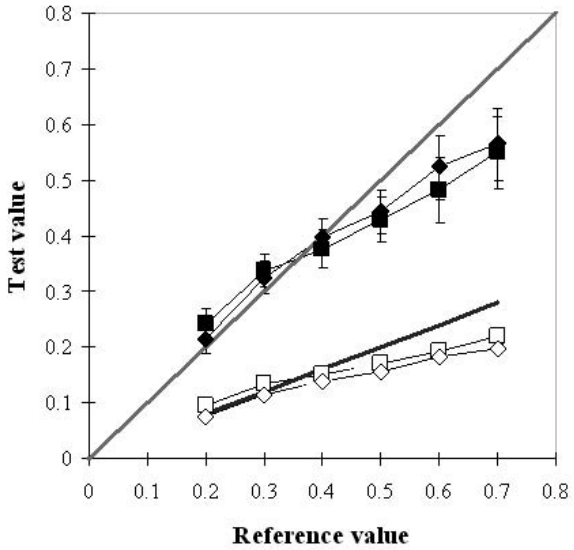

Figure 6.12: Compare Black Filter with Shadows with different β in position (*b*). Results of matching task for PG. Black figures represent results in plain view; white figures represent results under Black Filter. Squares represent Shadow with $\beta = 0.2$; Diamonds represent Shadow with $\beta = 0.3$; Perfect constancy under Filter is shown by a black diagonal for Squares and by a white diagonal for Diamonds. Ten observations per plotted point were performed.

better for low values and tend to be underestimated for higher values, when $\beta = 0.2$ (94% for reference

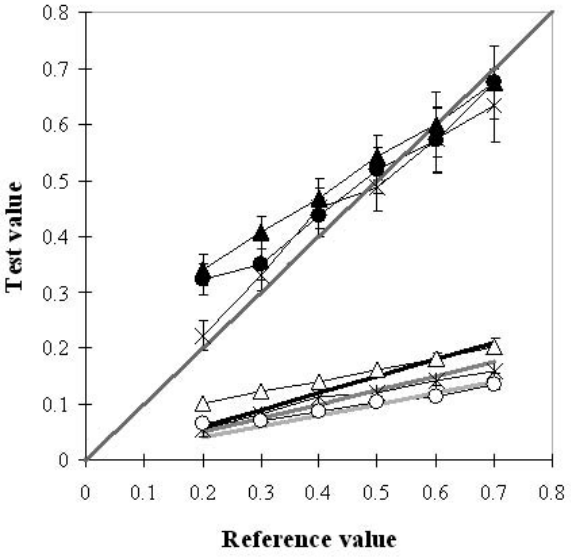

Figure 6.13: Compare Black Filter with Shadows with different β in position (*b*). Results of matching task for PG. Black figures represent results in plain view; white figures represent results under Black Filter. Triangles represent Shadow with $\beta = 0.4$; Stars represent Shadow with $\beta = 0.5$; Circles represent Shadow with $\beta = 0.6$; Perfect constancy under Filter is shown by a black diagonal for Triangles, by a white diagonal for Stars and by a gray diagonal for Circles. Ten observations per plotted point were performed.

value = 0.2), and when $\beta = 0.3$ (95.3% for reference value = 0.2). However, when $\beta = 0.4$, the results tend to be inverted (Figure 6.13): constancy is better for higher values (for reference value = 0.6, 100% when $\beta = 0.4$, 99.3% when $\beta = 0.5$ and 99.4% when $\beta = 0.6$). Constancy is observed for all results despite any β variation, even if shadow overlays the test square.

Compare White Filter with different Shadows (when β varies) in position (*b*)

Subject's answers were compared according to different Shadow blending values for a White Filter when Shadow lays on the test square. Filter with contrast parameter $\alpha = 0.5$ was compared with different Shadow blending values ($\beta = 0.2, 0.3, 0.4, 0.5, 0.6$) in Shadow position (*b*). Figures 6.14 and 6.15 show results for observer PG. Condition parameters are listed in previous Table 6.8, with Filter value = 1 and Shadow position (*b*). In Figures 6.14 and 6.15, we can see that accuracy of the observer is decreased when the reference value increases, despite any β parameter (See Table 6.11 for examples). Constancy is observed

β	0.2	0.3	0.4	0.5	0.6	**Reference value**
Constancy (%)	99.9	95.3	99.7	98.7	99.2	**0.2**
	91.3	91.8	94.6	93	97.8	**0.7**

Table 6.11: % constancy under Filter for reference values 0.3 and 0.7 according to β parameter. The accuracy highly decreases when the reference value increases, independently of β parameter, except for $\beta = 0.6$.

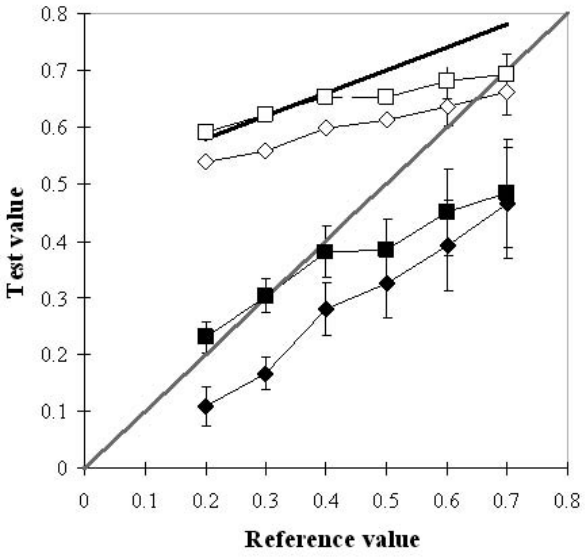

Figure 6.14: Compare White Filter with Shadows with different β in position (*b*). Results of matching task for PG. Black figures represent results in plain view; white figures represent results under White Filter. Squares represent Shadow with $\beta = 0.2$; Diamonds represent Shadow with $\beta = 0.3$; Perfect constancy under Filter is shown by a black diagonal for Squares and by a white diagonal for Diamonds. Ten observations per plotted point were performed.

for all results despite any β variation, even if shadow overlays the test square, but still the fact that Filter is White makes the task more difficult for the subject.

6.4.5 Results for Condition 5

This last condition compares scenes with different Shadow blurs. Two additional parameters as Shadow position ((*c*) or (*b*)) and Filter values (Black or White) are observed as well.

Compare Black Filter with different blurred Shadows in position (*c*)

These results compare subject's answers according to different Shadow blurs (low, medium or high) for a Black Filter when Shadow does not lay on the test square. Black Filter with contrast parameter $\alpha = 0.5$ was compared with different Shadow blurs. Figure 6.16 shows results for observer PG. Condition parameters are listed in Table 6.12. In Figure 6.16 we can see that accuracy of the observer is decreased when the

Positions	Filter value	Filter α	Shadow value	Shadow β	Shadow blur
(b, c)	0, 1	0.5	0	0.5	**low**
(b, c)	0, 1	0.5	0	0.5	**medium**
(b, c)	0, 1	0.5	0	0.5	**high**

Table 6.12: Condition 5 parameters (Shadow position, Filter and Shadow values, Filter and Shadow contrast parameters α and β). Shadows were differently blurred.

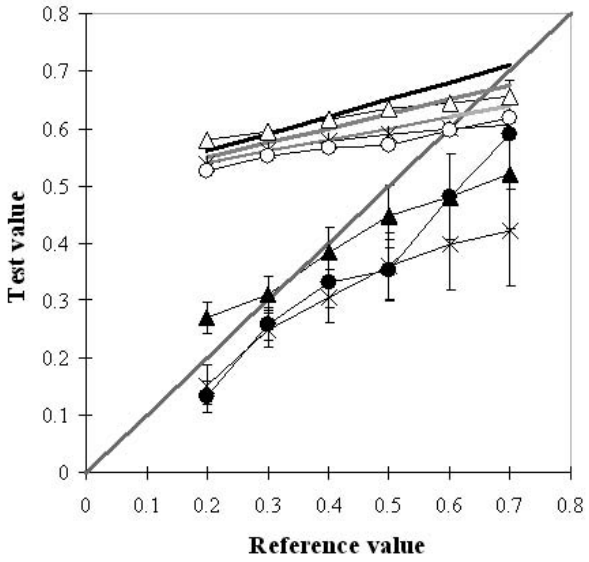

Figure 6.15: Compare White Filter with Shadows with different β in position (*b*). Results of matching task for PG. Black figures represent results in plain view; white figures represent results under White Filter. Triangles represent Shadow with $\beta = 0.4$; Stars represent Shadow with $\beta = 0.5$; Circles represent Shadow with $\beta = 0.6$; Perfect constancy under Filter is shown by a black diagonal for Triangles, by a white diagonal for Stars and by a gray diagonal for Circles. Ten observations per plotted point were performed.

reference value increases, despite any blur parameter (See Table 6.13 for examples). There is no effect of

Blur	Low	Medium	High	**Reference value**
Constancy (%)	99.7	99.3	98.4	**0.2**
	93.9	91.1	91.9	**0.7**

Table 6.13: % constancy under Filter for reference values 0.2 and 0.7 according to blur parameter. The accuracy decreases when the reference value increases, independently of blur parameter.

blur parameter on the lightness-matching task.

Compare White Filter with different blurred Shadows in position (*c*)

These results compare subject's answers according to different Shadow blurs (low, medium or high) for a White Filter when Shadow does not lay on the test square. White Filter with contrast parameter $\alpha = 0.5$ was compared with different Shadow blurs. Figure 6.17 shows results for observer PG. Condition parameters are listed in Table 6.12, with Filter value = 1. In Figure 6.17 we can see that accuracy of the observer is decreased when the reference value increases, despite any blur parameter (See Table 6.14 for examples). We can note that this decrease is bigger for White Filter than for Black Filter. No blur parameter was found, a misperception of contrast alteration is observed.

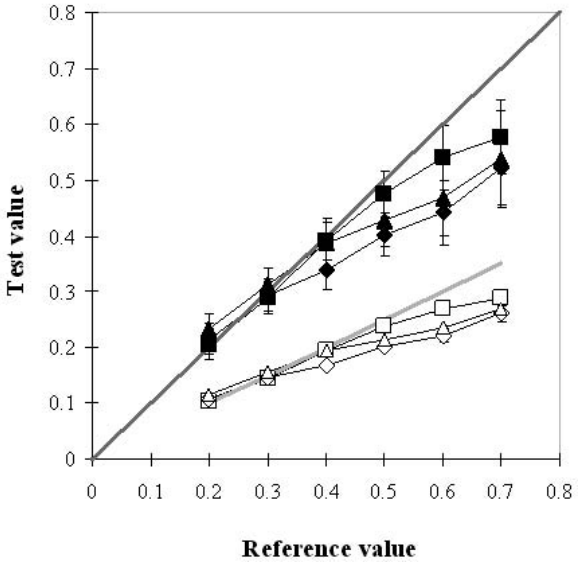

Figure 6.16: Compare Black Filter with Shadows with different blurs in position (*c*). Results of matching task for PG. Black figures represent results in plain view; white figures represent results under Black Filter. Squares represent low blur; Diamonds represent medium blur and Triangles high blur. Ten observations per plotted point were performed.

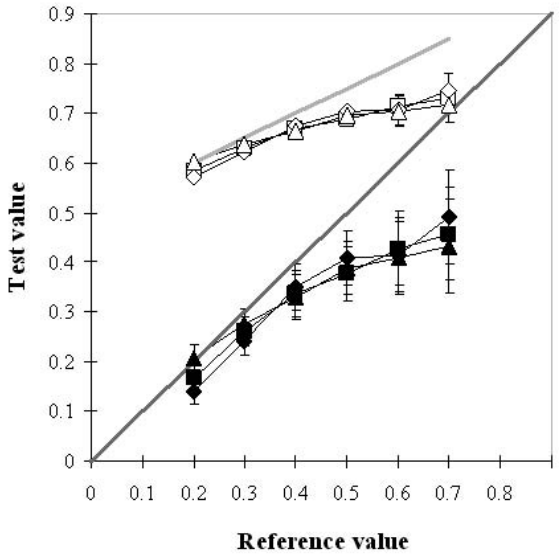

Figure 6.17: Compare White Filter with Shadows with different blurs in position (*c*). Results of matching task for PG. Black figures represent results in plain view; white figures represent results under White Filter. Squares represent low blur; Diamonds represent medium blur and Triangles high blur. Ten observations per plotted point were performed.

Blur	Low	Medium	High	**Reference value**
Constancy (%)	98.3	97	99.7	**0.2**
	87.9	89.5	86.7	**0.7**

Table 6.14: % constancy under Filter for reference values 0.2 and 0.7 according to blur parameter. The accuracy decreases when the reference value increases, independently of blur parameter.

Compare Black Filter with different blurred Shadows in position (*b*)

Here we compared answers according to different Shadow blurs (low, medium or high) for a Black Filter when Shadow overlays the test square. Black Filter with contrast parameter $\alpha = 0.5$ was compared with different Shadow blurs in Shadow position (*b*). Figure 6.18 shows results for observer PG. Condition parameters are listed in Table 6.12, with position (*b*). In Figure 6.18, the accuracy of the observer is

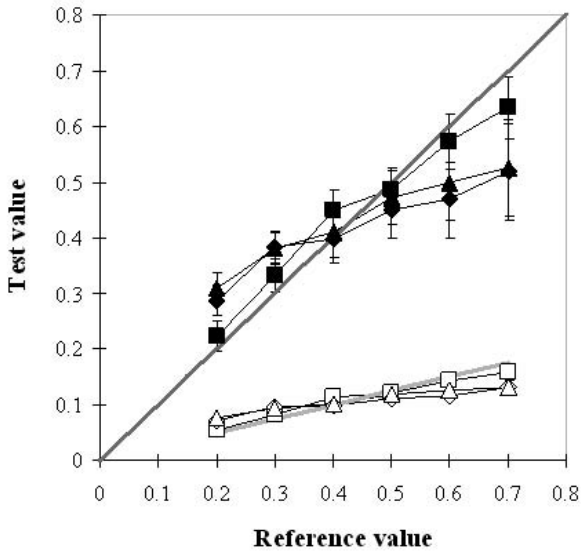

Figure 6.18: Compare Black Filter with Shadows with different blurs in position (*b*). Results of matching task for PG. Black figures represent results in plain view; white figures represent results under Black Filter. Squares represent low blur; Diamonds represent medium blur and Triangles high blur. Ten observations per plotted point were performed.

decreased when the reference value increases, except for low blur parameter (See Table 6.15 for examples). When the Shadow overlays the test square, we see a gentle effect of the blur parameter.

Compare White Filter with different blurred Shadows in position (*b*)

We compared answers according to different Shadow blurs (low, medium or high) for a White Filter when Shadow overlays the test square. White Filter with contrast parameter $\alpha = 0.5$ was compared with different Shadow blurs in Shadow position (*b*). Figure 6.19 shows results for observer PG. Condition parameters are listed in Table 6.12, with position (*b*) and Filter value = 1. In Figure 6.19, the accuracy of the observer is decreased when the reference value increases, except for low blur parameter (See Table 6.16 for examples).

Blur	Low	Medium	High	Reference value
Constancy (%)	98.7	100	99.8	**0.4**
	98.3	95.5	95.6	**0.7**

Table 6.15: % constancy under Filter for reference values 0.4 and 0.7 according to blur parameter. The accuracy gradually decreases when the reference value increases for medium and high blur parameters.

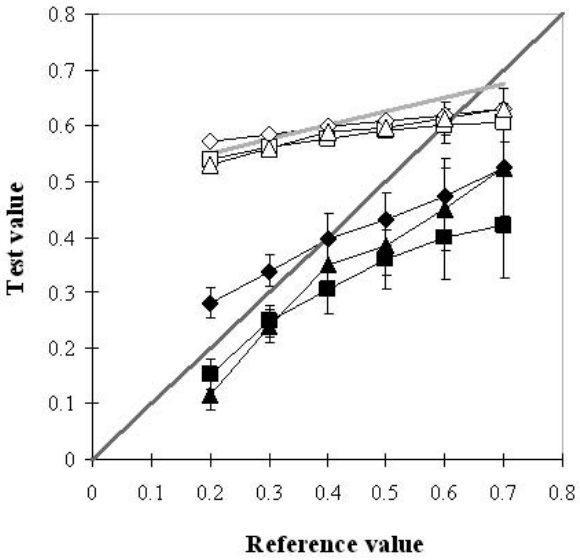

Figure 6.19: Compare White Filter with Shadows with different blurs in position (*b*). Results of matching task for PG. Black figures represent results in plain view; white figures represent results under White Filter. Squares represent low blur; Diamonds represent medium blur and Triangles high blur. Ten observations per plotted point were performed.

When the Shadow overlays the test square, we see no effect of the blur parameter when the Filter is White.

Blur	Low	Medium	High	Reference value
Constancy (%)	97.7	99.9	98.7	**0.4**
	93	95.6	95.6	**0.7**

Table 6.16: % constancy under Filter for reference values 0.4 and 0.7 according to blur parameter. The subject is less accurate with low blur parameter.

6.5 Discussion

The primary result of this study is that lightness constancy for surfaces seen through both achromatic filter and shadow is very high. The study used simulated displays, on a computer graphic monitor, in which both

filter and shadow are made to oscillate side-to-side, synchronously and in parallel. The result is found using an asymmetric matching task, which evokes judgments of the lightness of a test surface patch, seen through filter and possibly shadow, relative to that of a reference patch seen in plain view.

When both filter and shadow lie over the test surface, the observer's settings for the test value match very closely those of the reference patch being matched. This is shown most clearly in the results of Condition 2 (Figure 6.7); the two upper sets of data lie nearly along the diagonal line, which indicates perfect lightness constancy.

Results from this condition illustrate a second general finding of this study: results deviate systematically from perfect constancy in a manner consistent with a perceived additive shift. Reference surfaces lighter than the display mean value tend to be matched by somewhat darker test surfaces seen through filter and shadow, while reference surfaces darker than the display mean value tend to be matched by somewhat lighter test surfaces. The best-fit lines through such results, illustrated by the two sets of data at the bottom of Figure 6.7, have positive, non-zero, intercepts (the gray line shown was constrained to have an intercept of zero). One fits such results best by supposing that the perceived effect of a filter involves both a multiplicative term λ and an additive term $\mathbf{t}$:

$$\mathbf{b} = \lambda\mathbf{a} + \mathbf{t} \tag{6.4}$$

where the perceived value $\mathbf{b}$ of the surface viewed through a filter is related to its value $\mathbf{a}$, when perceived in plain view, through scaling by multiplier λ and by adding shift $\mathbf{t}$ (with $\mathbf{a}, \mathbf{b}, \mathbf{t} = [R, G, B]$).

Such a model for lightness perception is related closely to Metelli's episcotister model [Metelli, 1974] and to what Adelson terms an atmospheric transfer function [Adelson, 2000]; the trichromatic extension to this model was introduced by DaPos [Pos, 1989]. The results of Conditions 2 and 3 show that this model works in the case where both filter and shadow are perceived to lie over a surface, or the filter alone lies over the surface, and that independent estimates of filter and shadow lightness properties may be combined perceptually to generate accurate estimates of their joint effects.

The results also show that the effects of two manipulations which might be thought to affect the perceived depth of the filter, relative to that of the surfaces, had smaller effects on lightness judgments than expected. In Condition 2a, one might expect a greater perceived depth for the filter when the shadow is displaced away from the test surface (Figure 6.4; see also Condition 5, Figure 6.19), following the result of Kersten and colleagues [Kersten et al., 1996]. The greater perceived distance, in turn, might be thought to influence the observer's perception of the relative amounts of direct and filtered illumination received by underlying surfaces: a filter of identical physical effect, seen to lie far in front of the surfaces, may well be perceived as intrinsically darker than a filter closer to the surfaces, because the surfaces would receive more direct illumination in the former case. However, the results show no such effect. It may well be the case that a display in which filter distance is perceived to be varying, as in the original demonstration, is required for lightness effects to result.

Likewise, increasing the size of the shadow penumbra is a cue to increasing distance between filter and surfaces. Increasing shadow penumbra size may cause a filter more opaque and so altering asymmetric matches (Condition 5). There is a small trend towards darker settings with increasing shadow blur, which can be seen in Figure 6.16 (Figure 6.16, open symbols). The trend is weak, however. Not surprisingly, this trend is not found for "white" shadows, which fail to appear like shadows.

6.6 Summary

Lightness constancy is strong when surfaces are viewed through a transparent filter and a shadow. The results suggest that changes in shadow position, shadow blur or shadow blending parameter do not cause any appreciable change in an observer's ability to estimate lightness accurately. The results also suggest that the asymmetric matching task is difficult to perform when a white filter lies atop a dark test surface, an effect due possibly to the high contrast between filter and shadow. A systematic deviation from perfect constancy is observed as well, showing consistency with a perceived additive shift. A future study will use a

stereo display to produce a stronger illusion of depth and thus will increase the perceived distance between filter and its shadow.

Chapter 7

Conclusions

7.1 Summary of achievements

This thesis investigated the problem of defining an accurate model of transparency perception. This phenomenon shows that the visual system is able to decompose the retinal image into a background and a transparent-layer component. In other words, the visual system is able to identify as a single object a surface seen both in plain view and through a transparent overlay. It is also able to define the color of the filter itself. This ability fascinates many researchers, who emphasized its relation to different color phenomena, such as color constancy. However, despite the growing number of studies on this topic, the underlying mechanisms are still not well understood.

In the literature, several models of perceptual transparency have studied the relation of four colors at an *X-junctions*, one important source of information used by the visual system to infer transparency and to determine the parameters of the transparent layer. Investigating perceptual transparency is also challenging due to its interactions with different visual phenomena, but the most intensively studied conditions for perceptual transparency are those involving achromatic luminance and chromatic constraints. Two types of psychophysical models refer to different physical situations with different image-generation processes, the first one involving *additive* color mixtures, the second one resulting from *subtractive* color mixtures.

The General Convergence Model (GCM) combines both additive and subtractive color mixtures in showing that systematic chromatic changes in a linear color space, such as translation and convergence (or the combination of both), lead to perceptual transparency. This model emphasizes the fact that perceptual models must be considered rather than physical models, since it takes into account equiluminant transparent surfaces, absent in the real world. It also shows relations to color constancy phenomena. Some authors compared it to other models, such as the *Computational Model* [Nakauchi et al., 1999] or the *Invariant cone-excitation ratios* [Westland and Ripamonti, 2000], each of which was shown to be a special case of the GCM. However, this model seems to be a necessary but not a sufficient condition for transparency perception, since complementary hues appearing in the overlay cannot be perceived as transparent and some systematic deviations from the GCM related to subtractive mixtures are found. A first motivation of this thesis was to evaluate and define situations which tax the generality of the GCM.

We generated systematic chromatic changes consistent or not with the GCM, in adding several conditions, such as the magnitude of the chromatic change, as well as its elevation from the equiluminant plane. The stimulus was a simple bipartite field partially overlaid by a square. Observers classified each overlay as transparent or not. The main results support the GCM in showing that convergence and translation (except when equiluminant) lead to the perception of transparency, while shear and divergence do not. Large equiluminant translations were less often judged as transparent, but were consistent with the above observations concerning color changes crossing hue boundaries. However, other systematic chromatic changes, such as small shears and divergences were also classified as transparent, in contradiction with the GCM. Thus, vector length must be considered. This argument is developed in **Chapter 5** of the thesis.

A second experiment raises the question as to whether motion influences the perception of transparency. Five different systematic chromatic changes were generated. Additional parameters, such as configural complexity, luminance levels, magnitude of the chromatic change and shift directions were tested. Bipartite and checkerboard like stimuli configurations were shown to the observers. Vector lengths were defined in a more uniform color space to control them. The main results showed that observers' responses are influenced by each of the above cited parameters. Convergences appear significantly more transparent when motion is added for bipartite configuration, or when they are generated in a checkerboard configuration. The same effect with large equiluminant changes observed in the previous experiment is found for convergences and translations in the bipartite configuration: the resulting overlay tends to appear opaque. This effect is removed when the overlay moves. Shears are described as opaque, except when short vector lengths are combined with motion: the overlay tends to be transparent. Divergences are strongly affected by motion and vector lengths, and rotations by a combination of checkerboard configuration with luminance level and vector length. Thus, high order interactions were found which involves some of the experimental parameters. These results question the generality of the GCM.

Finally, the third experiment aimed to investigate the effects of shadows on the perception of a transparent filter. Shadows in visual scenes have a strong influence on visual perception. They are frequently present when we recognize natural objects, and they provide information about illumination and surface shape. Thus, shadow was used as three-dimensional cues to explore its effect on perceptual transparency. A lightness-matching task was conducted to evaluate how much constancy is seen by the subject among six experimental conditions, in which shadow position, shadow blur, shadow and filter blending values were varied. Comparisons between white and black filters were achieved as well. The results showed that lightness constancy is very high even if surfaces were seen under both filter and shadow. A systematic deviation from perfect constancy in a manner consistent with a perceived additive shift was also observed. Because the GCM includes additive mixture and is related to color and lightness constancy, these results are promising and may be explained ultimately by this model.

7.2 Perspectives

We have shown that several parameters including motion and configuration influence perceptual transparency. Three-dimensional cues such as shadow did not show any effect on the perception of a transparent overlay. Each proposed experiment can be independently extended and improved. Some directions for further work are proposed below.

- It has been observed in **Chapter 5** that motion has an effect on the systematic chromatic changes. In the experiment, the moving overlay kept the same circular movement for all trials with a speed of 120 deg./s. A natural extension of this study would be to consider different speeds, and see whether these effects are still visible.

- In the same experiment, various luminance levels were dispatched for surrounding bipartite (bipartite configuration) and for surrounding patches (checkerboard configuration) in the stimulus display. They were shuffled as shown in Figure 7.1. However, when they are arranged so as to create a smooth transition of luminance levels (similarly to the arrangement of color shuffle, by J. Koenderink [Hoffman, 1998]), overlays appear more distinguishable (See Figure 7.2; prints of Figures may not be representative about their effective appearance on a calibrated monitor). In this condition, the visual system may have more facilities to extract the overlay from the background. An experiment comparing both conditions (*shuffle* versus *homogeneous*) with respect to the different chromatic changes would be useful to assert this assumption.

- It has also been pointed out in **Chapter 5** that configural complexity plays a role according to the different chromatic shifts presented to the observer. Different interpretations may be possible for identical chromatic changes applied differently on the configuration display. For example, Figure 7.3

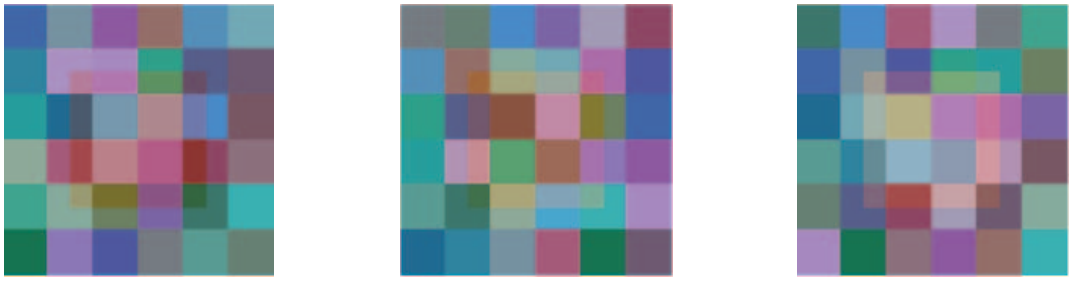

(*a*) (*b*) (*c*)

Figure 7.1: Checkerboard configuration with non homogeneous luminance arrangements. (*a*) Filter condition; (*b*) Equiluminant condition; (*c*) Illuminant condition.

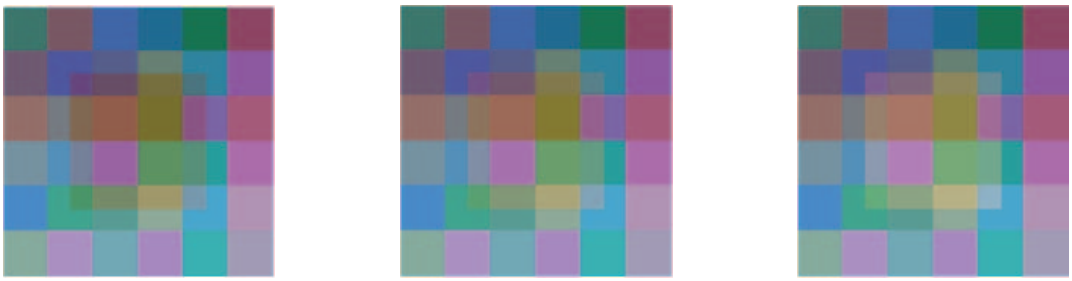

(*a*) (*b*) (*c*)

Figure 7.2: Checkerboard configuration with homogeneous luminance arrangements. (*a*) Filter condition; (*b*) Equiluminant condition; (*c*) Illuminant condition. All filters appear more distinguishable than those presented in Figure 7.1.

shows two different configurations with two different chromatic changes such as translations and shears. The resulting stimuli generated from translations show equivalent transparent overlays. However, for shears, compared to Figure 7.3 (*c*), a certain coherence is observed in Figure 7.3 (*d*), such as a cast shadow seen behind an object. Additional experiments must be performed with different configurations with respect to chromatic changes to evaluate possible resulting interpretations.

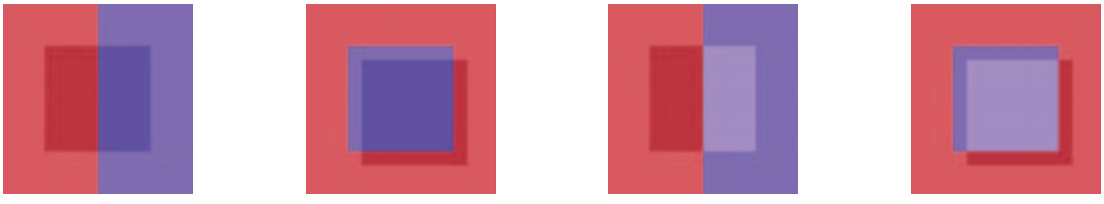

(*a*) (*b*) (*c*) (*d*)

Figure 7.3: Resulting stimuli generated from translations and shears with two different configurations. (*a*) Filter created from translations. (*b*) Filter created from translations, but with a different configuration. (*c*) Resulting stimulus from shears. (*d*) Resulting stimulus from shears, but with a different configuration. A cast shadow seems to appear behind a square object.

- A similar experiment as above involving configural interpretation would be to use stimuli such as shown in Figure 7.4. Implicit X-Junctions are created when the distribution of squares in Figure 7.4 (*d*) is homogeneous and when the colors of squares under the overlay are related to the colors around it by a simple translation. One possible study would be to define different L-Junction configurations with respect to different chromatic shifts to analyze possible interpretations by the visual system.

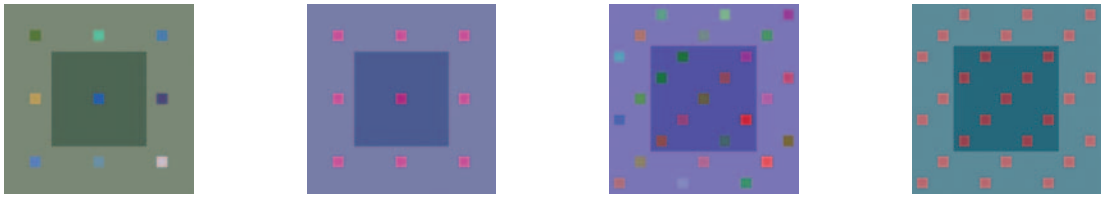

(*a*) (*b*) (*c*) (*d*)

Figure 7.4: L-Junctions and color coherence. (*a*) Filter created from translations in a L-Junction configuration without color coherence between square under the filter and squares around it. No transparency perception. (*b*) Filter created from translations in a L-Junction configuration with the color coherence between the square under the filter and squares around it. But still no transparency perception. (*c*) Filter created from translations in another L-Junction configuration without color coherence between squares under the filter and squares around it. No transparency perception. (*d*) Filter created from translations in a L-Junction configuration with color coherence between the square under the filter and squares around it. These L-Junctions create implicit X-Junctions and lead to transparency perception.

- The proposed experiment in **Chapter 6** addresses the influence of shadows on transparency in using simulated displays with both filters and shadows lying in front of surfaces. Results showed that lightness constancy is very high even if surfaces are seen under both filter and shadow. A similar display shown *in stereo* view would produce both a stronger illusion of depth difference between filter and surfaces and a greater effect on perceived lightness. Another experiment including chromaticities would be useful to see whether there are similar trends from perfect color constancy as well.

- Results in **Chapter 6** also show a systematic deviation from perfect lightness constancy in a manner consistent with a perceived additive shift. The GCM includes such additive chromatic changes. Thus, it would be interesting to test the GCM for color shadow perception. A display consisted of a color object with its cast shadow projected to the background (a series of color patches). A test surface would be viewed through the shadow and would be compared in appearance to a reference surface in plain view. The observer would adjust the color and lightness of the test square to the color of the surface square (reference square) so that colors look identical. Another variant would be that observer adjusts the color of a cast shadow by taking into account different color reflectance of the object. Such studies would help color shadow segmentations [Salvador, 2004].

Appendix A

Colorimetry

Colorimetry is a branch of color science that specifies numbers to colors from a physically defined visual stimulus. This approach is motivated by a desire to standardize perceived colors, in the sense when viewed by an observer with normal color vision and under the same observing conditions, stimuli with the same specification will be a complete color-match. We have seen in **Chapter 2** that the output of the cones from a light stimulus can be characterized by only three numbers. This *trichromacy principle* is the starting point of any *color space*, where only three numerical components will be sufficient to define color coordinates in a three-dimensional space. Different color spaces can be devised depending on different color representations, such as defined by physics, physiology or psychology (A complete chapter devoted to Colorimetry and color spaces can be found in [Wyszecki and Stiles, 1982]).

This Appendix introduces some of the color spaces used in this thesis (See **Chapters 4** and **5**), such as the reference color space *CIE XYZ*, another colorimetric color space such as *CIE LUV* and device-oriented *RGB* color spaces.

A.1 Colorimetric spaces

A colorimetry standard was defined by the *Commission Internationale de l'Eclairage* (CIE) in 1931 and continues to form the basis for the specification of color [Wyszecki and Stiles, 1982]. The CIE Colorimetric System comprises the essential standards and procedures of measurement that are necessary to make colorimetry a useful tool in science and technology. As we stated above, it was constructed on the basis of the principles of trichromacy. The CIE established the 1931 standard color-matching functions determined through psychophysical color matching experiments.

Color-matching experiment

As we have seen in **Chapter 2**, it is possible for many different spectral power distributions to produce identical color perceptions. This phenomenon is termed *metamerism*. It is useful to determine which lights produce identical color perceptions (always under a particular set of standard viewing conditions). *Additive color mixture* can be thus studied in an experiment where the observer is presented with two adjoining half-disks of projected light on a white screen. One half-disk is filled with light from one projector (test lamp) while the other half-disk is filled with light from three projectors (each from one primary light). The observer adjusts the quantities of these three primary lights until the resulting color perception matches that caused by the test lamp. Results of such color-matching experiments provide the amounts of three primaries, the *tristimulus values* of the spectrum, needed to match a unit amount of power at each wavelength of the visible spectrum (See Figure A.1 *(a)*). Color matching functions are related theoretically to the spectral

sensitivities of the three cones by linear transformations. The CIE 1931[1] defines a *Standard Colorimetric Observer* by providing two different but equivalent sets of color-matching functions that define two color coordinate systems, the RGB system and the XYZ system.

A.1.1 CIE XYZ

The *CIE RGB spectral primary system* is the first set of color-matching functions (See Figure A.1 *(a)*). Thus, the resulting equation for a color-match involving a monochromatic constituent E_λ of the equal-energy stimulus E is as follows:

$$E_\lambda = \bar{r}(\lambda)R + \bar{g}(\lambda)G + \bar{b}(\lambda)B \tag{A.1}$$

where $\bar{r}(\lambda), \bar{g}(\lambda), \bar{b}(\lambda)$ are the (spectral) tristimulus values of E_λ. However, the RGB color matching-functions present both positive and negative values. Since negative sources are not physically realizable,

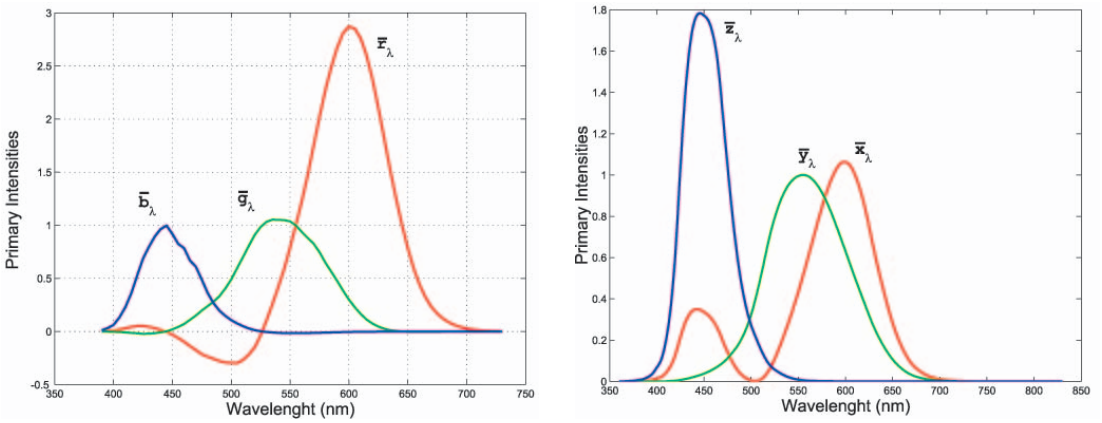

(*a*) (*b*)

Figure A.1: Color matching functions in the system of real primary stimuli R, G, B (*a*) and in the transformed system of imaginary primary stimuli X, Y, Z (*b*). (*a*) Spectral tristimulus values $\bar{r}(\lambda), \bar{g}(\lambda), \bar{b}(\lambda)$ of monochromatic stimuli E_λ of unit radiant power, with respect to the three fixed primary stimuli R, G, B, also monochromatic and of wavelengths $\lambda_R = 700, \lambda_G = 546.1, \lambda_B = 435.8$nm. (*b*) The CIE 1931 color-matching functions $\bar{x}(\lambda), \bar{y}(\lambda), \bar{z}(\lambda)$ based on the X, Y, Z primary stimuli (See text for explanation).

the definition of three hypothetical primary sources, such that all the spectral tristimulus values are positive, led to the second set of color-matching functions, which define the CIE XYZ color coordinate system. CIE RGB color-matching functions and CIE XYZ color-matching functions are related by a linear transformation. We report here an example of the transformation from the ITU-R BT.709 standard RGB values in the range [0, 1] to CIE XYZ tristimulus values in the range [0, 1]:

$$\begin{bmatrix} X \\ Y \\ Z \end{bmatrix} = \begin{bmatrix} 0.4125 & 0.3576 & 0.1804 \\ 0.2127 & 0.7152 & 0.0722 \\ 0.0193 & 0.1192 & 0.9502 \end{bmatrix} \begin{bmatrix} R \\ G \\ B \end{bmatrix} \tag{A.2}$$

This new colorimetric system always produces *positive* tristimulus values and represents all spectral colors in terms of these primaries (See Figure A.1 *(b)*). However, since their wavelengths have been chosen outside

[1] In 1931, the CIE established a standard colorimetric observer from experiments using a 2 deg. visual field. In 1964, another standard colorimetric observer was established with 10 deg. of visual field.

the visible spectrum, only a subset of this XYZ space can be physically produced. These primaries are also derived so that equal values of X, Y, and Z produce equal energy white and are arranged so that a single parameter, Y, determines the *luminance* of the color. The CIE XYZ standard is the reference space for comparing and storing color information, independently from devices and applications.

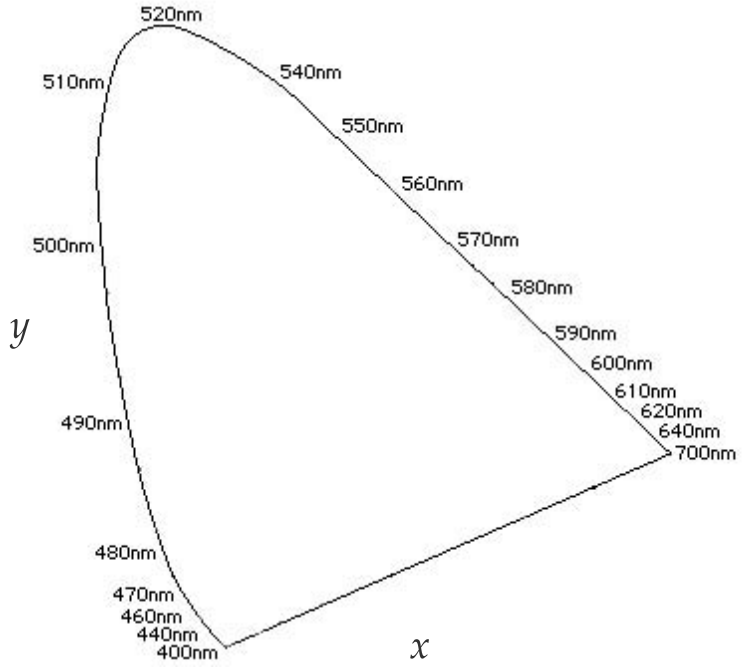

Figure A.2: Chromaticity diagram of CIE 1931 standard colorimetric observer in the transformed system of imaginary primaries X, Y, Z. Coordinates are obtained with $x = x/(X+Y+Z)$ and $y = y/(X+Y+Z)$.

A.1.2 CIE LUV

CIE tristimulus spaces are perceptually nonuniform, that is, equal perceptual differences between colors do not correspond to equal distances in the tristimulus space. The main aim in the development of uniform color spaces was to provide uniform practices for the measurement of color differences, something that cannot be done reliably in XYZ tristimulus spaces. The CIE has recommended two uniform color spaces: the CIE 1976 $L^*a^*b^*$-space and the CIE 1976 $L^*u^*v^*$-space. This last color space was used to characterize our stimuli in **Chapter 5**. The CIE 1976 ($L^*u^*v^*$)-*space* is defined in terms of non-linear transformations from CIE XYZ tristimulus values:

$$L^* = 116\left(\frac{Y}{Y_n}\right)^{1/3} - 16 \tag{A.3}$$

$$u^* = 13L^*(u' - u'_n) \tag{A.4}$$

$$v^* = 13L^*(v' - v'_n) \tag{A.5}$$

with the constraint that $Y/Y_n > 0.01$, L^* the *lightness* and u^*, v^* the *chromaticities*. The quantities u', v' and u'_n, v'_n are computed from:

$$u' = \frac{4X}{X + 15Y + 3Z} \quad v' = \frac{9Y}{X + 15Y + 3Z} \tag{A.6}$$

$$u'_n = \frac{4X_n}{X_n + 15Y_n + 3Z_n} \quad v'_n = \frac{9Y_n}{X_n + 15Y_n + 3Z_n} \tag{A.7}$$

The tristimulus values X_n, Y_n, Z_n are those of the white object-color stimulus. Usually, this white object-color stimulus is given by the spectral radiant power of the CIE standard illuminants, for example D_{65} (See **Chapter 2** for a definition of CIE standard illuminants). A chromaticity diagram is also defined from this space and is called the *CIE 1976 UCS diagram*, where v^* is plotted against u^*, and the resulting points in the diagram are only related to chromaticities when L^* is constant. In **Chapter 5**, we associate our vector lengths with the color difference ΔE^*_{uv}. This color difference between two stimuli, each given in terms of $L^*u^*v^*$, is calculated from:

$$\Delta E^*_{uv} = [(\Delta L^*)^2 + (\Delta u^*)^2 + (\Delta v^*)^2]^{1/2} \tag{A.8}$$

In our experiment, the first color is the surface's color seen in plain view and the second color is the filter's color obtained from one given color shift. This color-difference formula, defined by Equation A.8, is called the CIE 1976 ($L^*u^*v^*$) *color-difference formula*.

A.2 Device-oriented space

The CIE colorimetric system represents a fundamental international standard for color measurements. Device-oriented color representation systems allow the specification of color in devices such as television monitors, computer displays, color cameras or color printers. In these systems, colors depend on the equipment's characteristics [Hunt, 1998]. They appear different if the device settings are changed (if the phosphors of a monitor vary, the same color values produce a different color) or if they are reproduced in another device space (for example, color display on a monitor screen will appear different when printed). For this reason, a monitor used for psychophysical experiment must be properly calibrated and characterized.

A.2.1 RGB

The Red, Green, Blue (RGB) color space is used for capture and display devices. The primaries red, green and blue correspond to the three axes of a Cartesian coordinate system. Using an appropriate scale along each primary axis, the space can be normalized, so that all colors lie in the unit cube shown in Figure A.3. A transformation from RGB coordinates to rgb chromaticities is given by:

$$r = \frac{R}{R + G + B} \tag{A.9}$$

$$g = \frac{G}{R + G + B} \tag{A.10}$$

$$b = \frac{B}{R + G + B} \tag{A.11}$$

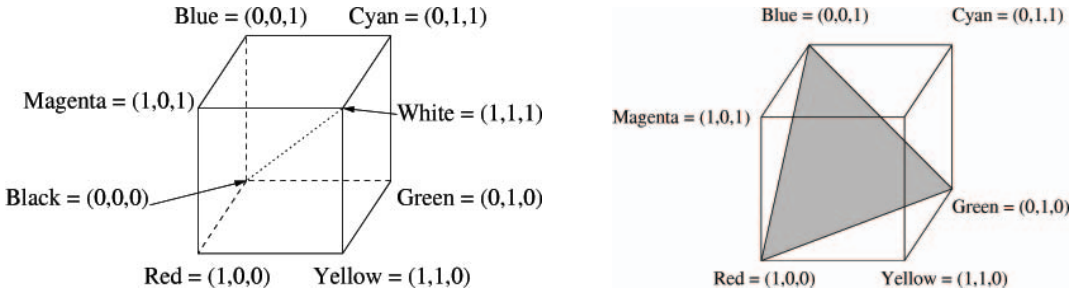

(*a*) (*b*)

Figure A.3: The RGB cube (*a*) and the unit plane in the RGB cube (*b*). The main diagonal of the cube, with equal amounts of each primary, represents the grays: black is $(0, 0, 0)$ and white is $(1, 1, 1)$. Each color is reproduced by an *additive mixture* of the three primaries. By dividing the R, G, B coordinates by their total sum, the r, g, b quantities are obtained, which give the three components of the *rgb* chromaticities.

Appendix B

Overview of Log-Linear Models

Statistical models used to fit the data in **Chapters 4** and **5** were *Log-Linear models* [Knoke and Burke, 1980]. These models were applied to analyze whether there is a possible interaction between the observers' responses and a perceptual factor (or explanatory variable, such as, for example, motion or configural complexity in our experiments). This interaction will thus be interpreted as an explanatory variable that affects observers' responses. In our studies, if a significant interaction is found, this variable affects the perception of transparency.

B.1 Poisson distribution

In our experiments, we performed data fitting using a Generalized Linear Model assuming the data to follow a *Poisson distribution* and using a logarithmic link function. The Poisson distribution is often used to model count data [Dobson, 2002]. If Y is the number of occurrences, its probability distribution can be written as

$$f(y) = \frac{\mu^y e^{-\mu}}{y!}, \quad y = 0, 1, 2, ... \tag{B.1}$$

where μ is the average number of occurrences. It can be shown that $E(Y) = \mu$ and $var(Y) = \mu$. This average μ often needs to be described as a *rate*, specified itself in terms of units of *exposure*. When exposure is constant, the explanatory variables are usually categorical. If there are a few explanatory variables, the data are summarized in a cross-classified table (See Section B.2). The response variable is the frequency or count in each cell of the table. The variables used to define the table are all treated as explanatory variables. The term *Log-Linear model*, which describes the role of the link function, is used for the generalized linear models appropriate for this situation. Before stating these models, it is important to have a notion of *cross-tabulations*.

B.2 Cross-tabulations

The first way to identify relationships between variables is to define *cross-tabulations*. The traditional method is to calculate percentages within categories of the independent variable [Knoke and Burke, 1980]. If the percentages differ by a significant amount (using a χ^2 test for independence) between or among categories, an association is said to exist. In order to use log-linear models, we have to replace a proportion (where the cell frequency is divided by the category total) by an *odds*. An odds is the ratio between the frequency of being in one category and the frequency of not being in that category. In a percentage table, two variables are unrelated if the percentages are identical or very close across all levels of the independent variable. Similarly, in an odds table, the variables are unassociated if all the conditional odds are equal or close to each other, and hence equal to the marginal odds as well.

Table B.1 shows an example of a cross-tabulation of one observer's responses according to responses type (*Transparent* or *Not Transparent*) related to filter motion (*Static* versus *Motion*), in our experiments described in **Chapters 5**. To compare directly two conditional odds, a single summary statistic can be done

	Transparent	**Not Transparent**	*Total*
Static filter	$f_{11} = 3$	$f_{12} = 13$	$f_{1.} = 16$
Motion filter	$f_{21} = 15$	$f_{22} = 1$	$f_{2.} = 16$
Total	$f_{.1} = 18$	$f_{.2} = 14$	$f_{..} = 32$

Table B.1: Cross-tabulation of responses type (**Transparent** or **Not Transparent**) and filter motion (**Static** or **Motion**).

by forming an *odds ratio* (See Equation B.2):

$$odds \quad ratio \quad (MT) = \frac{(f_{11})(f_{22})}{(f_{21})(f_{12})} \tag{B.2}$$

where M is the motion category and T the responses type category. A traditional measure of association for 2x2 tables, *Yule's Q*, is a simple function of the odds ratio:

$$Yule's \quad Q = \frac{(f_{11})(f_{22}) - (f_{12})(f_{21})}{(f_{21})(f_{12}) + (f_{11})(f_{22})} \tag{B.3}$$

where ranges in value are from -1.00 to $+1.00$, with zero indicating no relationship. In our experiment, the observed Yule's Q is of -0.97 meaning there is a high relationship between our variables: our observer tends to respond *Transparent* when the filter moves rather than when the filter is static.

B.3 Log-Linear Models

B.3.1 Saturated Models

Now we will find a model that will state the expected cell frequencies of a cross-tabulation (F_{ij}'s) as functions of parameters representing characteristics of the categorical variables and their relationships with each other. The frequencies expected under the model (the F_{ij}'s) must approximate the frequencies actually observed (the f_{ij}'s). One possible model for a 2x2 cross-tabulation, such as in Table B.1, is a *Saturated model*. This model is said saturated because all possible effect parameters are present in the model:

$$F_{ij} = \eta \tau_i^M \tau_j^T \tau_{ij}^{MT} \tag{B.4}$$

The F_{ij} represents the number of frequency of cases in cell i, j, which are expected to be present if the model is true. The η is the geometric mean of the number of cases in each cell in the table. It is a starting point from which effects are measured. The τ terms each represent effects which the variables have on the cell frequencies. The τ_i^M effects are present if the distribution on the response type variable across categories of the filter motion is unequal (non-rectangular) on the average. The τ_i^T effects are present if filter motion and response type are associated. Given these nine parameters, the four expected cell frequencies of Table B.1 can be represented by the model as shown in Table B.2. Since there are four cells in our 2x2 example table, the value of η is the fourth root of the product of the four expected cell frequencies. Because in the saturated model the expected cell frequencies are identical to the observed cell frequencies, we can now calculate all parameter estimates:

$$\eta = (f_{11} f_{12} f_{21} f_{22})^{1/4} = 4.92 \tag{B.5}$$

	Transparent	**Not Transparent**
Static filter	$F_{11} = \eta\tau_1^M\tau_1^T\tau_{11}^{MT}$	$F_{12} = \eta\tau_1^M\tau_2^T\tau_{12}^{MT}$
Motion filter	$F_{21} = \eta\tau_2^M\tau_1^T\tau_{21}^{MT}$	$F_{22} = \eta\tau_2^M\tau_2^T\tau_{22}^{MT}$

Table B.2: Expected cell frequencies for saturated model.

$$\tau_1^M = \frac{1}{\tau_2^T} = \frac{(f_{11}f_{12})^{1/2}}{\eta} = 1.27 \tag{B.6}$$

$$\tau_1^T = \frac{1}{\tau_2^M} = \frac{(f_{11}f_{21})^{1/2}}{\eta} = 1.36 \tag{B.7}$$

$$\tau_{11}^{MT} = \tau_{22}^{MT} = \frac{1}{\tau_{12}^{MT}} = \frac{1}{\tau_{21}^{MT}} = (\frac{f_{11}f_{22}}{f_{21}f_{12}})^{1/4} = 0.35 \tag{B.8}$$

Using these estimates (without rounding), we can exactly reproduce the four cell frequencies:

$$F_{11} = (4.92)(1.27)(1.36)(0.35) = 3 \tag{B.9}$$

$$F_{12} = (4.92)(1.27)(1/1.36)(1/0.35) = 13 \tag{B.10}$$

$$F_{21} = (4.92)(1/1.27)(1.36)(1/0.35) = 15 \tag{B.11}$$

$$F_{22} = (4.92)(1/1.27)(1/1.36)(0.35) = 1 \tag{B.12}$$

B.3.2 Non-saturated Models

A saturated model represents the cell frequencies of a cross-tabulation as a function of effects for the general mean (η), each variable and their relationships. The expected frequencies from a saturated model always perfectly match the observed frequencies. We can construct simpler models by setting some of the effect parameters to 1.00. Thus, the expected cell frequencies in our Table B.1 under a non-saturated model are:

$$F_{ij} = \eta\tau_i^M\tau_j^T \tag{B.13}$$

Additional models with other τ set to 1.00 include:

$$F_{ij} = \eta\tau_i^M \tag{B.14}$$

$$F_{ij} = \eta\tau_j^T \tag{B.15}$$

$$F_{ij} = \eta \tag{B.16}$$

These models are *hierarchical*, meaning that if a higher-order (interaction) term is included in the model, then all the related lower-order terms are also included.

B.3.3 Additive form

These general Log-Linear models are presented in their multiplicative form, but by taking natural logarithms of all the terms, the equations can be transformed into linear equations. In *Goodman's* notation, Equation B.4 has the log-linear form [Knoke and Burke, 1980]:

$$Ln(F_{ij}) = Ln(\eta\tau_i^M\tau_j^T\tau_{ij}^{MT}) \tag{B.17}$$

or

$$G_{ij} = \theta + \iota_i^M + \iota_j^T + \iota_{ij}^{MT}) \tag{B.18}$$

where the ι's are logs of the τ's, θ is the log of η and G_{ij} is the log of F_{ij}. The non-saturated models have similar log-linear expressions.

B.4 Testing for fit

To test which model provides the best fit, we will estimate the expected cell frequencies F_{ij}'s of each model seen above and comparing them to the observed frequencies f_{ij}'s using a *Pearson chi-square statistic* (χ^2):

$$\chi^2 = \sum_i \sum_j \frac{(f_{ij} - F_{ij})^2}{F_{ij}} \tag{B.19}$$

and comparing this with the central chi-squared distribution with $(I-1)(J-1)$ degrees of freedom [Dobson, 2002]. In this usual χ^2 test of independence, we seek to *reject* the null hypothesis of no association between the variables. We expect to find a large χ^2 value relative to df if the effect is significant. A *z-score* was also applied, based on a normal approximation of the transformed Poisson residuals. For a normal distribution, the z-score has the form:

$$z_x = \frac{X - \mu_x}{\sigma_x} \tag{B.20}$$

Appendix C

Motion and Configural Complexity: Complementary data

This appendix shows all results found in our study about the influence of motion and configural complexity on transparency perception, described in **Chapter 5**. This experiment investigated whether motion influences the perception of transparency generated by an overlay created from five different systematic chromatic changes. Bipartite and checkerboard like stimuli configurations were shown to the observers. A variety of chromatic transformations and changes in elevation from the equiluminant plane were studied for static versus motion overlays. Our main results showed that responses for stimuli generated from the five systematic chromatic variations vary according to several variables such as motion, configural complexity, vector length and luminance level. Higher order interactions were found with chromatic variations associated to luminance elevation, filter type and/or motion that change also quantitatively the observers' responses whatever the configuration or the absence/presence of motion are. Results are classified in the following Sections: observers' responses for convergences are presented in Section C.1, results for translations are shown in Section C.2, results for shears, divergences and rotations are described in Sections C.3 to C.5, respectively.

C.1 Convergences

Figure C.1 summarizes the number of responses of *all* observers (except PG) for convergences and are distributed as a function of luminance elevation according to each vector length ($\Delta E_{uv}{}^{*}$). Responses for each direction (or each filter type (FT)) are shown, according to configural complexity (CC) (such as bipartite and checkerboard configurations) and to static or moving filter condition (SM). Figure C.2 summarizes the number of responses of *each* observer (**LM**, **DT**, **PR** and **PG**) for convergences and are distributed as a function of luminance elevation according to each vector length ($\Delta E_{uv}{}^{*}$).

C.2 Translations

Figure C.3 summarizes the number of responses of *all* observers (except PG) for translations and are distributed as a function of luminance elevation according to each vector length ($\Delta E_{uv}{}^{*}$). Responses for each direction (or each filter type (FT)) are shown, according to configural complexity (CC) (such as bipartite and checkerboard configurations) and to static or moving filter condition (SM). Figure C.4 summarizes the number of responses of *each* observer (**LM**, **DT**, **PR** and **PG**) for translations and are distributed as a function of luminance elevation according to each vector length ($\Delta E_{uv}{}^{*}$).

C.3 Shears

Figure C.5 summarizes the number of responses of *all* observers (except PG) for shears and are distributed as a function of luminance elevation according to each vector length ($\Delta {E_{uv}}^*$). Responses for each direction (or each filter type (FT)) are shown, according to configural complexity (CC) (such as bipartite and checkerboard configurations) and to static or moving filter condition (SM). Figure C.6 summarizes the number of responses of *each* observer (**LM**, **DT**, **PR** and **PG**) for shears and are distributed as a function of luminance elevation according to each vector length ($\Delta {E_{uv}}^*$).

C.4 Divergences

Figure C.7 summarizes the number of responses of *all* observers (except PG) for divergences and are distributed as a function of luminance elevation according to each vector length ($\Delta {E_{uv}}^*$). Responses for each direction (or each filter type (FT)) are shown, according to configural complexity (CC) (such as bipartite and checkerboard configurations) and to static or moving filter condition (SM). Figure C.8 summarizes the number of responses of *each* observer (**LM**, **DT**, **PR** and **PG**) for divergences and are distributed as a function of luminance elevation according to each vector length ($\Delta {E_{uv}}^*$).

C.5 Rotations

Figure C.9 summarizes the number of responses of *all* observers (except PG) for rotations and are distributed as a function of luminance elevation according to each vector length ($\Delta {E_{uv}}^*$). Responses for each direction (or each filter type (FT)) are shown, according to configural complexity (CC) (such as bipartite and checkerboard configurations) and to static or moving filter condition (SM). Figure C.10 summarizes the number of responses of *each* observer (**LM**, **DT**, **PR** and **PG**) for rotations and are distributed as a function of luminance elevation according to each vector length ($\Delta {E_{uv}}^*$).

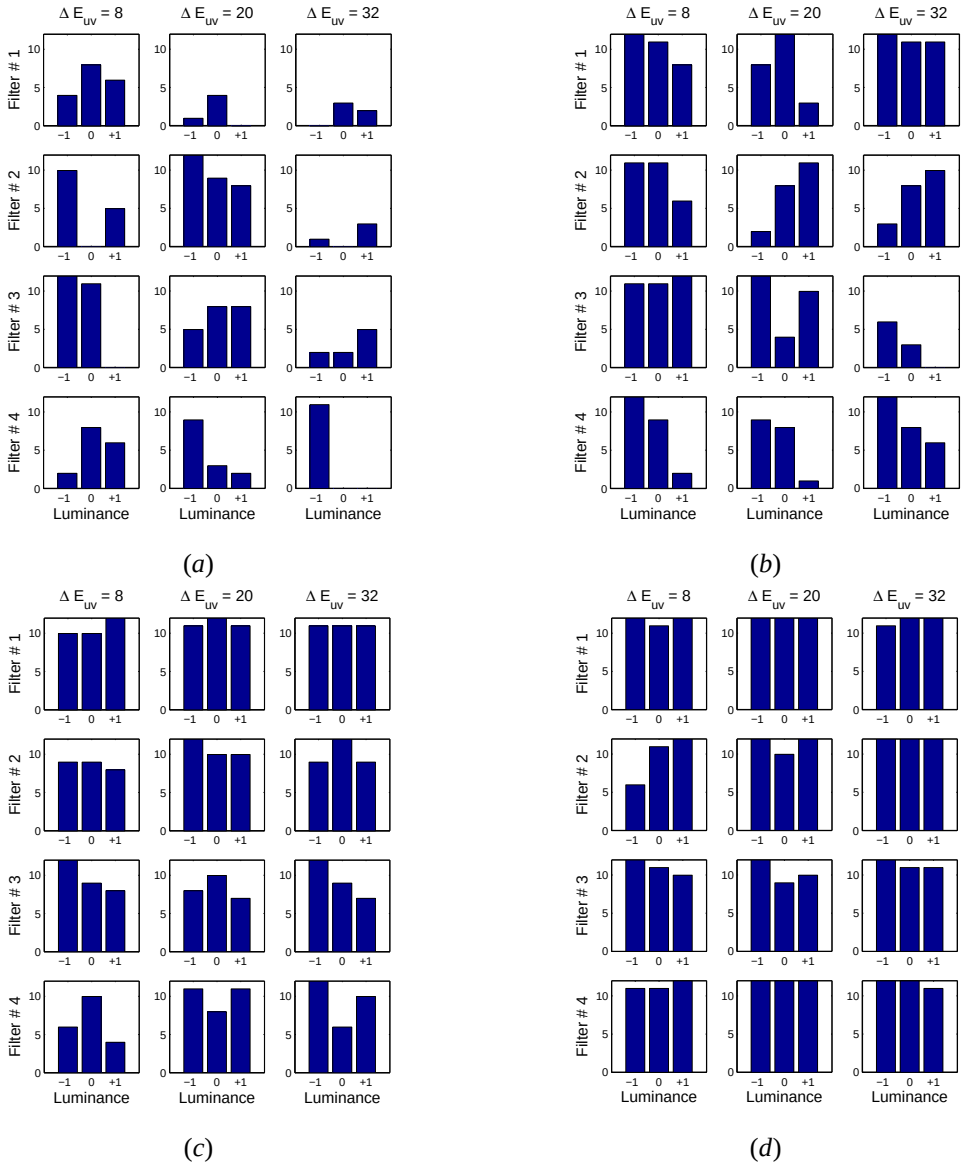

Figure C.1: Results for **convergences** for all observers (except PG). (*a*) **Bipartite** configuration with **static** filter. (*b*) **Bipartite** configuration with **moving** filter. (*c*) **Checkerboard** configuration with **static** filter. (*d*) **Checkerboard** configuration with **moving** filter. In *each set* of results, the first row (up) describes observers' cumulated responses for the first direction, or filter type 1 (FT). The second row shows observers' cumulated responses for filter type 2. The third row shows responses for filter type 3. The last row (down) illustrates observers' responses for filter type 4. All observers' responses are distributed as a function of luminance level (**(-1)**: Filter condition; **(0)**: Equiluminant condition; **(+1)**: Illuminant condition). The first column (left) shows observers' responses for $\Delta {E_{uv}}^* = 8$ in CIE LUV space, the second column depicts responses for $\Delta {E_{uv}}^* = 20$ and the last column (right) shows responses for $\Delta {E_{uv}}^* = 32$.

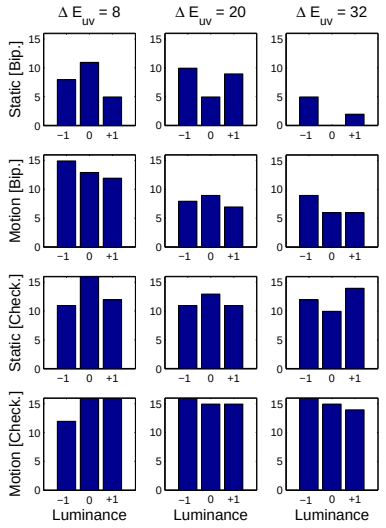

(*a*)

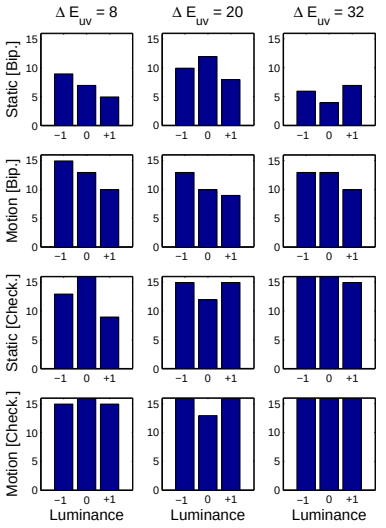

(*b*)

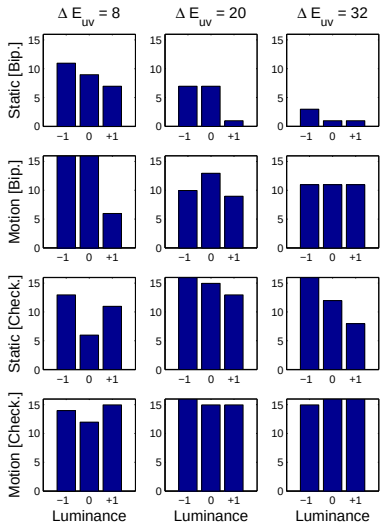

(*c*)

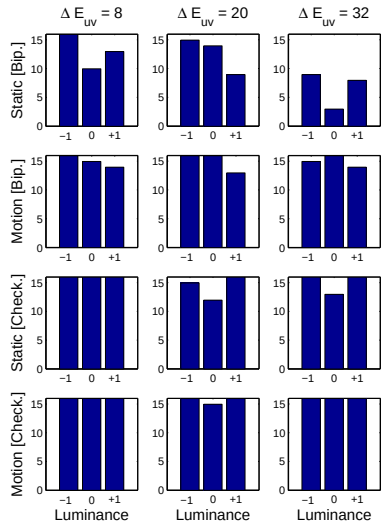

(*d*)

Figure C.2: Results for **convergences** for observers **LM** (*a*), **DT** (*b*), **PR** (*c*) and **PG** (*d*). The first row (up) describes observers' cumulated responses for bipartite configuration when filter is static (**Static [Bip.]**). The second row shows observers' cumulated responses when filter moves (**Motion [Bip.]**). The third row shows observers' cumulated responses for checkerboard configuration with static filter (**Static [Check.]**). The last row (down) illustrates observers' cumulated responses for checkerboard configuration when filter moves (**Motion [Check.]**). All observers' responses are distributed as a function of luminance level (**(-1)**: Filter condition; **(0)**: Equiluminant condition; **(+1)**: Illuminant condition). The first column (left) shows observers' responses for $\Delta {E_{uv}}^* = 8$ in CIE LUV space, the second column depicts responses for $\Delta {E_{uv}}^* = 20$ and the last column (right) shows responses for $\Delta {E_{uv}}^* = 32$.

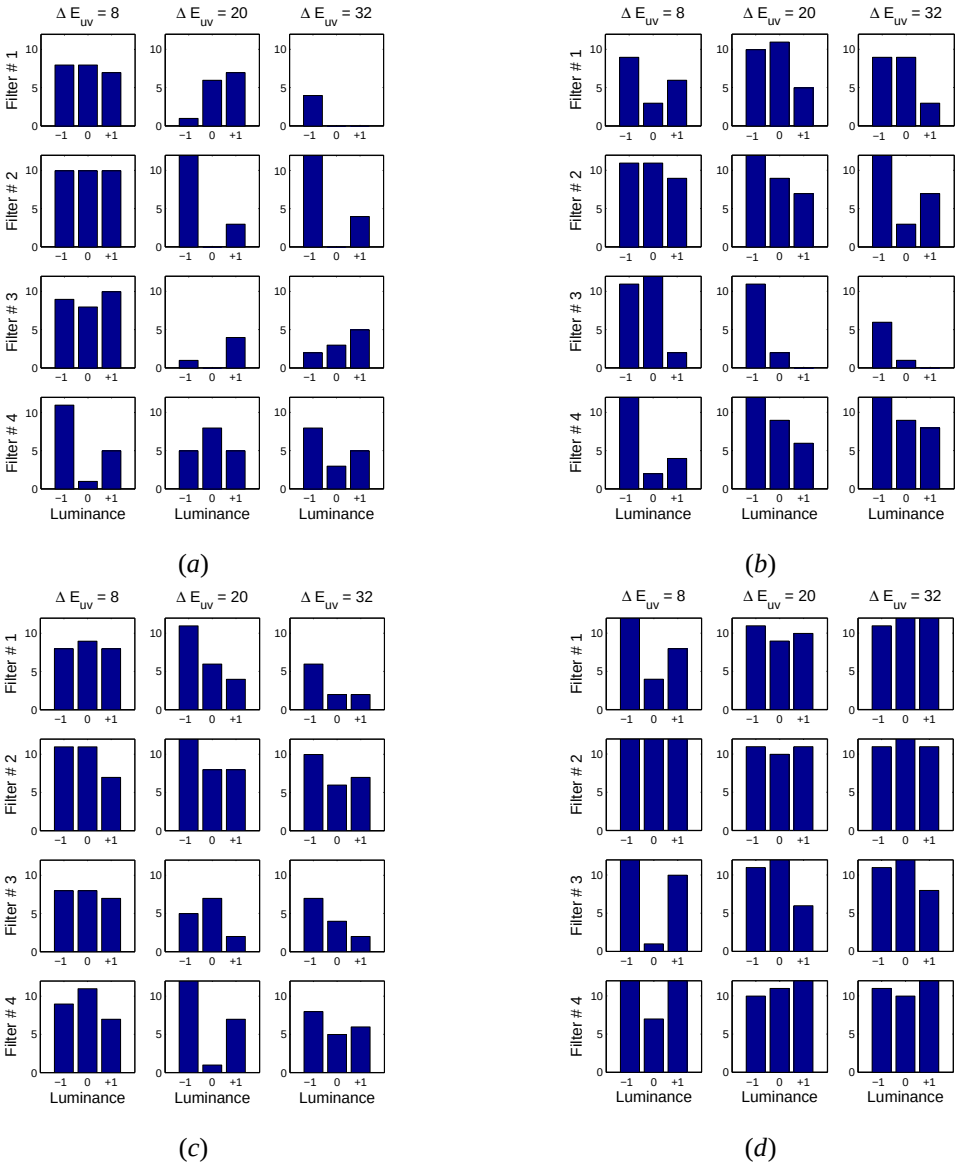

Figure C.3: Results for **translations** for all observers (except PG). (*a*) **Bipartite** configuration with **static** filter. (*b*) **Bipartite** configuration with **moving** filter. (*c*) **Checkerboard** configuration with **static** filter. (*d*) **Checkerboard** configuration with **moving** filter. In *each set* of results, the first row (up) describes observers' cumulated responses for the first direction, or filter type 1 (FT). The second row shows observers' cumulated responses for filter type 2. The third row shows responses for filter type 3. The last row (down) illustrates observers' responses for filter type 4. All observers' responses are distributed as a function of luminance level (**(-1)**: Filter condition; **(0)**: Equiluminant condition; **(+1)**: Illuminant condition). The first column (left) shows observers' responses for $\Delta {E_{uv}}^* = 8$ in CIE LUV space, the second column depicts responses for $\Delta {E_{uv}}^* = 20$ and the last column (right) shows responses for $\Delta {E_{uv}}^* = 32$.

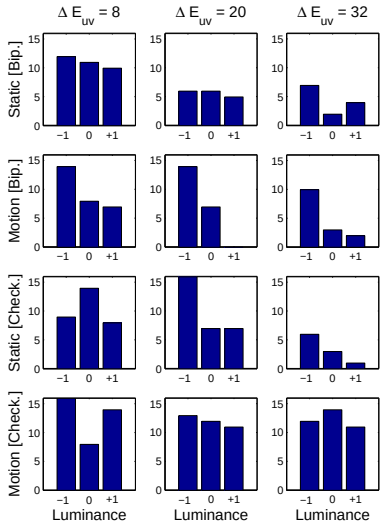

(*a*)

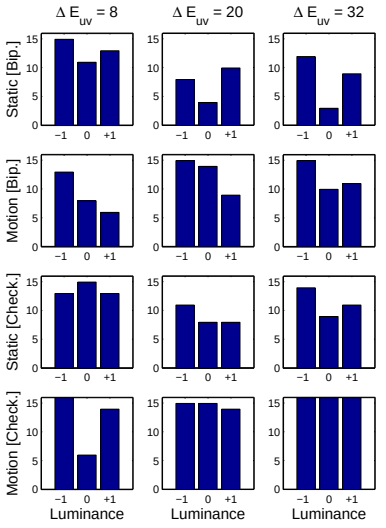

(*b*)

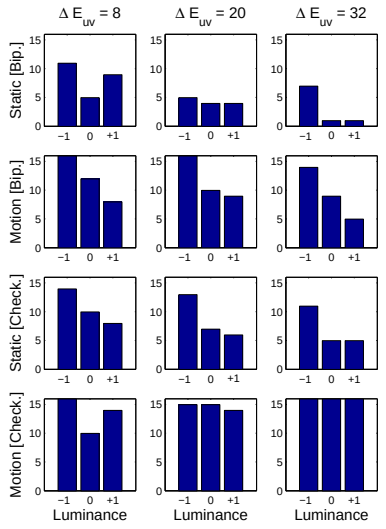

(*c*)

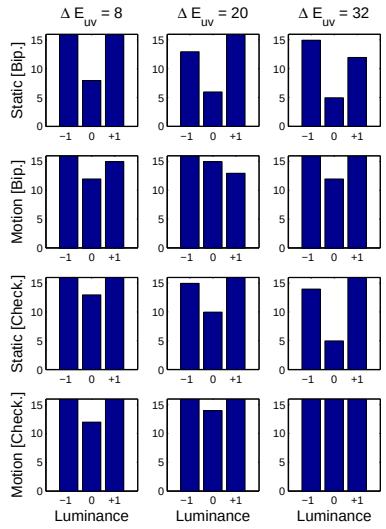

(*c*)

Figure C.4: Results for **translations** for observers **LM** (*a*), **DT** (*b*), **PR** (*c*) and **PG** (*d*). The first row (up) describes observers' cumulated responses for bipartite configuration when filter is static (**Static [Bip.]**). The second row shows observers' cumulated responses when filter moves (**Motion [Bip.]**). The third row shows observers' cumulated responses for checkerboard configuration with static filter (**Static [Check.]**). The last row (down) illustrates observers' cumulated responses for checkerboard configuration when filter moves (**Motion [Check.]**). All observers' responses are distributed as a function of luminance level (**(-1)**: Filter condition; **(0)**: Equiluminant condition; **(+1)**: Illuminant condition). The first column (left) shows observers' responses for $\Delta {E_{uv}}^* = 8$ in CIE LUV space, the second column depicts responses for $\Delta {E_{uv}}^* = 20$ and the last column (right) shows responses for $\Delta {E_{uv}}^* = 32$.

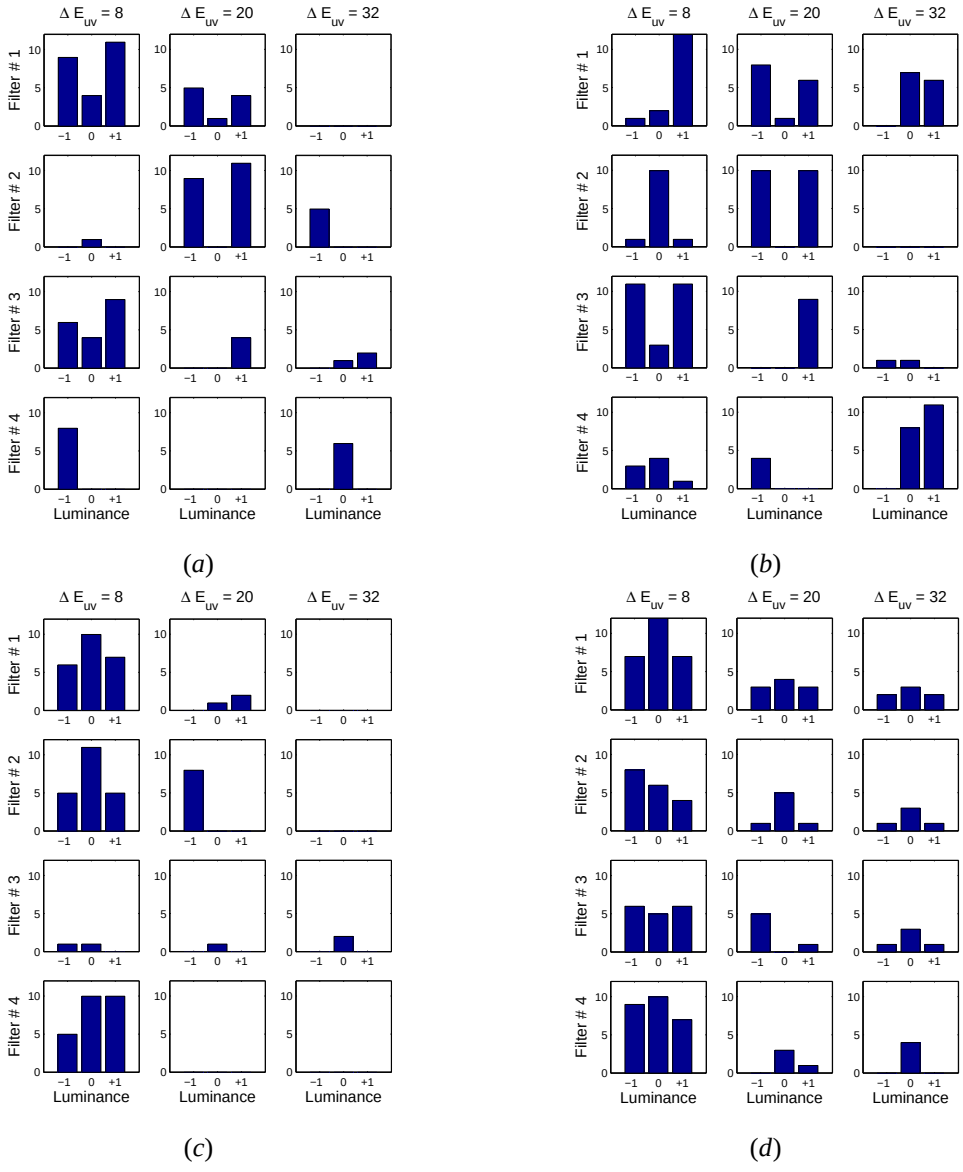

Figure C.5: Results for **shears** for all observers (except PG). (*a*) **Bipartite** configuration with **static** filter. (*b*) **Bipartite** configuration with **moving** filter. (*c*) **Checkerboard** configuration with **static** filter. (*d*) **Checkerboard** configuration with **moving** filter. In *each set* of results, the first row (up) describes observers' cumulated responses for the first direction, or filter type 1 (FT). The second row shows observers' cumulated responses for filter type 2. The third row shows responses for filter type 3. The last row (down) illustrates observers' responses for filter type 4. All observers' responses are distributed as a function of luminance level (**(-1)**: Filter condition; **(0)**: Equiluminant condition; **(+1)**: Illuminant condition). The first column (left) shows observers' responses for $\Delta {E_{uv}}^* = 8$ in CIE LUV space, the second column depicts responses for $\Delta {E_{uv}}^* = 20$ and the last column (right) shows responses for $\Delta {E_{uv}}^* = 32$.

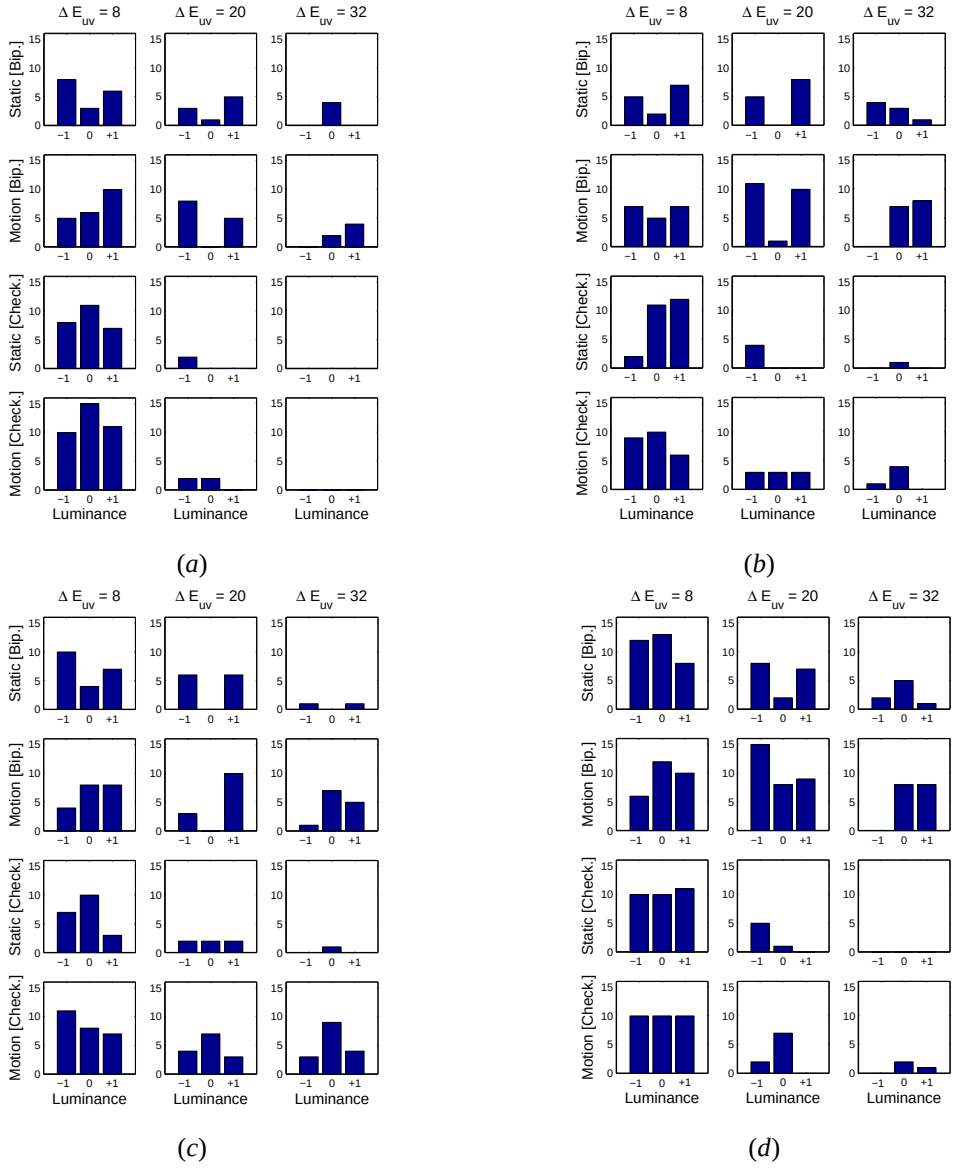

Figure C.6: Results for **shears** for observers **LM** (*a*), **DT** (*b*), **PR** (*c*) and **PG** (*d*). The first row (up) describes observers' cumulated responses for bipartite configuration when filter is static (**Static [Bip.]**). The second row shows observers' cumulated responses when filter moves (**Motion [Bip.]**). The third row shows observers' cumulated responses for checkerboard configuration with static filter (**Static [Check.]**). The last row (down) illustrates observers' cumulated responses for checkerboard configuration when filter moves (**Motion [Check.]**). All observers' responses are distributed as a function of luminance level (**(-1)**: Filter condition; **(0)**: Equiluminant condition; **(+1)**: Illuminant condition). The first column (left) shows observers' responses for $\Delta {E_{uv}}^* = 8$ in CIE LUV space, the second column depicts responses for $\Delta {E_{uv}}^* = 20$ and the last column (right) shows responses for $\Delta {E_{uv}}^* = 32$.

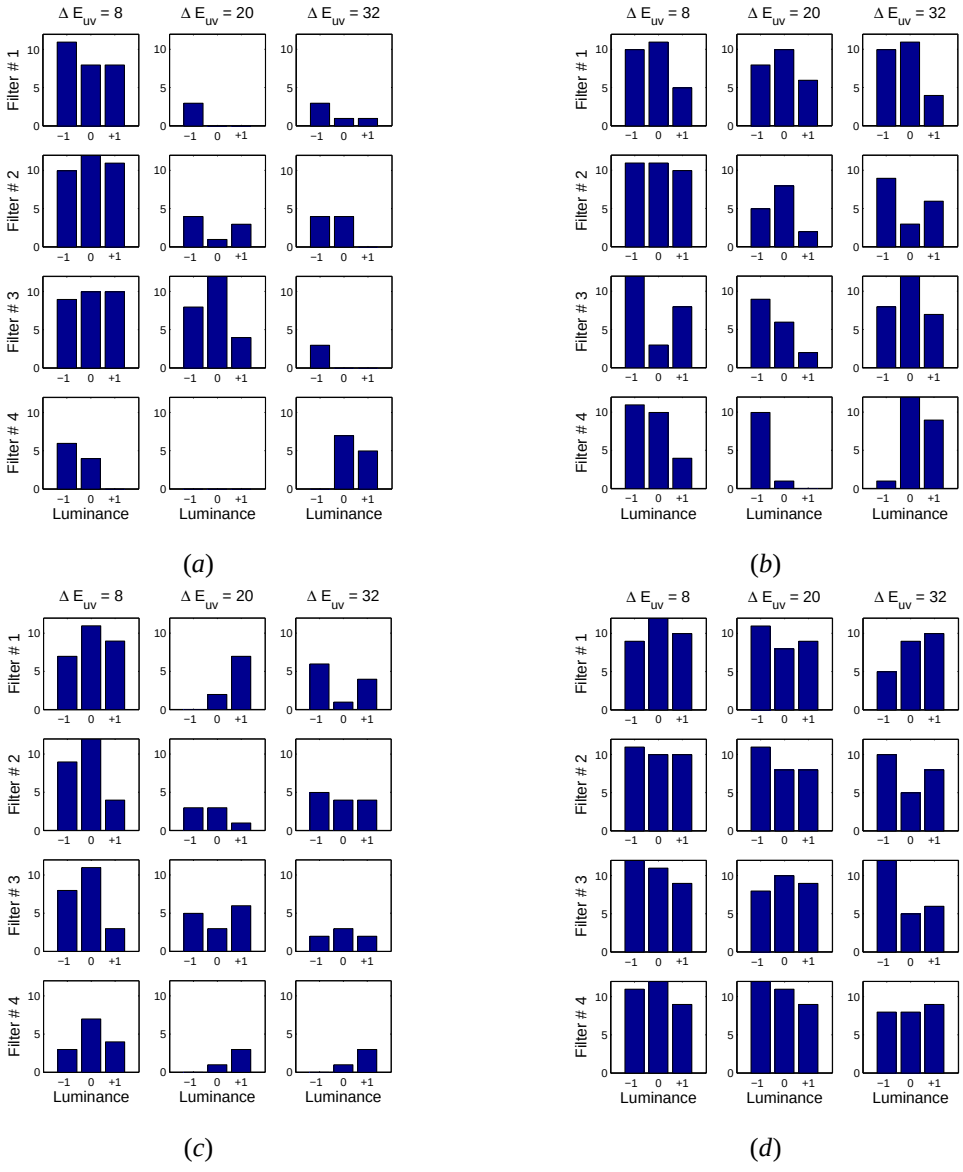

Figure C.7: Results for **divergences** for all observers (except PG). (*a*) **Bipartite** configuration with **static** filter. (*b*) **Bipartite** configuration with **moving** filter. (*c*) **Checkerboard** configuration with **static** filter. (*d*) **Checkerboard** configuration with **moving** filter. In *each set* of results, the first row (up) describes observers' cumulated responses for the first direction, or filter type 1 (FT). The second row shows observers' cumulated responses for filter type 2. The third row shows responses for filter type 3. The last row (down) illustrates observers' responses for filter type 4. All observers' responses are distributed as a function of luminance level (**(-1)**: Filter condition; **(0)**: Equiluminant condition; **(+1)**: Illuminant condition). The first column (left) shows observers' responses for $\Delta {E_{uv}}^* = 8$ in CIE LUV space, the second column depicts responses for $\Delta {E_{uv}}^* = 20$ and the last column (right) shows responses for $\Delta {E_{uv}}^* = 32$.

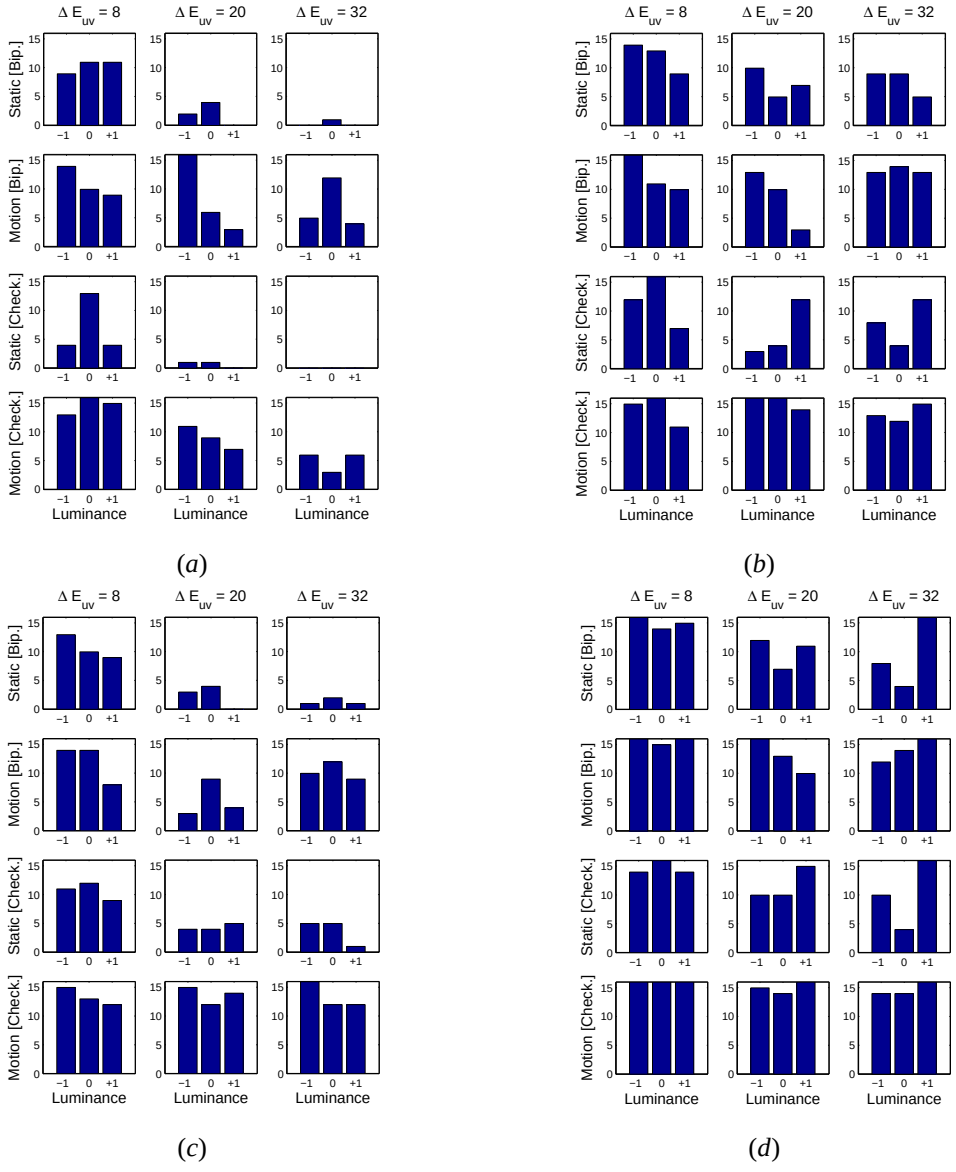

Figure C.8: Results for **divergences** for observers **LM** (*a*), **DT** (*b*), **PR** (*c*) and **PG** (*d*). The first row (up) describes observers' cumulated responses for bipartite configuration when filter is static (**Static [Bip.]**). The second row shows observers' cumulated responses when filter moves (**Motion [Bip.]**). The third row shows observers' cumulated responses for checkerboard configuration with static filter (**Static [Check.]**). The last row (down) illustrates observers' cumulated responses for checkerboard configuration when filter moves (**Motion [Check.]**). All observers' responses are distributed as a function of luminance level (**(-1)**: Filter condition; **(0)**: Equiluminant condition; **(+1)**: Illuminant condition). The first column (left) shows observers' responses for $\Delta {E_{uv}}^* = 8$ in CIE LUV space, the second column depicts responses for $\Delta {E_{uv}}^* = 20$ and the last column (right) shows responses for $\Delta {E_{uv}}^* = 32$.

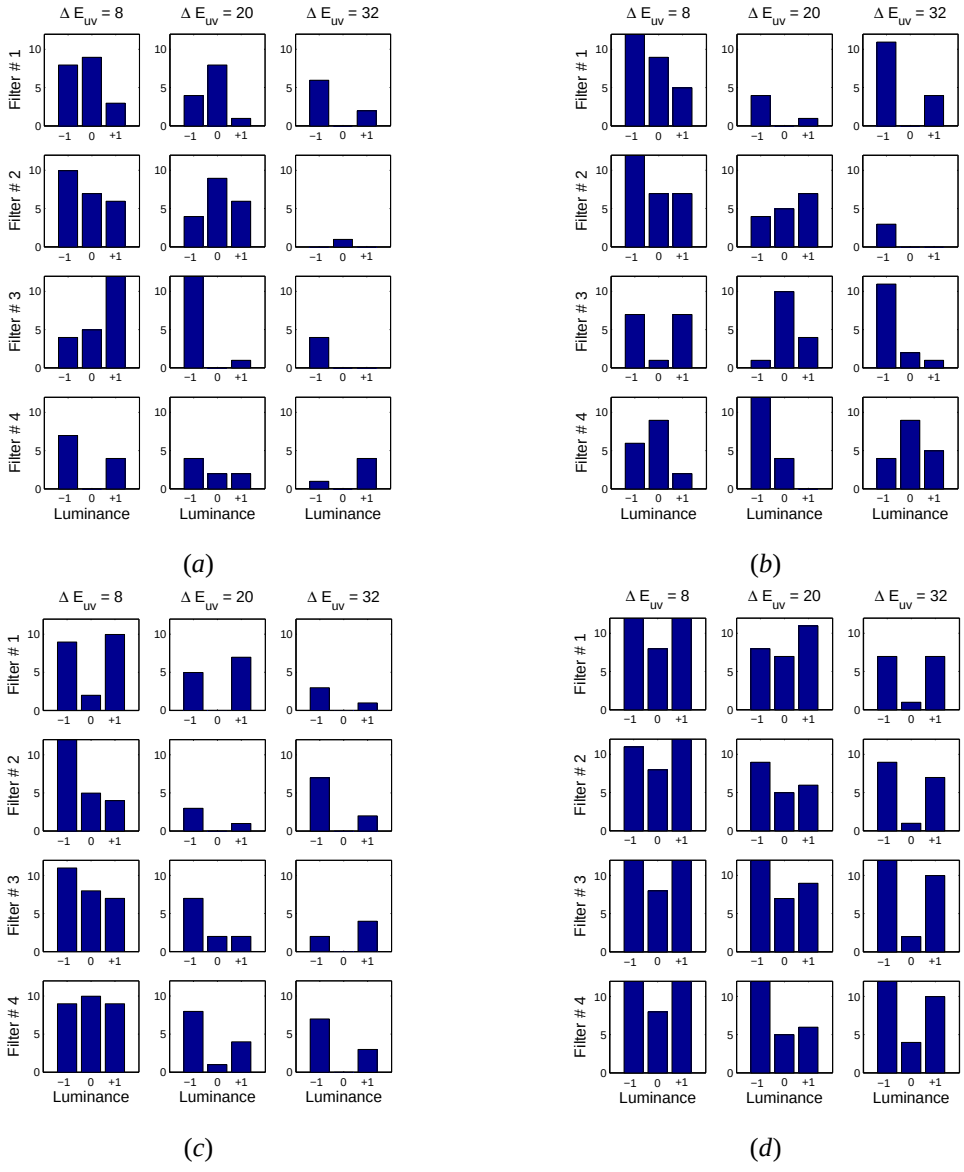

Figure C.9: Results for **rotations** for all observers (except PG). (*a*) **Bipartite** configuration with **static** filter. (*b*) **Bipartite** configuration with **moving** filter. (*c*) **Checkerboard** configuration with **static** filter. (*d*) **Checkerboard** configuration with **moving** filter. In *each set* of results, the first row (up) describes observers' cumulated responses for the first direction, or filter type 1 (FT). The second row shows observers' cumulated responses for filter type 2. The third row shows responses for filter type 3. The last row (down) illustrates observers' responses for filter type 4. All observers' responses are distributed as a function of luminance level (**(-1)**: Filter condition; **(0)**: Equiluminant condition; **(+1)**: Illuminant condition). The first column (left) shows observers' responses for $\Delta {E_{uv}}^* = 8$ in CIE LUV space, the second column depicts responses for $\Delta {E_{uv}}^* = 20$ and the last column (right) shows responses for $\Delta {E_{uv}}^* = 32$.

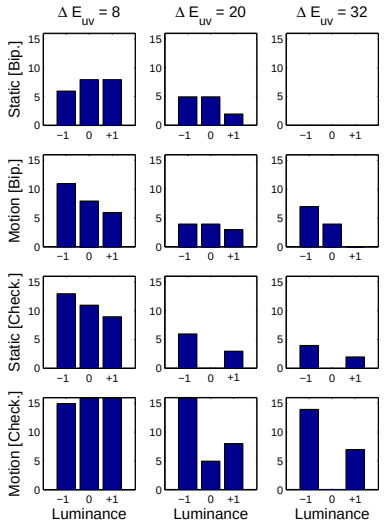

(*a*)

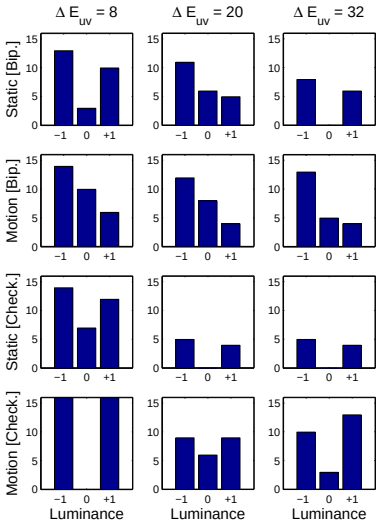

(*b*)

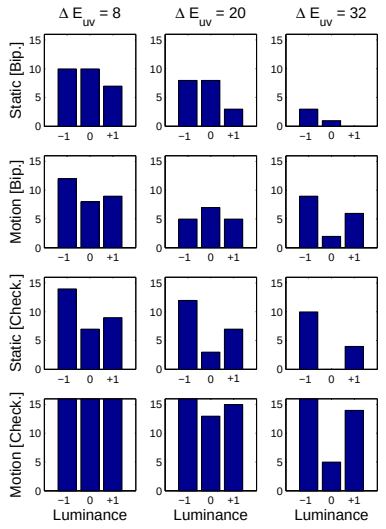

(*c*)

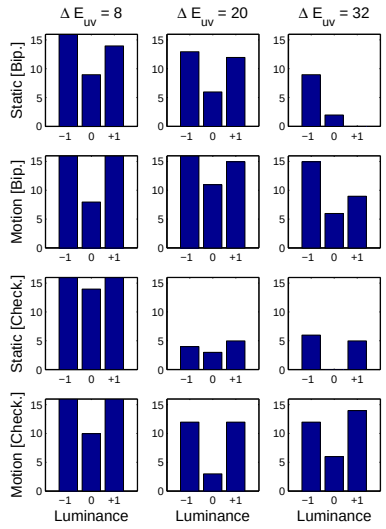

(*c*)

Figure C.10: Results for **rotations** for observers **LM** (*a*), **DT** (*b*), **PR** (*c*) and **PG** (*d*). The first row (up) describes observers' cumulated responses for bipartite configuration when filter is static (**Static [Bip.]**). The second row shows observers' cumulated responses when filter moves (**Motion [Bip.]**). The third row shows observers' cumulated responses for checkerboard configuration with static filter (**Static [Check.]**). The last row (down) illustrates observers' cumulated responses for checkerboard configuration when filter moves (**Motion [Check.]**). All observers' responses are distributed as a function of luminance level (**(-1)**: Filter condition; **(0)**: Equiluminant condition; **(+1)**: Illuminant condition). The first column (left) shows observers' responses for $\Delta {E_{uv}}^* = 8$ in CIE LUV space, the second column depicts responses for $\Delta {E_{uv}}^* = 20$ and the last column (right) shows responses for $\Delta {E_{uv}}^* = 32$.

List of Tables

List of Figures

Bibliography

E. H. Adelson. Perceptual organization and the judgment of brightness. *Science*, 262:2042–2044, 1993.

E. H. Adelson. Lightness perception and lightness illusions. In *The New Cognitive Neurosciences*, pages 339–351. M. Gazzaniga, Cambridge, MA: MIT Press, 2nd ed., 2000.

E. H. Adelson and P. Anandan. Ordinal characteristics of transparency. *AAAI-1990 Workshop on qualitative vision (Boston)*, pages 77–81, 1990.

B. L. Anderson. A theory of illusory lightness and transparency in monocular and binocular images: the role of contour junctions. *Perception*, 26:419–453, 1997.

K-H. Bäuml. Color constancy: the role of image surfaces in illuminant adjustment. *JOSA*, A 16(7):1521–1530, 1999a.

K-H. Bäuml. Simultaneous color constancy: how surface color perception varies with the illuminant. *Vision Research*, 39:1531–1550, 1999b.

J. Beck. Additive and substractive color mixture in color transparency. *Percept. Psychophys.*, 23:265–267, 1978.

J. Beck, K. Prazdny, and R. Ivry. The perception of transparency with achromatic colors. *Percept. Psychophys.*, 35:407–422, 1984.

Y. M. M Bishop, S. E. Fienberg, and P. W. Holland. *Discrete Multivariate Analysis: Theory and Practice*. MIT Press, Cambridge, 1975.

M. G. Bloj, D. Kersten, and A. C. Hurlbert. Perception of three dimensional shape influences colour perception through mutual illumination. *Nature*, 402:877–879, 1999.

H. Boyaci, K. Doerschner, and L. T. Maloney. Perceived surface color in binocularly viewed scenes with two light sources differing in chromaticity. *Journal of Vision*, 4(9):664–679, 2004.

H. Boyaci, L. T. Maloney, and G. Hersh. The effect of perceived surface orientation on perceived surface albedo in binocular-viewed scenes. *Journal of Vision*, 3(8):541–553, 2003.

O. J. Braddick, K. A. Wishart, and W. Curran. Directional performance in motion transparency. *Vision Research*, 42:1237–1248, 2002.

D. H. Brainard. Color constancy in the nearly natural image: 2. achromatic loci. *J. Opt. Soc. Am.*, 15(2): 307–325, 1998.

D. H. Brainard, W. A. Brunt, and J. M. Speigle. Color constancy in the nearly natural image: 1. asymmetric matches. *J. Opt. Soc. Am.*, 14(9):2091–2110, 1997.

E. Brenner, J. S. Ruiz, E. M. Herráiz, F. W. Cornelissen, and J. B.J. Smeets. Chromatic induction and the layout of colours within a complex scene. *Vision Research*, 43:1413–1421, 2003.

M. H. Brill. Physical and informational constraints on the perception of transparency and translucency. *Computer Vision, Graphics And Image Processing*, 28:356–362, 1984.

M. H. Brill. The perception of a colored translucent sheet on a background. *Color research and application*, 19(1):34–36, 1994.

R. O. Brown and D. I. A. MacLeod. Color appearance depends on the variance of surround colors. *Current Biology*, 7:844–849, 1997.

I. Bülthoff, D. Kersten, and H. H. Bülthoff. General lighting can overcome accidental viewing. *Investigative Ophtalmology and Visual Science, Suppl.*, 35(4):1741, 1994.

J. Wei C. S. Barnes and S. K. Shevell. Chromatic induction with remote chromatic contrast varied in magnitude, spatial frequency, and chromaticity. *Vision Research*, 39(21):3561–3574, 1999.

V. A. Casagrande. A third parallel visual pathway to primate area v1. *Trends Neurosci.*, 17(7):305–310, 1994.

P. Cavanagh and Y. G. Leclerc. Shape from shadows. *Journal of Experimental Psychology: Human Perception and Performance*, 15(1):3–27, 1989.

V. J. Chen and C. M. Cicerone. Subjective color from apparent motion. *Journal of Vision*, 2(6):424–437, 2002.

V.J. Chen and M. D'Zmura. Test of a convergence model for color transparency. *Perception*, 27:595–608, 1998.

C. Chubb, G. Sperling, and J. A. Solomon. Texture interactions determine perceived contrast. In *Proceedings of the National Academy of Sciences*, number 86, pages 9631–9635, USA, 1989.

F. Ciurea and B. Funt. Failure of luminance-redness correlation for illuminant estimation. In *IS&T/SID Twelfth Color Imaging Conference*, Scottsdale, AZ, USA, November 2004.

P. B. Delahunt and D. H. Brainard. Color constancy under changes in reflected illumination. *Journal of Vision, in press*, 2004a.

P. B. Delahunt and D. H. Brainard. Does human color constancy incorporate the statistical regularity of natural daylight? *Journal of Vision*, 4:57–81, 2004b.

A. M. Derrington, J. Krauskopf, and P. Lennie. Chromatic mechanisms in the lateral geniculate nucleus of macaque. *J. Physiology*, 357:241–265, 1984.

A. J. Dobson. *An Introduction to Generalized Linear Models*. Chapman and Hall/CRC, 2nd edition, 2002.

M. D'Zmura, P. Colantoni, K. Knoblauch, and B. Laget. Color Transparency. *Perception*, 26:471–492, 1997.

M. D'Zmura, O. Rinner, and K. R. Gegenfurtner. The colors seen behind transparent filters. *Perception*, 29:911–926, 2000.

M. D'Zmura and B. Singer. The spatial pooling of contrast in contrast gain control. *JOSA A*, 13:2135–21405, 1996.

M. D'Zmura and B. Singer. Contrast gain control. In *Color vision: From genes to perception*, pages 369–385. K. R. Gegenfurtner and L. T. Sharpe (Eds), Cambridge University Press, UK, 1999.

W. Ehrenstein. *Modifications of the brightness phenomenon of L. Hermann (Translated by A. Hogg from 'Über Abwandlungen der L. Hermannschen Helligkeitserscheinung', Zeitschrift für Psychologie, 150, 83Ű91)*. New York: Springer., s. petry and g. e. meyer edition, 1941/1987.

V. Ekroll and F. Faul. Perceptual transparency in neon color spreading displays. *Perception and Psychophysics*, 64(6):945–955, 2002.

V. Ekroll, F. Faul, R. Niedere, and E. Richter. The natural center of chromaticity space is not always achromatic: a new look at color induction. *Proc. Natl. Acad. Sci. U. S. A.*, 99:13352–13356, 2002.

V. Ekroll, F. Faul, and R. Niederee. The peculiar nature of simultaneous colour contrast in uniform surrounds. *Vision Research*, 44(15):1765–1786, 2004.

S. A. Engel, X. Zhang, and B. A. Wandell. Color tuning in human visual cortex measured using functional magnetic resonance imaging. *Nature*, 388:68–71, 1997.

F. Faul and V. Ekroll. Psychopysical model of chromatic perceptual transparency based on substractive color mixture. *J. Opt. Soc. Am. A*, 19(6):1084–1095, 2002.

D. H. Foster. Does color constancy exist? *Trends in Cognitive Sciences*, 7(10):439–443, 2003.

D. H. Foster, K. Amano, and S. M. C. Nascimento. Colour constancy from temporal cues: better matches with less variability under fast illuminant changes. *Vision Research*, 41:285–293, 2001.

K. R. Gegenfurtner. Colouring the cortex. *Nature*, 388:23–24, 1997.

K. R. Gegenfurtner. Reflections on colour constancy. *Nature*, 402:855–856, 1999.

K. R. Gegenfurtner. Color in the cortex revisited. *Nature Neurosci.*, 4(4):339–340, 2001.

K. R. Gegenfurtner. Cortical mechanisms of colour vision. *Nature*, 4:563–572, 2003.

K. R. Gegenfurtner and D. C. Kiper. Color vision. *Annu. Rev. Neurosci.*, 26:181–206, 2003.

P. Gerardin, P. Roud, S. Süsstrunk, and K. Knoblauch. Motion influences the effects of systemic chromatic changes. In *CGIV 2004, IS&T's Second European Conference on Color in Graphics, Imaging and Vision*, Aachen, Germany, April 2004.

P. Gerardin, S. Süsstrunk, and K. Knoblauch. Study of systematic chromatic changes in color space to model color transparency. In *IS&T/SPIE Human Vision and Electronic Imaging Conference, vol. 5007*, Santa Clara, CA, January 2003a.

P. Gerardin, S. Süsstrunk, and K. Knoblauch. Systematic chromatic changes underlying color transparency. In *Perception, Vol. 32 (supplement: 26th European Conference on Visual Perception)*, Paris, France, September 2003b.

W. Gerbino, C. I. Stultiens, J. M. Troost, and C. M. de Weert. Transparent layer constancy. *J. Exp. Psychol. Hum. Percept. Perform*, 16(1):3–20, 1990.

J. Golz and D. I. A. MacLeod. Influence of scene statistics on colour constancy. *Nature*, 415:637–640, 2002.

J. Hagedorn and M. D'Zmura. Color appearance of surfaces viewed through fog. *Perception*, 29:1169–1184, 2000.

D. J. Heeger. Normalization of cell responses in cat striate cortex. *Visual Neuroscience*, 9:181–197, 1992.

H. V. Helmholtz. *Optique Physiologique*. re-edition by J. Galay (1989), 1867.

E. Hering. *Outlines of a theory of the light sense*. Cambridge, Mass., Harvard University Press, 1964.

D. D. Hoffman. *Visual Intelligence*. W. W. Norton and Compagny Ltd., 1998.

I. P. Howard and P. A. Duke. Monocular transparency generates quantitative depth. *Vision Research*, 43: 2615–2621, 2003.

R. W. G. Hunt. *Measuring Colour*. Fountain Press, England, 3nd ed. edition, 1998.

J. M. Hupe and N. Rubin. Perceived motion transparency can override luminance/color cues which are inconsistent with transparency. In *ARVO*, 2000.

J. M. Hupe and N. Rubin. The oblique plaid effect. *Vision Research*, 44(5):489–500, 2004.

A. Hurlbert and K. Wolf. Color contrast: a contributory mechanism to color constancy. *Prog Brain Res.*, 144:147–160, 2004.

E. N. Johnson, M. J. Hawken, and R. Shapley. The spatial transformation of color in the primary visual cortex of the macaque monkey. *Nature Neurosci.*, 4:409–416, 2001.

P. K. Kaiser and R. M. Boynton. *Human color vision*. Optical Society of America, washigton dc, 2nd ed. edition, 1996.

G. Kanizsa. *Organization in Vision*. New York: Praeger, 1979.

D. Kersten, D. C. Knill, P. Mamassian, and I. Bülthoff. Illusory motion form shadows. *Nature*, 379(31), 1996.

B-G. Khang and Q. Zaidi. Accuracy of color scission for spectral transparencies. *Journal of vision*, 2: 451–466, 2002a.

B-G. Khang and Q. Zaidi. Cues and strategies for color constancy: perceptual scission, image junctions and transformational color matching. *Vision Research*, 42:211–226, 2002b.

B-G. Khang and Q. Zaidi. Illuminant color perception of spectrally filtered spotlights. *Journal of vision*, 4 (9):680–692, 2004.

D. C. Kiper, S. B. Fenstemaker, and K. R. Gegenfurtner. Chromatic properties of neurons in macaque area v2. *Visual neurosci.*, 14:1061–1072, 1997.

K. Knoblauch. Vision des couleurs chez les primates. *Primatologie*, 2:29–59, 1999.

K. Knoblauch. Color vision. In *Steven's Handbook of Experimental Psychology, Third Edition, Sensation and Perception*, pages 41–75. John Wiley and Sons, 2002.

K. Knoblauch and M. Dojat. Transparence, constance et apparence des couleurs. *Pour La Science*, Dossier Hors Séries(2):16–19, 2003.

K. Knoblauch and S. K. Shevell. Relating cone signals to color appearance: failure of monotonicity in yellow/blue. *Vis. Neurosci.*, 18(6):901–906, 2001.

K. Knoblauch and S. K. Shevell. Color appearance. In *The Visual Neurosciences*. L. M. Chalupa and J. S. Werner, MIT Press, November 2003.

D. Knoke and P. Burke. *Log-Linear Models*. Sage University Paper, vol. 20 edition, 1980.

K. Koffka. *Principles of Gestalt Psychology*. New York: Harcourt, Brace, and World, 1935.

B. B. Lee. Paths to colour in the retina. *Clin. Exp. Optom.*, 87(4–5):239–248, 2004.

P. Lennie. Single units and visual cortical organization. *Perception*, 27:889–935, 1998.

P. Lennie and M. D'Zmura. Mechanisms of color vision. *Crit. Rev. Neurobiol.*, 3:333–400, 1988.

P. Lennie, J. Krauskopf, and G. Sclar. Chromatic mechanisms in striate cortex of macaque. *J. Neurosci.*, 10:649–669, 1990.

F. Long and D. Purves. Natural scene statistics as the universal basis of color context effects. *PNAS*, 100 (25):15190–15193, 2003.

R. B. Lotto and D. Purves. An empirical explanation of color contrast. *PNAS*, 97(23):12834–12839, 2000.

D. I. A. MacLeod. New dimensions in color perception. *Trends in Cognitive Sciences*, 7(3):97–99, 2003.

P. Mamassian, D. C. Knill, and D. Kersten. The perception of cast shadows. *Trends in cognitive sciences*, 2(8):289–295, 1998.

P. R. Martin. Colour through the thalamus. *Clin. Exp. Optom.*, 87(4–5):249–257, 2004.

S. C. Masin. An experimental comparison of three- versus four-surface phenomenal transparency. *Percept. Psychophys.*, 35(4):325–332, 1984.

J. C. Maxwell. Experiments on colour as perceived by the eye with remarks on colour blindness. *Trans. of the R. Society of Edinburg*, 21:275–298, 1855.

P. McOwan and A. Johnston. Motion transparency arises from perceptual grouping: evidence from luminance and contrast modulation motion display. *Current Biology*, 6(10):1343–1346, 1996.

F. Metelli. The perception of transparency. *Scientific American*, 230:90–98, 1974.

F. Moradi and S. Shimojo. Perceptual-binding and persistent surface segregation. *Vision research*, 44: 2885–2899, 2004.

K. Moutoussis and S. Zeki. Responses of spectrally selective cells in macaque area v2 to wavelengths and colors. *J. Neurophysiol.*, 87(4):2104–2112, 2002.

S. Nakauchi, P. Silfsten, J. Parkkinen, and S. Usui. Computational theory of color transparency: recovery of spectral properties for overlapping surfaces. *JOSA*, A 16(11):2612–2624, 1999.

K. Nakayama, S. Shimojo, and V. Ramachandran. Transparency: relation to depth, subjective contours, luminance and neon color spreading. *Perception*, 19:497–513, 1990.

J. L. Nieves, A. García-Beltrán, and J. Romero. Response of the human visual system to variable illuminant conditions: An analysis of opponent-colour mechanisms in colour constancy. *Ophthal. Physiol. Opt.*, 20 (1):44–58, 2000.

J. F. Norman, T. E. Dawson, and S. R. Raines. The perception and recognition of natural object shape from deforming and static shadows. *Perception*, 29:135–148, 2000.

D. Osorio, D. L. Ruderman, and T. W. Crownin. Estimation of errors in luminance signals encoded by primate retina resulting from sampling of natural images with red and green cones. *J. Opt. Soc. Am. A*, 15(1):16–22, 1998.

F. Pavani and U. Castiello. Binding personal and extrapersonal space through body shadows. *Nature Neurosciences*, 7(1):13–14, 2004.

B. Pinna, G. Brelstaff, and L. Spillman. Surface color from boundaries: a new 'watercolor' illusion. *Vision Research*, 41:2669–2676, 2001.

B. Pinna, J. S. Werner, and L. Spillman. The watercolor effect: a new principle of grouping and figure-ground organization. *Vision Research*, 43:43–52, 2003.

O. Da Pos. *Trasparenze*. Icone s.r.l., first edition, 1989.

O. Da Pos. The perception of transparency with chromatic colours. In *Research in perception: Proceedings of the meeting in memory of Fabio Metelli, Padova, November 13-14, 1997*. Logos, first edition, 1999.

O. Da Pos and P. Bressan. Chromatic induction in neon colour spreading. *Vision Research*, 43:697–706, 2003.

A. M. Puerta. The power of shadows: shadow stereopsis. *J.O.S.A. A.*, 6(2):309–311, 1989.

N. Qian, R. A. Andersen, and E. H. Adelson. Transparent motion perception as detection of unbalanced motion signal. *J. Neurosciences*, 14:7357–7366, 1994.

R. R development core team: A language and environment for statistical computing. r. foundation for statistical computing, vienna, austria. http://www.R-project.org., 2004.

O. Rinner and K. R. Gegenfurtner. Time course of chromatic adaptation for color appearance and discrimination. *Vision Research*, 40:1813–1826, 2000.

C. Ripamonti, M. Bloj, K. Mitha, S. Greenwald, R. Hauck, S. I. Maloney, and D. H. Brainard. Measurements of the effect of surface slant on perceived lightness. *Journal of Vision*, 4(9):747–763, 2004.

C. Ripamonti and S. Westland. Transparency perception. In *Color science: Exploiting digital media*, pages 3–22. John Wiley and Sons Limited, l. w. mcdonald edition, 2001.

C. Ripamonti and S. Westland. Prediction of transparency perception based on cone-excitation ratios. *J. Opt. Soc. Am. A*, 20(9):1673–1680, 2003.

R. Robilotto, B-G. Khang, and Q. Zaidi. Sensory and physical determinants of perceived achromatic transparency. *Journal of vision*, 2:388–403, 2002.

R. Robilotto and Q. Zaidi. Perceived transparency of neutral density filters across dissimilar backgrounds. *Journal of vision*, 4(9):183–195, 2004.

R. W. Rodieck, R. K. Brening, and M. Watanabe. Contrast sensitivity: the origin of parallel visual pathways. *MIT Press*, pages 117–144, 1993.

A. Roorda, A. B. Metha, P. Lennie, and D. R. Williams. Packing arrangement of the three cone classes in primate retina. *Vision Res.*, 41:1291–1306, 2001.

A. Roorda and D. R. Williams. The arrangement of the three cone classes in the living human eye. *Nature*, 397:520–522, 1999.

E. Salvador. *Shadow Segmentation and Tracking in Real-Worl Conditions*. PhD thesis, EPFL, 2004.

D. Schluppeck and S. A. Engel. Color opponent neurons in v1: A review and model reconciling results from imaging and single-unit recording. *Journal of Vision*, 2:480–492, 2002.

R. M. Shapley and M. J. Hawken. Parallel retino-cortical channels and luminance. In *Color Vision (From genes to perception)*, pages 221–234. Cambridge University Press, 1999.

S. K. Shevell and J. Wei. Chromatic induction: border contrast or adaptation to surrounding light? *Vision Research*, 38:1561–1566, 1998.

S. K. Shevell and J. Wei. A central mechanism of chromatic contrast. *Vision Research*, 40(23):3173–3180, 2000.

B. Singer and M. D'Zmura. Color contrast induction. *Vision Research*, 34:3111–3126, 1994.

B. Singer and M. D'Zmura. Contrast gain control: a bilinear model for chromatic selectivity. *JOSA A*, 12: 667–685, 1995.

M. Singh. Lightness constancy through transparency: internal consistency in layered surface representations. *Vision Research*, 44:1827–1842, 2004.

M. Singh and B. L. Anderson. Perceptual assigment of opacity to translucent surfaces: the role of image blur. *Perception*, 31:531–552, 2002a.

M. Singh and B. L. Anderson. Toward a perceptual theory of transparency. *Psychological review*, 109(3): 492–519, 2002b.

M. Singh and D. D. Hoffman. Part boundaries alter the perception of transparency. *Psychological science*, 9:370–378, 1998.

V. C. Smith and J. Pokorny. Spectral sensitivity of the foveal cone photopigments between 400 and 500nm. *Vision Research*, 15:161–171, 1975.

H. Smithson and Q. Zaidi. Colour constancy in context: Roles for local adaptation and levels of reference. *Journal of Vision*, 4(9):693–710, 2004.

R. J. Snowden and F. A. J. Verstraten. Motion transparency: making models of motion perception transparent. *Trends in Cognitive Sciences*, 3(10):369–377, 1999.

A. Stockman and L. T. Sharpe. The spectral sensitivities of the middle- and long-wavelength-sensitive cones derived from measurements in observers of known genotype. *Vision Research*, 40(13):1711–1737, 2000.

M. Tommasi. A ratio model of perceptual transparency. *Percept. Mot. Skills*, 89(3 Pt 1):891–897, 1999.

H. F. J. M. van Tuijl. A new visual illusion: Neonlike color spreading and complementary color induction between subjective contours. *Acta Psychologica*, 39:441–445, 1975.

T. Wachtler, T. D. Albright, and T. J. Sejnowski. Nonlocal interactions in color perception: nonlinear processing of chromatic signals from remote inducers. *Vision Research*, 41:1535–1546, 2001.

J. M. Wallace and P. Mamassian. The efficiency of depth discrimination for non-transparent and transparent stereoscopic surfaces. *Vision Research*, 44(19):2253–2267, 2004.

B. A. Wandell. Color appearance: the effects of illumination and spatial pattern. *Proc. Natl. Acad. Sci. USA*, 90(21):9778–9784, 1993.

B. A. Wandell. *Foundations of Vision: Behavior, Neuroscience and Computation*. Sinauer Associates, May 1995.

T. Watanabe and P. Cavanagh. Depth capture and transparency of regions bounded by illusory and chromatic contours. *Vision Research*, 32(3):527–532, 1992.

T. Watanabe and P. Cavanagh. Surface decomposition accompanying the perception of transparency. *Spat. Vis.*, 7(2):95–111, 1993a.

T. Watanabe and P. Cavanagh. Transparent surfaces defined by implicit x-junctions. *Vis. Res.*, 33(16): 2339–2346, 1993b.

T. Watanabe, G. L. Zimmerman, and P. Cavanagh. Orientation-contingent color aftereffects mediated by subjective transparent structure. *Perception and Psychophysics*, 52(2):161–166, 1992.

S. Westland and C. Ripamonti. Invariant cone-excitation ratios may predict transparency. *JOSA*, A 17(2): 255–264, 2000.

S. Westland, C. Ripamonti, and O. Da Pos. Conditions for perceptual transparency. *Journal of Electronic Imaging / Special issue on Retinex*, in press.

D. Wollschlager, A. M. Rodriguez, and D. D. Hoffman. Flank transparency: transparent filters seen in dynamic two-color displays. *Perception*, 30(12):1423–1426, 2001.

D. Wollschlager, A. M. Rodriguez, and D. D. Hoffman. Flank transparency: the effects of gaps, line spacing, and apparent motion. *Perception*, 31(9):1073–1092, 2002.

G. Wyszecki and W. S. Stiles. *Color Science: Concepts and Methods, Quantitative Data and Formulae*. John Wiley and Sons, 1982.

Y. Xiao, Y. Wang, and D. J. Felleman. A spatially organized representation of colour in macaque cortical area v2. *Nature*, 421:535–539, 2003.

T. Young. On the theory of light and colours. *Phil. Trans. R. Soc.*, 92:12–18, 1802.

S. Zeki. Color coding in rhesus monkey prestriate cortex. *Brain res.*, 53:422–427, 1973.

S. Zeki. Color coding in the cerebral cortex: the responses of wavelength-selective and color-coded cells in monkey visual cortex to changes in wavelength composition. *Neuroscience*, 9:767–781, 1983.

Curriculum Vitae

Peggy GERARDIN
Image and Visual Representation Group (IVRG, LCAV)
School of Computer and Communications Sciences (I&C)
Ecole Polytechnique Fédérale de Lausanne (EPFL)
1015 Lausanne, Switzerland
Phone: +41 21 693 1274; Fax: +41 21 693 4312
Email: Peggy.Gerardin@epfl.ch
Web: http://lcavwww.epfl.ch/∼gerardin/

Research Experience

2001-2004 Research assistant in the Image and Visual Representation Group (IVRG, LCAV) of the Ecole Polytechnique Fédérale de Lausanne (EPFL), Lausanne, Switzerland.

- **Research fields:** Color perception, color image segmentation, image quality.
- **Topics:** Color transparency, transparency and motion, transparency and shadow.

Teaching Experience

2003 Lecturer for one class on Image Quality Evaluations in the course of Digital Photography, at the Ecole Polytechnique Fédérale de Lausanne (EPFL), Lausanne, Switzerland.

2003 Supervision of Semester and Diploma projects. **Diploma Project:** *Detection of Moving Color Transparency*, 9th semester, March 2003 to September 2003. **Semester Project:** *Shadow perception and its application to shadow detection*, 6th semester, March 2003 to June 2003.

2002 Teaching assistant for the course of Color Imaging, at the Ecole Polytechnique Fédérale de Lausanne (EPFL), Lausanne, Switzerland. **Lecturer:** One class on Color Transparency. **Assistant:** Exercises and projects.

2002 Teaching assistant for the course of Digital Photography, at the Ecole Polytechnique Fédérale de Lausanne (EPFL), Lausanne, Switzerland. **Lecturer:** One class on Image quality. **Assistant:** Exercises and projects.

Education

2001-2004 PhD student in the Image and Visual Representation Group (IVRG, LCAV) of the Ecole Polytechnique Fédérale de Lausanne (EPFL), Lausanne, Switzerland.

2000 DEA in Cognitive Sciences, option Neurosciences, (University Lyon1, University Lyon2, France). **Master thesis:** *FMRI study on human color perception*, (unity of INSERM 438, RMN Bioclinique Laboratory, Grenoble, France. Co-supervisors: Michel Dojat (INSERM 438) and Kenneth Knoblauch (INSERM 371)).

1999 Maîtrise in Cognitive Sciences, option Neurosciences, (University Lyon1, University Lyon2, Ecole Normale Supérieure de Lyon, France). **Diploma thesis:** *Extraocular deafferentation effects on a manual pointing task towards a memorized visual target*, (Institut des Sciences Cognitives, UMR 5015 CNRS, Bron, France. Supervisor: Driss Boussaoud (Group of .Neurophysiology of Action.)).

Fellowship

2003 Fellowship from the Swiss National Foundation from **September 2003 to March 2004** at the University of California, Irvine (UCI), Cognitive Science Dept., in Michael D'Zmura's Laboratory.

Graduate Courses

Additional grades obtained during PhD thesis in: Face Perception, Prof. Donald D. Hoffman, UCI. The Mind Body Problem, Prof. Donald D. Hoffman, UCI.

Technical Skills

Computer platforms: SUN.

Operating systems: UNIX, MS/DOS, Linux, Windows.

Programming languages: Matlab, Octave.

Visual stimulus display: MatVis, VSG 2/5.

Word processing: Word, LaTeX, PowerPoint, Excel.

Languages

French: Mother tongue.

English: Fluent oral, written.

Publications

Journal Papers

- P. Gerardin, P. Roud, S. Süsstrunk & K. Knoblauch, **Influence of Configural and Perceptual Factors on the Perception of Transparency**. To be submitted.

Conferences

- P. Gerardin, P. Roud, S. Süsstrunk & K. Knoblauch, **Motion influences the Effects of Systemic Chromatic Changes**. In Proc. CGIV 2004, IS&T's Second European Conference on Color in Graphics, Imaging and Vision, Aachen, Germany, April 5-8, 2004.
- P. Gerardin, S. Süsstrunk, & K. Knoblauch, **Systematic Chromatic Changes underlying Color Transparency**. Perception, Vol. 32 (supplement: 26th European Conference on Visual Perception, Paris, 2003), p. 52, 2003.
- P. Gerardin, S. Süsstrunk, & K. Knoblauch, **What systematic chromatic changes are necessary to perceive color transparency?** in 17th Symposium of the International Color Vision Society, Seattle, 2003.
- P. Gerardin, S. Süsstrunk & K. Knoblauch, **Study of Systematic Chromatic Changes in Color Space to model Color Transparency**. In Proc. IS&T/SPIE Human Vision and Electronic Imaging Conference, vol. 5007, Santa Clara, CA, January 21-24 2003.
- L. Piettre, M. Dojat, P. Gerardin, C. Segebarth & K. Knoblauch, **Transition screen strongly enhances activation in occipital ventral cortex during perception of colored stimuli**, in 9th ESMRMB-ISMRM conference, Glasgow (UK), 2001.
- L. Piettre, M. Dojat, P. Gerardin, C. Segebarth & K. Knoblauch, **Perception of coloured stimuli. Enhancement of the activations in the occipital ventral cortex by the use of a transition screen**, in NeuroImage 13, Number 6, 2001, Part 2 of 2 Parts, S929.

Theses

- P. Gerardin, **Configural and Perceptual Factors Influencing the Perception of Color Transparency**. Ph. D. Thesis accepted to the Ecole Polytechnique Federale de Lausanne (EPFL), January 2005.
- P. Gerardin, **FMRI study on human color perception**, Master thesis in Cognitive Sciences, July 2000, INSERM 438, RMN Bioclinique Laboratory, Grenoble, France.
- P. Gerardin, **Extraocular deafferentation effects on a manual pointing task towards a memorized visual target**, Diploma thesis in Cognitive Sciences, Institut des Sciences Cognitives, UMR 5015 CNRS, Bron, France.